POLITECNICO DI MILANO

Facoltà di Ingegneria Industriale

Corso di Laurea Magistrale in
Ingegneria Meccatronica e Robotica

CRACK IDENTIFICATION METHOD FOR MECHANICAL STRUCTURES

Relatore: *Prof. Francesco Braghin*

Co-relatore: *Ing. Giancarlo Galli*

Tesi di Laurea di:

Gianmaria Celico Fadini
Matricola : 784454

Anno Accademico 2013 - 2014

TABLE OF CONTENT

FIGURE LIST

TABLE LIST

ABSTRACT

Detection of cracks in a mechanical component is one of the most important aspect in industrial field. These elements are in fact responsible for sudden ruptures or failure and may therefore be a serious danger to the overall security of a mechanical structure indeed.
In this paper will be completely illustrated a new approach to crack identification. The method presented is part of the ***N**on **D**estructive **T**esting (NDT).*
It is know that a damage induces a nonlinear behaviour in the system analysed. Even in presence of small depth cracks, the dynamic behaviour of structures with breathing cracks forced by harmonic excitation is characterized by the appearance of sub-harmonic and super-harmonics in the response spectrogram. This is the main expression of the system nonlinearity.
With the objective of developing a crack identification method, great part of this study is focused on the study of super-harmonic frequencies of the system response. These frequencies are used to weigh the non-linearity of system behaviour at each frequency considered.
Dealing with the presence of a single crack, the study follows the intuition that the non-linearity of system behaviour tend to be switched off when the crack is located in correspondence of a nodal point of the mode of interest. Since the objective is to track the gap between non-linear and linear behaviour of a cracked structure, it is necessary to create an index that can be used in a later stage to locate the damage. This index, named *Non-Linearity Index,* evaluate these frequencies in which the behaviour is approximately linear and use them in conjunction with the nodal point location information to identify the position of the crack.
Nodal point location can be obtained by analytical way for simple geometries as well as by Finite Element Analysis for complex geometries where an analytical solution is not available.
Multiple advantages are related with the use of the crack identification method discussed in this paper. Nodal points information can be achieved from the study of an undamaged model of the structure that is more easily solvable respect to a system where a crack needs to be modelled. Finally the fact that it is possible to obtain information useful to crack identification directly from the measures of one single point of the structure. These facts make the method costly and versatile indeed.

SOMMARIO

L'identificazione delle cricche in un componente meccanico riveste uno degli aspetti più importanti in campo industriale. Questi elementi sono infatti responsabili di rotture improvvise e disservizi che a volte possono essere un serio pericolo per la sicurezza complessiva di una struttura meccanica.
In questo lavoro sarà illustrato in modo completo un nuovo approccio all'identificazione delle cricche. Il metodo presentato fa parte di quelli che vengono comunemente chiamati ***C**ontrolli **N**on **D**istruttivi (CND).*
È risaputo che un danneggiamento introduce una non linearità all'interno del sistema. Anche in presenza di piccole cricche, il comportamento dinamico di una struttura con una cricca aperta, quando forzata con un eccitazione armonica, è caratterizzato dalla presenza di frequenze sub e super armoniche nello spettrogramma della risposta. Questa è la principale espressione della non-linearità del sistema.
Con l'obiettivo di sviluppare un metodo di identificazione delle cricche, gran parte del lavoro si è focalizzato sullo studio delle frequenze super-armoniche della risposta del sistema. Queste frequenze sono usate per pesare la non-linearità del sistema ad ogni frequenza considerata.
Considerando la presenza di una singola cricca nel sistema, lo studio segue l'intuizione che la non-linearità del sistema tende a svanire quando la cricca viene a trovarsi in corrispondenza di un punto nodale del modo di vibrare di interesse. Siccome l'obiettivo è quello di tracciare la distanza tra risposta non-lineare e lineare di una struttura criccata è necessario creare un indice da utilizzare successivamente per la localizzazione del danneggiamento. Questo indice, chiamato *Non-Linearity Index,* valuta queste frequenze in cui il comportamento è approssimativamente lineare e le utilizza in unione alle informazioni sulla posizione del nodi del modo per identificare la posizione della cricca.
La posizione dei nodi della curvatura può essere ottenuta per via analitica nel caso di geometrie semplici oppure attraverso un analisi ad elementi finiti per geometrie complesse dove una soluzione analitica non è possibile.
I vantaggi nell'utilizzo del metodo di identificazione delle cricche discusso in questa relazione sono molteplici. Le informazioni sulla posizione dei nodi della curvatura possono essere ricavate dallo studio di una struttura non danneggiata e quindi, più facilmente risolvibile rispetto ad una in cui la cricca debba essere modellata. Infine il fatto che sia possibile ricavare informazioni utili all'identificazione della cricca direttamente dalle rilevazioni fatte in un unico punto della struttura. Questi fatti rendono il metodo poco costoso e soprattutto versatile.

INTRODUCTION

In industrial field, every critical product needs to be checked to verify its integrity and compliance with applicable regulations. It is well known that a crack, even of reduced dimension, when subjected to fatigue stress, grows and propagates leading to a sudden failure. Cracks are not easily detectable so, for their identification, detailed investigations are required indeed.

The sudden failure of structural components is very costly and may be catastrophic in term of human life and property damage. One of the most important aspects of evaluation of structural systems and ensuring their lifetime safety is structural damage detection. Some structures such as large bridges should be continuously monitored to detect possible damage (e.g. cracks) for ensuring uninterrupted service due to damage growth.

The presence of a crack not only causes a local variation in the mechanical characteristics of the structure at its location, but it also has a global effect that involves the entire structure. For this reason, the dynamic characterization of cracked structures can be used for damage detection in non-destructive tests and, among the various techniques, vibration-based methods offer an effective means of detecting fatigue cracks in structures [1-5].

There are two main categories of crack models used in detection methods: open crack models and breathing crack models. Consequently, vibration based methods are also classified into two categories: the linear approaches and the nonlinear approaches.

The majority of identification techniques involve the use of measured structural responses under dynamic excitation. When a structure experience fatigue phenomenon for example, some cracks may occur in the structure. These cracks cause changes in structural parameters (e.g., the stiffness of a structural member such as beam elements), which, in turn, change dynamic properties (such as natural frequencies and mode shapes).

Crack detection of beam elements involve in two different aspects: the first is the effects of cracks on eigen parameters as a forward problem and the second one may be considered as how to detect the location and qualification of cracks as an inverse problem. The inverse problem may be defined as determination of the internal structure of a physical system from the system's measured behaviour of identification of the unknown input that gives rise to measured output signal. To address the solutions of an inverse problem for a cracked beam, it is necessary to know "forward solutions", which are the results of determination of cracked beam natural frequencies knowing the crack parameters.

Non-destructive testing methods like ultrasonic testing, X-ray, etc., are generally useful for the purpose. These methods are costly and time consuming for long components, e.g., railway tracks, long pipelines, etc.
Vibration-based methods can offer advantages in such cases. This is because measurement of vibration parameters like natural frequencies is easy. Further, this type of data can be easily collected from a single point of the component. This factor lends some advantages for components that are not fully accessible. This also helps to do away with the collection of experimental data from a number of data points on a component, which is involved in a prediction based on, for example, mode shapes.
Several approaches have been used for modelling a crack in a beam, in the following chapter, a series of method of investigation for the detection of crack in beams will be presented, these methods formed the base for the development of our method of analysis. The available theories for this argument are too numerous to be dealt all completely, so we decide to focus on the most used.
After highlighting what are the characteristics of each technique and the results obtained from researchers, this text will move to a purely theoretical discussion of the concepts on which the new approach to crack identification is based and in particular some theoretical recall of *Vibration of Continuous Systems*, *Modes of Vibration* and *Non-Linear behavior*. Crack identification method will be then introduced and explained in all its aspects.
Last part of this paper is dedicated to the experimental validation of the method presented, this is done on a real physical model created and with the cooperation of both analytical or numerical solutions of the geometry considered.
Data obtained from multiple acquisitions are used to create a theoretical coefficient that permits to locate the crack present in the structure.

Chapter 1 STATE OF THE ART

In this part, a series of methods for crack identification are presented. During the last fifteen years several approaches have been used for modelling a crack in a beam. The methods presented use different techniques with all positive or negative characteristic, in some of them the crack is modelled by appropriately reducing the section modulus or by a local flexibility matrix in other approaches the crack is represented by a rotational spring. A finite element method has also been used for study of the vibration of cracked components.

1.1 Modelling of transverse vibration of short beams

S. P. Lele and S. K. Maiti presented this study in 2001[1], based on frequency measurements and extended to short beams taking into account the effects of shear deformation and rotational inertia through the Timoshenko beam theory and representing the crack by a rotational spring. The method is able to measure change in crack length from the change in the first natural frequency. Particularly, in the paper, were presented a method for solving forward problem (determination of frequencies of beams knowing the crack parameters), for inverse problem (determination of crack location knowing the natural frequencies) and crack extension estimation. A crack located at distance L_1 from the fixed end of a cantilever (Fig. 1) is represented by a rotational spring of stiffness K_1, whose magnitude is given by :

$$K_t = \frac{EBW^4}{72\pi \int_0^a a(f\left(\frac{a}{W}\right))^2 da} \tag{1}$$

Where $f(a/W)$ is given by:

$$\begin{aligned}\left[f\left(\frac{a}{W}\right)\right]^2 = a(1\cdot 2769 - 3\cdot 105\frac{a}{W} + 14\cdot 878\,\frac{a^2}{W^2} - 25 \\ \cdot 8\,\frac{a^3}{W^3} + 45\cdot 32\,\frac{a^4}{W^4} - 51\cdot 33\,\frac{a^5}{W^5} + 64 \\ \cdot 39\,\frac{a^6}{W^6} - 62\cdot 96\,\frac{a^7}{W^7} + 200\cdot 9\,\frac{a^8}{W^8} - 243 \\ \cdot 2\,\frac{a^9}{W^9} + 83\cdot 16\frac{a^{10}}{W^{10}} + 225\cdot 6\,\frac{a^{12}}{W^{12}})\end{aligned} \tag{2}$$

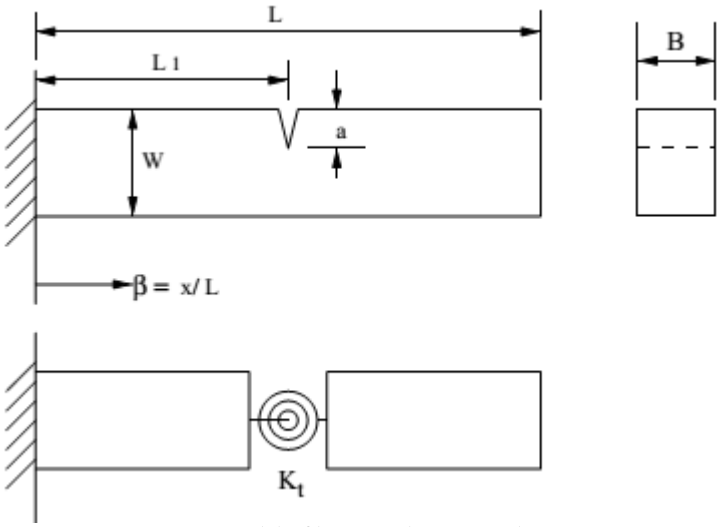

Fig. 1 – Model of beam with rotational spring.

The governing equations of flexural vibration are given by Timoshenko as follows:

$$EI\frac{\partial^2 y}{\partial x^2} + k'\left(\frac{\partial y}{\partial x} - \psi\right)AG - \rho I\frac{\partial^2 \psi}{\partial t^2} = 0 \tag{3}$$

$$\rho\frac{\partial^2 y}{\partial t^2} - k'\left(\frac{\partial^2 y}{\partial x^2} - \frac{\partial \psi}{\partial x}\right)G = 0 \tag{4}$$

where y is the transverse deflection, ψ the angle of rotation due to bending moment, E the modulus of elasticity, G the modulus of rigidity, A the area of cross-section, I the area moment of inertia, ρ the density and k' the numerical shape factor for the cross-section.
The solutions for these equations can be written in the following form:

$$\begin{aligned} Y &= A_1\cosh(bp\beta) + A_2\sinh(bp\beta) + A_3\cosh(bq\beta) + A_4\sinh(bq\beta) \\ \Psi &= A_1'\sinh(bp\beta) + A_2'\cosh(bp\beta) + A_3'\cosh(bq\beta) + A_4'\sinh(bq\beta) \end{aligned} \tag{5}$$

Where Y is the amplitude function of y and ψ the amplitude function of ψ.
For a cracked beam (Fig. 1), the two segments lying on the other side of the crack can be analysed separately.

The solution for the two segments can be written as follows:

$$\begin{aligned} Y_1 &= C_1 \cosh(bp\beta) + C_2 \sinh(bp\beta) + C_3 \cosh(bq\beta) + C_4 \sinh(bq\beta) \\ \Psi_1 &= C_1' \sinh(bp\beta) + C_2' \cosh(bp\beta) + C_3' \cosh(bq\beta) + C_4' \sinh(bq\beta) \\ Y_2 &= C_5 \cosh(bp\beta) + C_6 \sinh(bp\beta) + C_7 \cosh(bq\beta) + C_8 \sinh(bq\beta) \\ \Psi_2 &= C_5' \sinh(bp\beta) + C_6' \cosh(bp\beta) + C_7' \cosh(bq\beta) + C_8' \sinh(bq\beta) \end{aligned} \tag{6}$$

The last part of the theory are the boundary conditions and the conditions for continuity of displacement, moment and shear force at the crack location and the jump in the slope. This leads to a long characteristic equation used to solve forward and inverse problems.

Forward problem

For the determination of the natural frequencies for a given crack location and size, the rotational spring stiffness is given as input. The characteristic equation is solved to get the frequency parameter b. In turn, the natural frequency ω is determined using the equation :

$$b^2 = \frac{\rho A L^4 \omega^2}{EI} \tag{7}$$

Inverse problem

The characteristic equation for the Timoshenko beam with a crack is written in the form :

$$K = -\frac{|\Delta_1|}{|\Delta_2|} \tag{8}$$

The method of Nandwana and Maiti is utilized to obtain the solution. Since the rotational spring stiffness representing the crack is independent of the vibration mode, the point of intersection of three (minimum) curves gives the location of the crack.

1.1.1 Crack extension measurement

In this case, the objective is to estimate $\Delta a = a_2 - a_1$, from the knowledge of ω_1 and ω_2 which correspond to crack lengths. The starting crack length a_1 is specified. For some dimensionless parameters (b and s), it is clear that there is a dependence on material properties. If b is to remain the same for two different values of frequency, there is a need for adjusting either E or ρ. Choosing to adjust E, the corrected modulus $\bar{E}$ corresponding to $\bar{\omega}$ is given by :

$$\frac{\rho A L^4 \omega^2}{EI} = \frac{\rho A L^4 \bar{\omega}^2}{EI} \Rightarrow \frac{E}{\bar{E}} = \left(\frac{\omega}{\bar{\omega}}\right)^2 \quad (9)$$

There is an improvement accuracy with this E correction. That was demonstrated through case studies.

1.1.2 Results

The method has been tested considering various geometric combinations and two sets of material properties. One important fact is the nature of the crack, in this case of study is introduced in the beam with wire cut machining.
The results of the Timoshenko beam model are in good agreement with the FEM results in the entire range of L/W ratio. For shorter beams, the difference between the results by the Euler-Bernoulli model and the FEM, as expected, increases. This shows the effect of rotational inertia and shear deformation. The present model predicts the first natural frequency with the highest accuracy when the FEM results are taken as the basis.
Since the interest lies in the detection of a crack anywhere in the whole span of the beam, it is logical to express the percentage error taking the beam length as the basis. The percentage error is therefore given by the difference between the predicted and actual crack locations expressed as a percentage of the beam length.
From the range of crack locations and sizes considered in the numerical studies, the errors in prediction of natural frequencies are observed to be ≤ 1%
for the first mode of vibration for beams with $L/W \geq 3$. For the second and third mode, the errors are of the order of 10%. The errors in detection of crack location and estimation of crack extension are ≤ 10%. Based on the experimental study, the errors in the prediction of natural frequencies and detection of crack location are of the order of 10%. The maximum error in estimation of crack extension is about 34%.

1.2 Crack detection in beams using kurtosis

Natural frequencies have been the most appealing damage indicator because they can be easily measured and are less contaminated by experimental noise.
The main disadvantage of using natural frequency changes for crack detection is the fact that significant cracks may cause small changes in natural frequencies, which may go undetected due to measurements errors. In an effort to overcome these difficulties, research has been focused on using changes in mode shapes. Mode shapes are more sensitive to local damag compared to changes in natural frequencies but has some drawbacks. The presence of a crack may not significantly influence lower modes that are usually measured from vibration tests. Extracted mode shapes are usually affected by experimental noise and the duration of measurements increases considerably if a detailed mode shape has to be estimated.
In this paper, the fundamental vibration mode of a cracked cantilever beam is analysed and both the location and size of the crack are estimated. The location of the crack is detected by a sudden change in the spatial variation of the analysed response, while the size of the crack is related to the kurtosis measure. The proposed technique forms a Kurtosis-based crack detector, which takes into account the non-Gaussianity of the vibration signal in order to efficiently detect both the location and the size of the crack [2]. Compared to existing methods for crack detection, the proposed kurtosis-based prediction scheme is attractive due to low computational complexity and inherent robustness against noise.
This model has been successfully applied to simply supported, cantilever, and fixed–fixed cracked beams. Experiments were finally conducted on Plexiglass Beam.

Mathematical background

Let $\{X(k)\}$ be a real random zero-mean process that is fourth-order stationary. The kurtosis is a measure of the heaviness of the tail in the distribution of the $X(k)$ sequence. If outliers or abrupt changes in the $X(k)$ appears then the non-Gaussianity of the signal is powered, making heavier the tails of the distribution and destroying its symmetry, resulting in high values of the kurtosis parameter. In this way, the kurtosis could be used to establish an effective statistical test in identifying abrupt changes in signals, such as those produced in the vibration signals from cracked beams due to the existence of a crack.
The KCD (*Kurtosis Crack Detector*) is based on the property of kurtosis to identify deviations from Gaussianity in band-limited random process. This non-Gaussianity

could vary with different structural conditions, i.e., reduction of the stiffness due to the occurrence of a crack, and, thus, changes in the mode shapes of vibration.
The output vector of the KCD scheme is constructed as:

$$\hat{k}_4 = |\hat{\gamma}_4 - \bar{\gamma}_4| \tag{10}$$

where $\hat{\gamma}_4$ is the vector with the estimated $\hat{\gamma}_4$ values derived at each position of the sliding M-sample window across the N-sample vibration signal and $\bar{\gamma}_4$ is the sample mean value of $\hat{\gamma}_4$. In this way, the values of the output vector $\hat{k}_4$ outside the area of the crack location are almost zeroed, obviously enhancing the visual inspection of the existence of a crack in the KCD output.

Analysis

A cantilever beam of length L, of uniform rectangular cross-section $w \times w$ with a crack located at L_c is considered as shown in Fig. 2(a). The crack is assumed to be open and have uniform depth α. Due to the localized crack effect, the beam can be simulated by two segments connected by a massless spring (Fig. 2(b)).

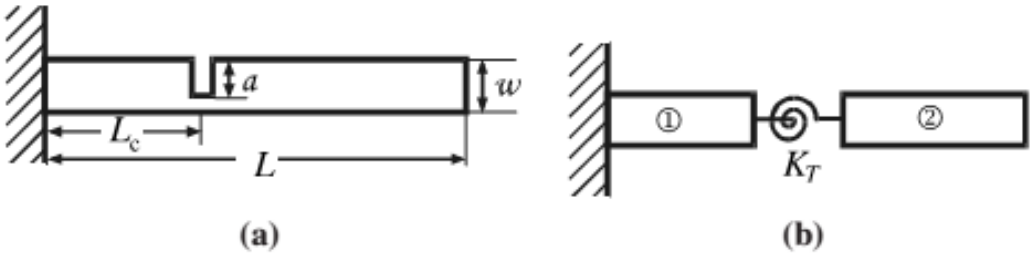

Fig. 2 – (a) Cantilever beam under study; (b) cracked cantilever beam model.

In this analysis, since only bending vibrations of thin beams are considered, the rotational spring constant is assumed to be dominant in the local flexibility matrix.
For numerical simulations a Plexiglas beam of total length 30 cm and rectangular cross-section $2x2\ cm^2$ is considered. A crack of relative depth 20% is introduced at $x = 4\ cm$ from clamped end.
From the first analysis we can see that the displacement data reveal no local features that directly indicate the existence of the crack.

1.2.1 Determination of crack location

To determine the location of the crack was investigate the values of kurtosis on simulated response data. The estimated kurtosis versus distance along the beam is presented in Fig. 3. It can be seen that in all cases the estimate of kurtosis exhibits a peak value at x = 4 cm where the crack is located. It can be also observed that the peak value increases with increasing crack depth indicating that kurtosis is related to crack depth.

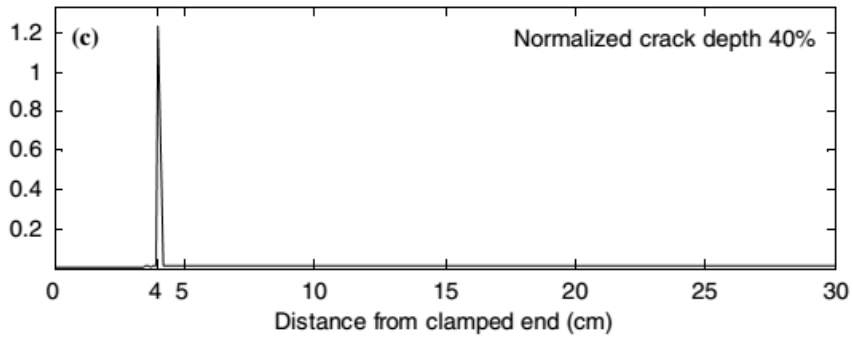

Fig. 3 – Estimated kurtosis as a function of distance along the cracked beam

To estimate the size of the crack, the dependence of the kurtosis estimate on both crack location and depth was systematically investigated. For that purpose, the vibration modes of the beam were calculated for relative crack depths varying from 5% up to 50% in steps of 5%, while the crack location was varied from 2 cm to 10 cm from the clamped end. The results are presented in Fig. 4.

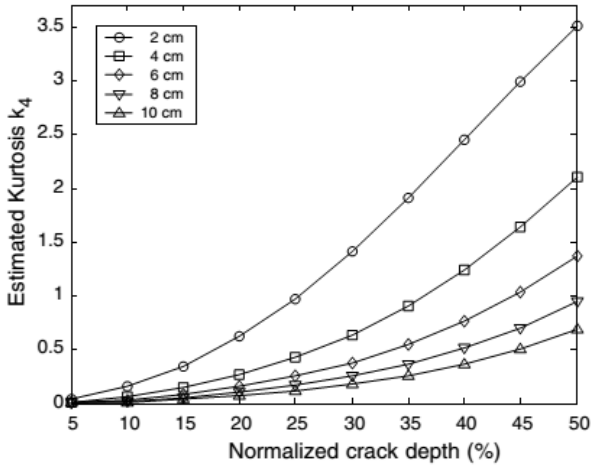

Fig. 4 – Estimated kurtosis versus normalized crack depth

It can be seen that kurtosis increases with increasing crack depth. For a given crack depth, the rate of increase depends on crack location. The increment of the increase is higher for cracks close to the clamped end and decreases gradually as the crack location is shifted towards the free end. Consequently, cracks in the vicinity of the clamped end could be more easily and accurately determined.
The method was tested on noise robustness using different crack depths and noise presence.

1.2.2 Experimental results

To validate the analytical results an experiment on a Plexiglas beam has been performed. A crack of relative crack depth 30% was introduced at x = 6 cm from the clamped end. An electromagnetic vibrator by Link and two B&K accelerometers were used for the experiment. Harmonic excitation was utilized via a 2110 B&K analyzer and the fundamental mode of vibration was investigated. The vibration amplitude was measured with a sampling distance of 7.5 mm, which was the effective diameter of the accelerometer used, so that a total number of 39 measuring points were obtained. Mode shape was measured by using two calibrated accelerometers mounted on the beam. One accelerometer was kept at the clamped end as the reference input, while the second one was moved along the beam to measure the mode amplitude. For that purpose, a miniature accelerometer weighting 2.5 g was used. It can be seen that there is a main clear peak at x = 6 cm and smaller in different positions Fig. 5.

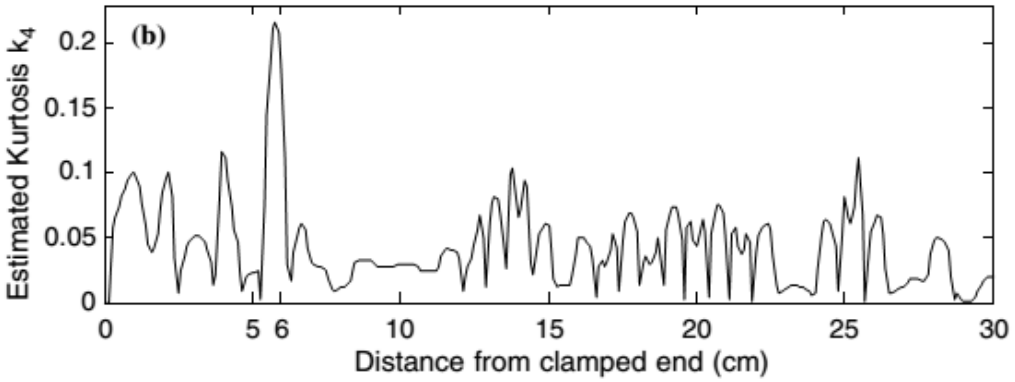

Fig. 5 – Estimation of Kurtosis along the length of the beam

1.2.3 Conclusion

The numerical results were confirmed by the application of the method to experimental mode shapes of a cracked cantilever beam. Using the noisy experimental data, the location and size of a crack were detected with reasonable accuracy. In conclusion, the presented results provide a foundation of using kurtosis as an efficient crack detection tool. Compared to existing methods for crack detection, it is attractive due to its low computational complexity and robustness against noise.

1.3 Detection of crack using wavelet finite element methods

In this methodology, developed by B. Li, X.F. Chen, J.X. Ma, Z.J [3], the detection of crack location and size takes advantage of wavelet finite element methods (WFEM). First, the beam is discretized into a set of wavelet finite elements, and then the natural frequencies of the beam with various crack locations and sizes are accurately obtained. The frequency response functions, function of crack location and size, are approximated by means of surface-fitting techniques. Measured natural frequencies are used in a crack detection process and the crack location and size can be identified by finding the point of intersection of three frequency contour lines.
In order to overcome the difficulties that traditional FEM have, wavelet spaces have been employed as approximate spaces and then wavelet finite element methods (WFEM) have been derived. By comparison with the conventional FEM, WFEM lend several advantages for modal analysis of crack problems. A main attractive feature is that WFEM have the ability to accurately represent fairly general functions with a small number of wavelet coefficients, as well as to characterize the smoothness of such functions from the numerical behaviour of these coefficients. WFEM. The frequency response function (FRF), as a function of crack location and size, is approximated through surface-fitting techniques and three-dimensional plots of FRFs are shown. Then, for a particular crack location and size, the three frequency contour lines of the beam are obtained under the situation that measured natural frequencies of crack beams are set as input. The crack location and size can be identified through finding the points of intersection of the three contour lines.

Analysis

The basic idea of WFEM, which is similar to the traditional FEM, is to discretize a body into an assemble of discrete finite elements which are interconnected at the

nodal points on element boundaries. The displacement field is approximated over each wavelet-based finite element, in terms of the nodal displacements.
For a one-dimensional wavelet-based finite element, the nodal displacements can be represented by the shape functions, whose forms are as follows:

$$N = \varphi T \tag{11}$$

where T stands for the transform matrix, and denotes the Daubechies wavelet scaling function collection. While for an arbitrary two-dimensional wavelet-based finite element, the shape functions are given as

$$N = N_x \otimes N_y \tag{12}$$

Where $\otimes$ is Kronecker symbol, N_x and N_y are the shape functions in the horizontal (x) and vertical (y) directions, respectively.
After constructing wavelet-based shape functions, the procedures of construction of the stiffness matrix K_e and the mass matrix M_e can be achieved as in the traditional FEM. The forms of both matrixes are represented as:

$$\begin{aligned} K_e &= \int_{\Omega} (LN)^T D(LN)\, dxdy \\ M_e &= \int_{\Omega} \rho N^T N\, dxdy \end{aligned} \tag{13}$$

where L and D denote the generalized strain and the elasticity matrix, respectively and finally is the beam density. The superscript T stands for the transpose of a matrix or a vector. For the model is used a uniform beam with an open crack located at $\beta = e/L$ (Fig. 6).

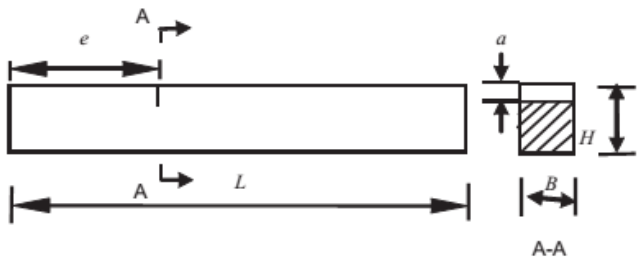

Fig. 6 – Beam model

L, H, and B represent the length, height and width of the beam, respectively. e and a are the crack location and crack size, respectively. ☒ and ☒ stand for the normalized crack position and normalized crack size, respectively.
Suppose that the crack is located between two wavelet-based finite elements, and the numbers of two nodes are Le and Ri, respectively (Fig. 7). The crack introduces a local flexibility that is a function of the crack depth, the flexibility changes the stiffness of the beam. Also in this case, as usual, the crack is represented by a massless rotational spring with a computable stiffness K_t.

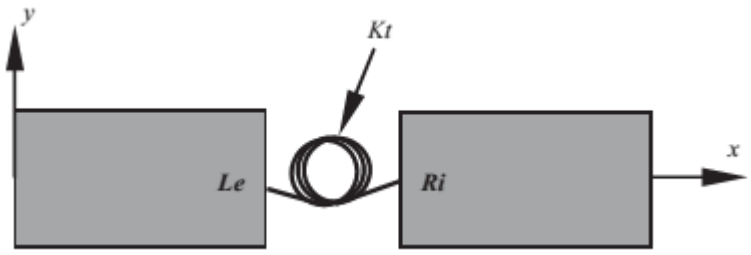

Fig. 7 – Model used to describe the crack

The continuity conditions at the crack position indicate that the left and right nodes have the same vertical deflection, while their rotations are connected through the stiffness matrix K_c

$$K_c = \begin{bmatrix} K_t & -K_t \\ -K_t & K_t \end{bmatrix} \tag{14}$$

Hence, we can assemble K_c into the global stiffness matrix, K, through employing a single dof of the vertical deflection of both nodes Le and Ri. The global mass matrix of cracked beam is equal to the uncracked. Using the displacement-based formulation in conjunction with the principle of virtual displacement, the equations of the beam motion can be then written as:

$$MY + K\ddot{Y} = 0 \tag{15}$$

Supposing that a time harmonic solution for the nodal displacements can be represented as

$$Y = A \sin \omega_i t \tag{16}$$

where A is the amplitude of the nodal displacements. This leads to

$$[-\omega_i^2 M + K]\{A\} = 0 \;\rightarrow\; \det(K - \omega_i^2 M) = 0 \tag{17}$$

Finally, the effective values of the natural frequencies can be found through solving generalized eigenvalues of last equation written.

1.3.1 Crack identification methods

Since the crack location and the crack size influence the changes in the natural frequencies of a cracked beam, a particular frequency can correspond to different crack locations and crack sizes. This can be observed from three-dimensional plots of the first three natural frequencies of the free–free beam (Fig. 8). On this basis, a contour line, which has the same frequency resulting from a combination of different crack locations and crack sizes (for a particular mode) can be plotted in a curve with crack position and crack size as its axes.

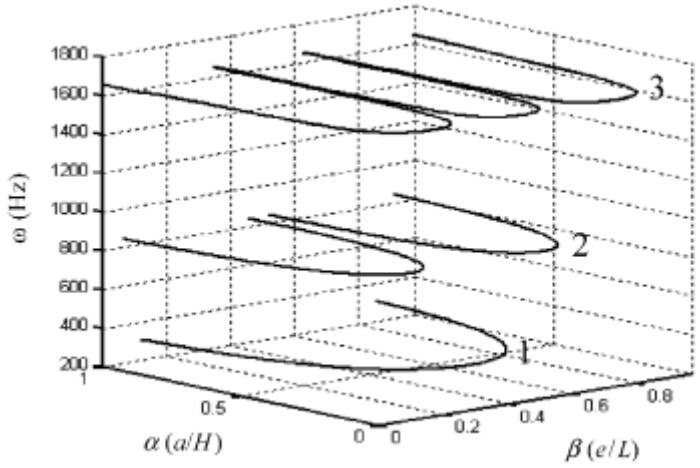

Fig. 8 – First three natural frequencies of the free–free beam

The development of a crack, at a certain location, corresponds to a sudden reduction of the bending stiffness of the beam, and furthermore leads to a shift of the natural frequency. The inverse problem of the crack identification is to predict the location β and depth α of a crack once the value of natural frequencies ω_i is measured.

$$(\alpha, \beta) = g_i(\omega_i) \tag{18}$$

If the crack coincides the vibration node of one mode, the frequency for that mode remains almost unchanged. Therefore a minimum of three curves is required to identify the two unknown parameters of crack location and size.

1.3.2 Experimental verification

Test specimens were steel beams with $0.032 \text{ x } 0.016\ m^2$ rectangular cross-section and 0.72m long. The corresponding material properties were:

$$\text{E} = 206 \text{ GPa}, \qquad \nu = 0.29, \qquad \rho = 7650 \text{ kg}/m^3$$

The crack in each beam was simulated by a cut normal to the beams' longitudinal axis, with a controlled depth. In order to avoid the nonlinear characteristics of an opening and closing crack, the thickness of the cut was carefully defined, taking into account that both sides of the crack were not supposed to make contact during the dynamic bending of the beam.
To have better results, it is also studied the correction of Young's Modulus, infact the evaluation of the natural frequencies through the characteristic equation of the free–free beams requires the knowledge of the material properties. Quoted values of Young's modulus are not sufficiently accurate for this purpose. The problem can be overcome by an iterative approach, which uses the undamaged natural frequencies of the beams to determine an effective value of the Young's modulus E.

$$\det\left(\omega_i^2 M - E_m \frac{K}{E}\right) = 0 \tag{19}$$

where E_m is the corrected value of Young's modulus E. It should be noted that the physical significance for the correction of Young's modulus E is not to change the value E, but to narrow the error between the numerical model and real-life situation. In fact, this is a zero setting procedure.

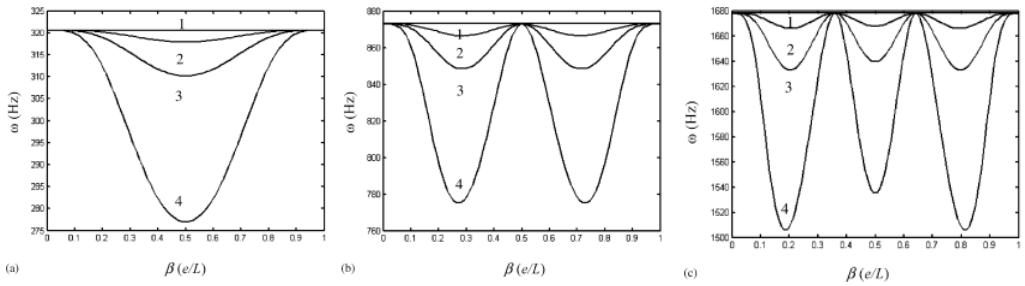

Fig. 9 – Variations of the first three natural frequencies vs crack size

Tab. 1 – Results from WFEM and FEM obtained

Crack Case	Natural frequencies (Hz)					
	WFEM (Error %)			FEM (Error %)		
	Mode 1	Mode 2	Mode 3	Mode 1	Mode 2	Mode 3
1	315.8(0.06)	859.0(0.05)	1648.9(0.01)	315.8(0.06)	860.6(0.14)	1657.3(0.50)
2	316.0(0.03)	857.9(0.01)	1636.6(0.25)	316.0(0.03)	859.4(0.19)	1644.5(0.74)
3	316.8(0.06)	852.8(0.16)	1607.7(0.89)	316.8(0.06)	854.2(0.33)	1614.5(1.32)
4	313.1(0.03)	833.1(0.79)	1539.1(1.59)	313.1(0.03)	834.3(0.93)	1544.0(1.91)
5	316.0(0.03)	855.8(0.07)	1648.0(0.03)	316.0(0.03)	857.4(0.26)	1656.5(0.55)
6	314.5(0.13)	842.0(0.17)	1627.1(0.04)	314.5(0.13)	843.4(0.32)	1635.1(0.53)
7	310.2(0.45)	813.4(1.02)	1588.2(0.49)	310.2(0.45)	814.5(1.15)	1595.6(0.96)
8	307.7(0.75)	866.3(0.47)	1563.2(1.90)	307.7(0.75)	782.0(10.16)	1570.0(2.35)
9	311.5(0.06)	851.0(0.33)	1645.6(0.05)	311.5(0.06)	852.5(0.15)	1654.2(0.47)
10	307.7(0.20)	843.4(0.12)	1651.7(0.01)	307.7(0.20)	844.9(0.30)	1660.2(0.53)
11	298.4(0.74)	828.4(0.41)	1656.5(0.06)	298.4(0.74)	844.9(0.58)	1665.0(0.03)
12	290.9(4.27)	812.8(0.94)	1674.1(0.13)	290.9(4.27)	814.0(1.09)	1682.5(0.63)
13	314.0(0.32)	862.8(0.05)	1647.9(0.15)	315.0(0.64)	839.7(2.72)	1552.9(5.63)
14	305.6(0.86)	859.4(0.05)	1615.1(0.54)	305.6(0.86)	861.0(0.14)	1622.7(1.01)
15	294.5(1.03)	865.8(0.02)	1582.1(0.51)	294.5(1.03)	867.4(0.16)	1588.7(0.93)
16	277.0(4.49)	873.0(0.02)	1534.8(2.46)	276.9(4.45)	874.6(0.16)	1540.1(2.81)

In order to obtain natural frequencies with high accuracy, the wavelet finite element analysis is performed. Must be noted that using fewer wavelet-based finite elements is possible to obtain higher analytical accuracy. The result of the WFEM and FEM is tabulated in Table 1.
The investigation leads to understand that there is a correlation between the variations of the first three natural frequencies with crack size for some of the crack locations of a free–free beam. (see Fig. 9)

1.3.3 Conclusions

The methods leads to good results, the predicted crack positions and crack sizes are in good agreement with the actual values. The average error of crack locations without E correction is 11.64%. While the average error of crack locations with E correction is 2.65%. The average error of crack sizes without E correction is 22.1%. While the average error of crack sizes with E correction is 5.62%.
Through an approach for Young's modulus correction, the error between theoretical analysis and experimental studies, which are caused by boundary condition and material parameters, can be greatly reduced. Experimental results verify that the present method can be utilized to detect crack location as well as crack size. The procedure for detection of crack is simple and general. It is believed that this procedure can be easily extended to complex structures, such as rotor, blade, etc. with multiple cracks.

1.4 Free vibration behaviour of a cracked cantilever beam

Understanding the vibration behaviour of a simple structural element containing a single crack is the first step towards diagnosing damage on more complex structures. This study [4] is based on cracks that occurred in metal beams obtained under controlled fatigue-crack propagation. The beams were clamped in a heavy vise and struck in order to obtain a clean impulse modal response. Spectrograms of the free-decay responses showed a time drift of the frequency and damping: the usual hypothesis of constant modal parameters is no longer appropriate.
Extracted worms show that the second mode of a beam with a deep crack is modulated in frequency by the first mode. In fact, the dominant mode opens and closes the crack, thereby modulating the beam stiffness, which affects higher modal frequencies. The first state is difficult for a small crack to reach since high-amplitude excitation is required to fully open the crack.
One of the main focus on this paper is about the assumption of the crack as always open, in many other works this was the main hypothesis, in this case the author tries to explain why it's not correct to use that case.
Narrow slots cannot exhibit the behaviour of a crack in metallic structures for many reasons:

- A mechanical slot has a measurable width which prevents any interaction between the two faces of the slot. In such cases, the slot behaves as a hinge. It closes under a negative load and is already open at zero load. However, interactions between crack faces are possible and do in fact occur, resulting in event that is known as crack closure effects (Fig. 10).

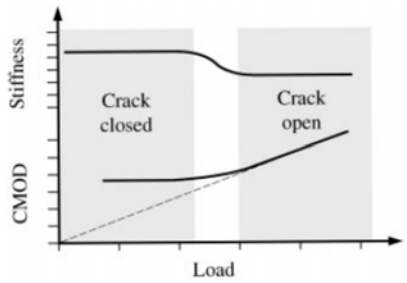

Fig. 10 – Crack behaviour influenced from external load

A cracked beam will exhibit the static behaviour of an uncracked beam until the applied load is sufficiently high to overcome the closure load.

Consequently, the opening force generated by the vibration must be greater than this load in order to fully open the crack (Fig. 11).

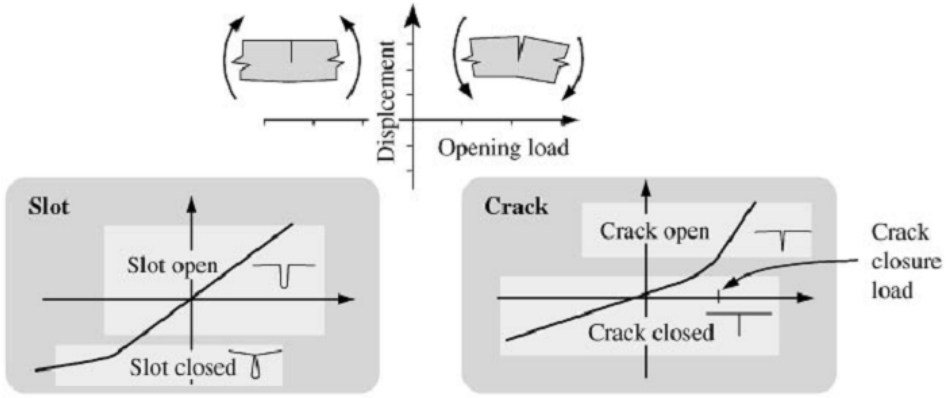

Fig. 11 – Crack behaviour

- The roughness of the fracture surface, corrosion debris in the crack, plastic deformation left in the wake of a propagating crack, strain-induced phase transformation in the fatigue process zone and hydraulic wedging produced by oil trapped in the crack are all phenomena leading to crack closure. Moreover, these phenomena can play a role in the vibration damping.
- A crack can be only partially open with an appropriate strain distribution. Consequently, the free-decay response of a cracked beam exhibits three consecutive vibrational states: fully open to closed, partially open to closed and remaining closed. On the other hand, a slot generates two vibrational states: open to closed and remaining open (see Fig. 12).

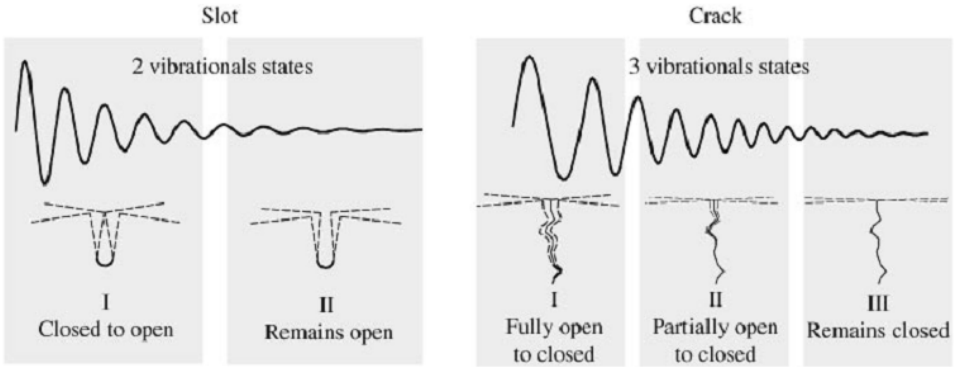

Fig. 12 – Vibrational states

The target is a match between modelling and experimental measurements. On the one hand, better crack modelling must include non-linear stiffness, hysteresis effects and a damping function of the crack opening. Some of the usual modal-analysis hypotheses are no longer valid with a real crack.
Almost all crack diagnosis algorithms based on dynamic behaviour call for a reference signature. In fact, these algorithms fail when the reference signature is not available, is not taken in the same operating condition or is not measured on an identical structure. Many algorithms are based on a modal shape, a frequency or a damping shift, and are not accurate enough to detect early cracks with a small relative cross-section less than 10%. These algorithms cannot work without a previous reference signature. This paper proposes a few new ways to detect cracks without using a reference signature.
For the experiments, beams of square cross-section (2.5 cm x 2.5 cm), 24.5 cm long, were machined from an AISI 4340 steel plate. A semi-circular groove 0.2 cm deep was machined around the beam, 7.5 cm from one of its extremities, to keep the crack straight.

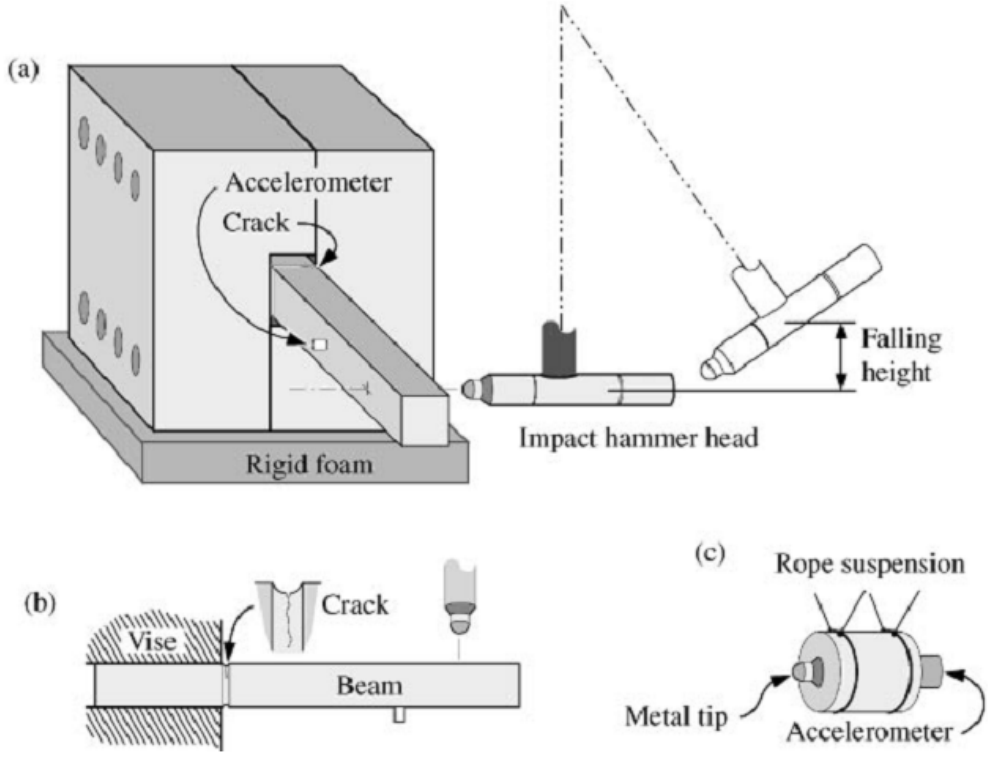

Fig. 13 – Experimental setup

The fatigue cracks were produced by cycling in pure bending (four-point bending fixture) in lab air (30-40% RH), at low frequency (1-5 Hz) on a servo hydraulic 100-kN-capacity testing rig.
An impact hammer with a known fall height generates an excitation centred on the neutral axis of the beam in order to minimise torsional vibration (Fig. 13).
The repeatability of the clamping device and the measurement set-up was tested by mounting, measuring and dismantling the uncracked beam 10 times. The first and second modes had a frequency of 660.60 ± 0.02 and 3536.31 ± 0.11 Hz, respectively, with a 30-ppm or 0.003% standard deviation.
For both modes, the damping ratio estimates had less than 1% dispersion between consecutive mountings: the damping ratio appeared more sensitive than the frequency. The overall repeatability was good enough to superimpose the time traces for many milliseconds for different mountings.
The observed frequency and damping behaviour are similar to those reported by other authors: the frequency drops and damping increases with crack depth as illustrated in Fig. 14 for the first two modes. Note that a small crack induces small frequency and damping shifts between measurements taken on the cracked specimen and the reference specimen. As illustrated in Fig. 15, the beam oscillates in period T1 when the crack is closed and in period T2 when the crack is open. Since the stiffness decreases when the crack is open, T2 is larger than T1 and increases with crack depth along with its statistical occurrence. Modal damping also appears as a function of the crack depth. The damping behaviour is quite complex and decreases with crack depth in some cases.

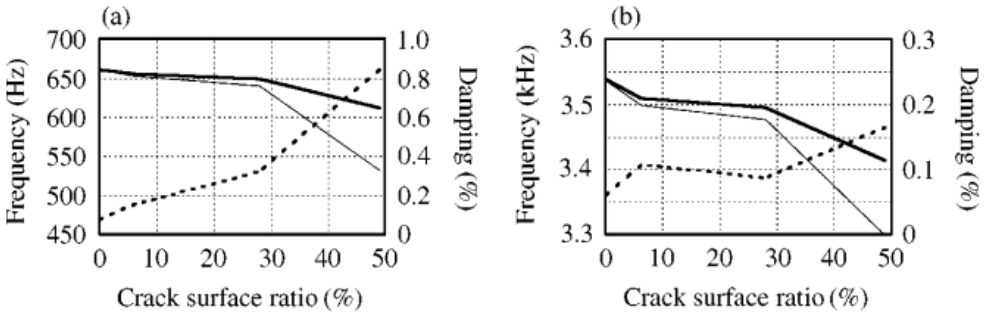

Fig. 14 – Influence of crck depth on damping

The time drift of the modal frequency is also explained by the existence of two periods, as illustrated in Fig. 16. Observe in Fig. 11 that the crack closure load moves up the elbow on the transfer function. At high motion amplitude, the mean

frequency is a function of the two periods. With the decreasing amplitude present in a free-decay response, period T1 gradually dominates statistically.

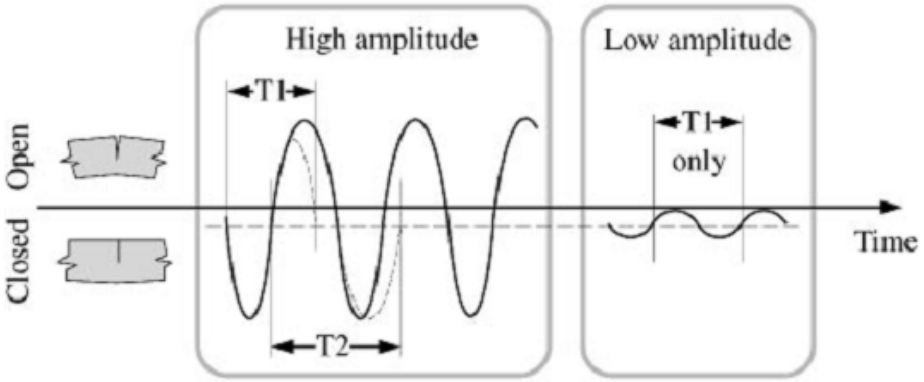

Fig. 15 – Influence of the crack on periodic oscillation

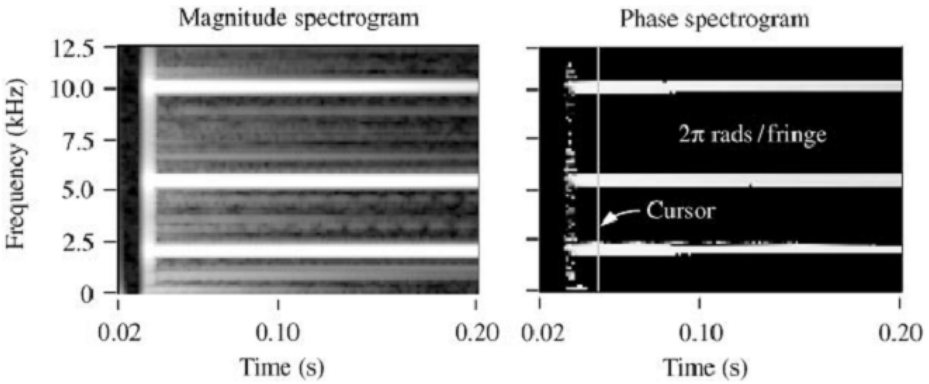

Fig. 16 – Phase spectrogram

The magnitude of the short-time fast Fourier transform (STFFT) is defined as a spectrogram. The right portion of Fig. 16 shows the phase spectrogram of a suspended uncracked beam to illustrate a constant phase (frequency) behaviour. The sensitivity of the phase spectrogram is a function of the single/noise ratio and inter-modal frequency distance. Phase spectrograms have revealed that every structure shows a time drift behaviour of the modal frequency in its free-decay response. The amplitude of the behaviour is a function of the geometry and the material.

Analysis

Spectrograms are based on the Fourier transform, which models the signal as a sum of constant amplitude and frequency sines. The corresponding signal model has only three degrees of freedom: amplitude, phase and frequency. When the amplitudes and

frequencies are no longer constant over the spectral window, the Fourier transform yields inaccurate results. To overcome this limitation, a sinusoid extraction algorithm was developed using a model with seven degrees of freedom.
The term “worm transform” has been used to describe this algorithm because the modulated sinusoid was extracted ring by ring and the rings then linked together to obtain a continuous time function for both amplitude and phase.
Fig. 17 presents the time-frequency free-decay response for the two first bending modes of the beam with the deepest crack.

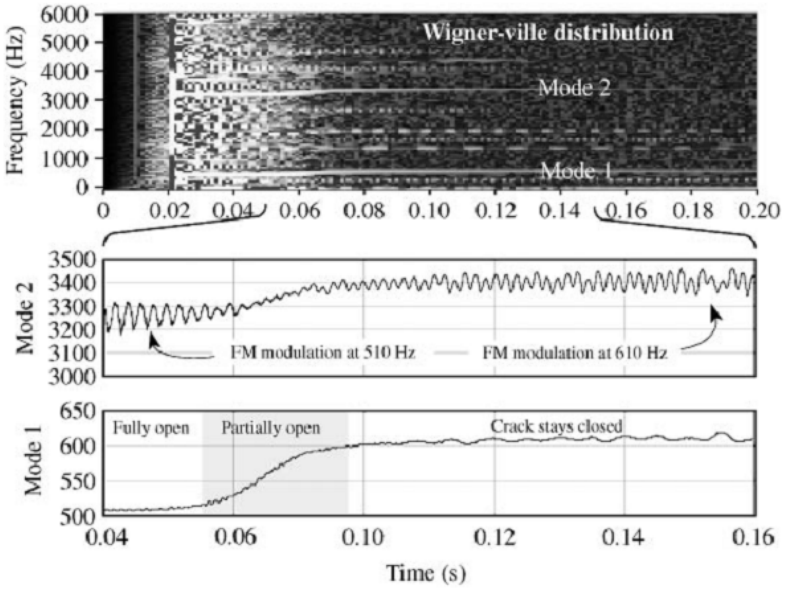

Fig. 17 – Time-frequency free-decay response

The modal frequencies extracted by worm transform are a good illustration of how the second mode of a cracked beam is modulated in frequency by the "rst mode. The mode with the dominant amplitude opens and closes the crack, thereby modulating the beam stiffness and affecting high-order instantaneous modal frequencies and amplitudes. Three vibration states are easy to observe on a deep crack beam: one where the crack is alternately fully open and fully closed, a second with a crack partially open, and a third with an alternating force acting on a closed crack. High harmonic contents characterise the first state.
In the third state, the crack stays closed, since the peak force is smaller than the crack's intrinsic closure load. However, the modulating force acts on closed-crack widths, thus modulating the crack stiffness and the second mode frequency.
The behaviour can be described on the basis of two time scales: on a large scale, the mean stiffness determines the average modal frequency while, on a small scale, the

instantaneous stiffness modulates the modal frequency. The dominant mode, which opens and closes the crack, is affected only by the mean stiffness, whereas high-order mode frequencies follow the instantaneous stiffness.
It should be noted that a mode might have more than one frequency component at the same time; for example, in the first state, the first bending mode of a cracked beam must include its visible harmonics on a spectrogram. Actually, this mode is a distorted sinusoid, since the crack opens and closes synchronously with the sinusoid from the modal motion. On the opposite side of the record, when the amplitude is not enough to allow crack breathing, the first mode can be described by one frequency component because the corresponding sinusoid is not distorted.

Amplitude-dependent modal damping

In general, the classical damping ratio must be carefully used to characterise a non-linear system since the related viscous damping hypothesis and uncoupled modes are no longer valid. It is worth noting that most of the present-day modal software is designed in terms of fitting constant modal frequencies rather than an amplitude-dependent frequency mode.
The peak/rms ratio is proposed as being a simple tool better designed to globally characterise ADMD. Note that the peak/energy ratio yields a similar result.
When beam #2 is struck with a screwdriver, the human ear perceives a diminishing sound amplitude with an increasing impact force around 1 kN: with increasing impact force the clear tonality becomes a short low-frequency damped noise. The impact amplitude also influences the modal amplitude distribution. This variation is explained, on the one hand, by a modal excitation efficiency, which is a function of an impact point *vs* modal shape, and a modal shape, which is a function of the vibration state. On the other hand, after a few milliseconds, the modal amplitude is also a function of the modal damping, itself a function of the vibration state (Fig.18).
The instantaneous damping modulation can be explained by crack breathing as follows:

- When fully open, a crack acts like a hinge and contributes slightly to structure damping.
- When partially open, a crack crushes the crack surface oxidation by-products and dust, breathes air and trapped oil in and out and in this way increases the damping.
- When fully closed, a crack has little effect on the structure damping.

The highest damping value occurs when a dominant mode partially opens the crack, allowing the higher-order modes to open and close the crack.

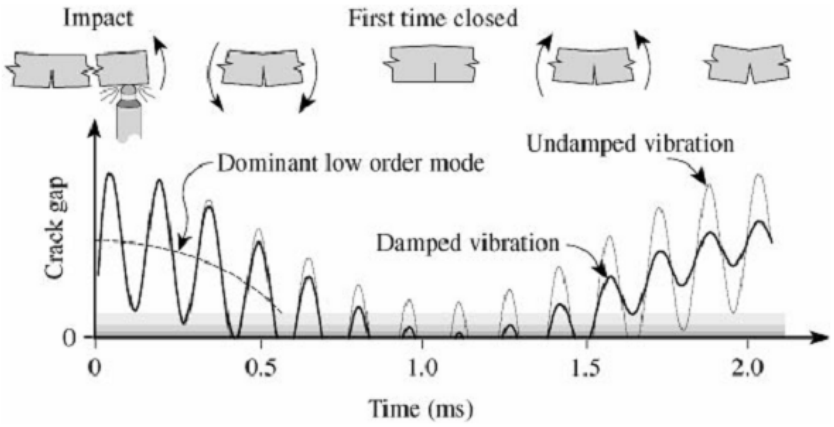

Fig. 18 – Influence on modal amplitude distribution

It is concluded that lower-order modes are a!ected by the average damping corresponding to crack states whereas high-order modes react instantaneously to the damping modulated by crack breathing. The resulting global damping is a fairly complex function of excitation and time.

1.4.1 Crack detection

Criteria based on damping, harmonic distortion, the bispectrum, the frequency spectrogram and the coherent modulated power were tested.
Since the non-linear behaviour of a crack is accentuated in the first vibration state, an appropriate impact force is needed to fully open the crack. Smaller cracks, however, call for a higher impact force yet high impact amplitude may damage the structure and also generate non-linear components on an uncracked structure. Whatever the technique used, detection of small cracks is therefore usually restricted to the measurement of the third vibrational state.
The harmonic distortion criterion can easily detect a crack if enough record length is provided in the first vibrational state. When a strong impact is not possible without damage, the second and especially the third vibrational states do not generate enough distortion to allow detection of a small crack.
Tests were also performed with a bispectral transform from which the auto-bicoherence yields better results than the auto-bispectrum. It was found that bispectral transform has limited success on beam #1, it is thought to be due to:

- the spread of high-order spectral components due to frequency drifts;
- high-frequency components whose amplitude is greater for the uncracked beams;
- more frequency components present on uncracked beam due to high damping of cracked beam that has wiped off many frequencies;
- non-linearity of the measurement apparatus itself.

Finally crack-detection accuracy is defined by the product of the accuracy of the frequency estimate and the ratio of the 'crack length' over the 'corresponding frequency drift'.

1.4.2 Conclusions

A cantilever beam with a fatigue crack shows a modal behaviour dependent on the vibration state of the crack opening. When the amplitude allows full opening, the amplitude-dominant mode generates harmonics and modulates the higher-order modes. With the crack partially open, the damping reaches its highest value for most modes. When the tvibration amplitude decreases and becomes too small to open the crack, many modal frequencies increase and modal damping diminishes. Consequently, the modal frequencies, modal damping and amplitude distribution between modes are all a function of the
excitation amplitude, this also reduces the repeatability of measurements.
The frequency spectrogram and a criterion based on the coherent power of amplitude modulation have detected fatigue cracks with a 6.2% surface ratio.

1.5 Crack detection based on the anti-resonance technique

In this paper is presented an alternative technique for crack detection in a Timoshenko beam based on the first anti-resonant frequency [5].
In order to characterize the local discontinuity due to cracks, a rotational spring model based on fracture mechanics is proposed to model the crack. Subsequently, the proposed method is verified by a numerical example of a simply-supported beam with a crack. The effect of the crack size on the anti-resonant frequency is investigated. The position of the crack of the simply-supported beam is also determined by the anti-resonance technique. The proposed technique is further applied to the "contaminated" anti-resonant frequency to detect crack damage, which is obtained by adding 1-3% noise to the calculated data.

The crack of the beam is assumed to be open, and with a uniform depth in width. The length, height and width of the beam are *L*, *H* and *B*, respectively. And there is a crack at a distance L_c from the left end of the beam, as shown in Fig. 19.
In the analysis, a steel beam is considered, thus, the influence of material damping on the resonant frequencies is ignored, and only bending vibrations are considered.

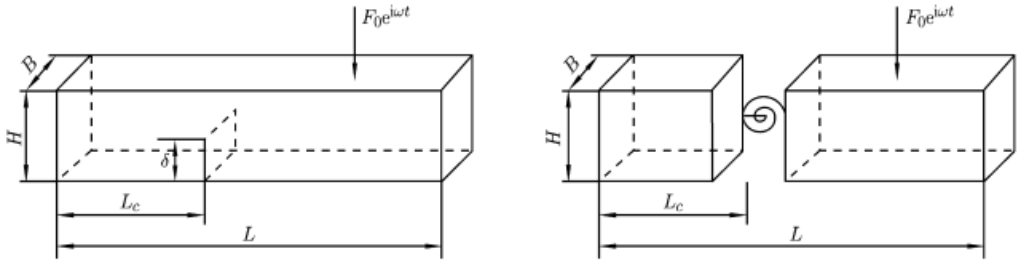

Fig. 19 – Beam model

The stiffness of the rotational spring can be denoted as:

$$K_T = \frac{1}{c} \qquad c = \frac{5.346H}{EI} f(s)$$

$$f(s) = 1.862s^2 - 3.95s^3 + 16.37s^4 - 37.226s^5 + 76.81s^6 - 126.9s^7 + 172s^8 - 43.97s^9 + 66.56s^{10} \tag{20}$$

where *c* is the local flexibility due to a crack, *f(s)* is the non-dimensional local compliance function, $s = \delta/H$, is the relative crack depth, δ is the depth of the crack. Each segment of the beam separated by the crack and the applied force can be viewed as an individual component, and the dynamic equation governing the flexural vibration of each segment of the beam is:

$$\kappa AG = \left(\frac{\partial^2 W_i}{\partial x^2} - \frac{\partial \phi_i}{\partial x}\right) = \rho A \frac{\partial^2 W_i}{\partial t^2} \tag{21}$$

$$EI \frac{\partial^2 \phi_i}{\partial x^2} + \kappa AG \left(\frac{\partial^2 W_i}{\partial x^2} - \phi_i\right) = \rho I \frac{\partial^2 \phi_i}{\partial t^2} \qquad i = 1,2,3 \tag{22}$$

where κ is the shear correction factor, *G* is the modulus of rigidity of the materials, Φ is the slope of the deflection curve due to bending deformation, *W* is the flexural

displacement and the beam has a constant cross-section area *A* and area inertia *I*. Its material properties, Young's modulus *E* and mass density ρ, are also constant.
After some demonstrations, the use of separation of variables and the introduction of boundary conditions it can be found that the vibration solution to each equation can be depicted as follows:

$$w_i = A_i cosh(\alpha_1\beta) + Bsinh(\alpha_1\beta) + C_i cos(\alpha_2\beta) + D_i sin(\alpha_2\beta) \quad (23)$$

$$\phi_i = m_1 A_i Sh(\alpha_1\beta) + m_1 BCh(\alpha_1\beta) - m_2 C_i sin(\alpha_2\beta) + m_2 D_i cos(\alpha_2\beta) \quad (24)$$

To calculate the mechanical impedances of the cracked Timoshenko beam is considered that the driving-point impedance at an arbitrary position x along the beam length can be derived according to the expression

$$Z(x) = \frac{F_0}{j2\pi f\omega(x)} \quad (25)$$

where *j* is the unit of an imaginary number, *w(x)* is the corresponding displacement and *f* is the frequency.
The crack identification procedure follows these steps.

1. The cracked beam is excited by a harmonic force with wide scanning frequencies, and the driving force is moved from the left end to the right end of the beam. At the same time, the mechanical impedance at each driving point location is measured, which can be computed numerically according to the previous equation, and some graphs describing the mechanical impedance characteristics are given.
2. The first anti-resonant frequencies are extracted from the graphs, and a figure correlating the first anti-resonant frequency with the driving point location along the beam is plotted. A discontinuity in the figure is seen, which corresponds to the crack of the beam. Thus, the crack of the beam is identified by monitoring the presence of the discontinuity.

1.5.1 Analysis

In order to demonstrate the validity of the technique proposed in the above section, a numerical example of a simply-supported beamwith a crack is presented.

In the example, the steel beamgeometries and material properties are as follows: length = *1 m*, height = *0.2 m*, width = *0.2 m*, Young's modulus $E = 210\times109\ Pa$, shear modulus $G = 79\times109\ Pa$, $\kappa = 0.85$, and density $\rho = 7860\ kg/m3$. The crack is located at *0.3 m* from the left end of the beam, which was stimulated by the harmonic force *10 N*.

The mechanical impedances under several cracked beam scenarios are presented in comparison with those of the intact beam scenario in Fig. 20.

From Fig. 20 it is found that the presence of a crack induces the reduction of the resonant frequency and the anti-resonant frequency of the Timoshenko beam, and with an increase of crack depth both the first resonant frequency and the first anti-resonant frequency decrease gradually.

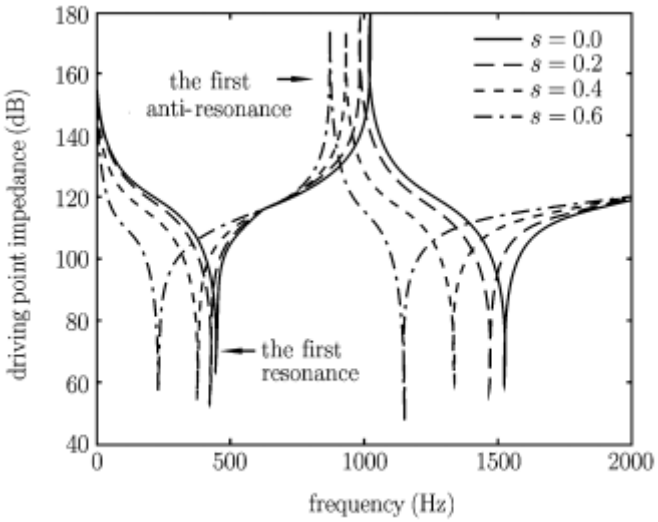

Fig. 20 – Variation of mechanical impedance vs depth of the crack.

In this paper, the effects of the driving point location on the mechanical impedance of the simply supported Timoshenko beam are also investigated. Fig. 21, indicates the variation of mechanical impedance with the variation of the force location in the case of the intact beam (a) and those in the case of cracked beam with a crack located somewhere at 0.3 m from the left end of the beam (b). It can be found that when the driving force moves from an end to near the midpoint of the beam, the first natural frequency remains constant, whereas the first anti-resonant frequency increases and approaches the second natural frequency gradually, and the magnitude of the fist anti-resonance decreases more quickly in the case of a cracked beam than in the case of the intact beam.

The crack of the beam will be located using the first anti-resonant frequency information, which is extracted from the mechanical impedance graphs corresponding to different driving points. Must be noted that, when a crack in the simply-supported beam is presented, the decrease of the first anti-resonant frequency is much larger with the Euler beam theory applied than that with the Timoshenko beam theory applied.
The study shows that the peak value of the first anti-resonant frequency curves decreases as the depth of the crack increase in the case of different cracked beam scenarios and the driving point location corresponding to the peak value is no longer just in the midpoint of the beam, but excursive from the midpoint. When the driving force goes through the midpoint and approaches the right end, the first resonance frequency decreases gradually.

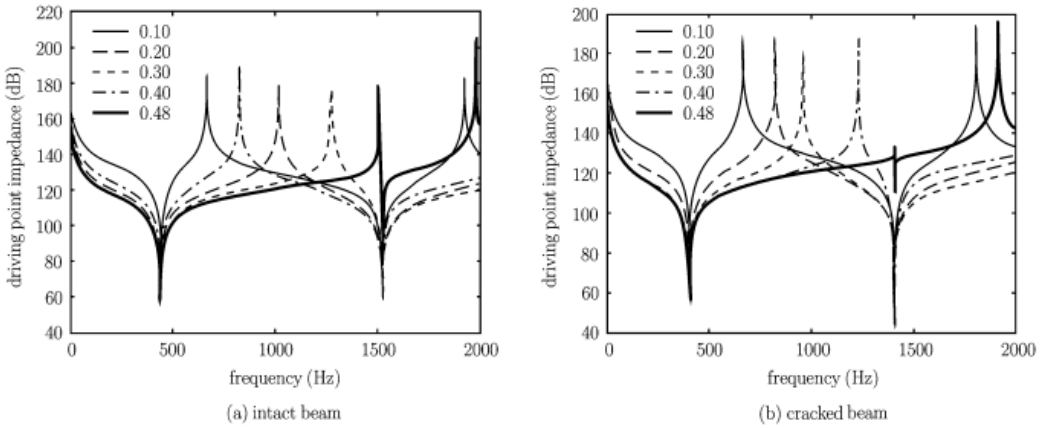

Fig. 21 – Variation of mechanical impedance vs force location

The most important finding, however, is that the curves corresponding to different cracked beam cases show some discontinuities at the position *0.3 m* from the left end of the cracked beam. It seems that the discontinuity indicates the appearance of the crack damage and the predicted crack location is coincident with the assumed crack location. It is also found that as the depth of the crack increases, the discontinuities become more accentuated.
Fig. 22 shows the changes in the first anti-resonant frequency curves with the variable depths of the beam crack under 1% and 3% noise cases. From this figure can be noted that the beam crack can be located, this verifies the robustness of the proposed crack identification technique.

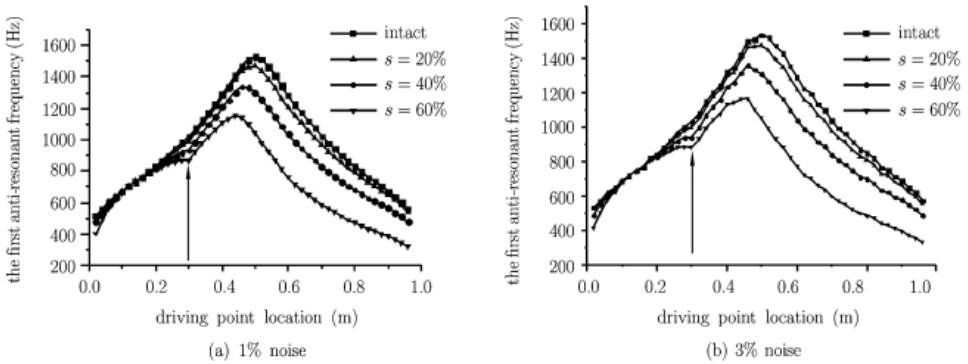

Fig. 22 – The first anti-resonant frequency with variable depths of the crack

To verify the proposed crack identification method an experiment on a steel beam has been performed. In this experiment, a 384 mm long steel beam of rectangular cross-section $18 \times 13\ mm^2$ was simply supported at a steel support.

A crack of relative crack depth 60% was introduced at a distance of 286 mm from the left end of the beam. Harmonic excitation was used via a vibrator and the driving force was kept constant and was shifted in steps from the left to the right end of the beam. Based on the first anti-resonant frequencies extracted, the curves of the first anti-resonance versus driving point location were plotted in intact and cracked beam cases. The experimental results are coincident with the calculated results in intact and cracked beam cases. The calculated results showed that in the thin beam example the effects of different beam theories on the first anti-resonant frequency were quite small. It has also been found that the presence of 60% crack damage induced the notable decrease of the first anti-resonant frequency and a discontinuity occurred at a distance of about 280 mm from the left end of the steel beam, which corresponds to the location of crack in the steel beam (Fig. 23).

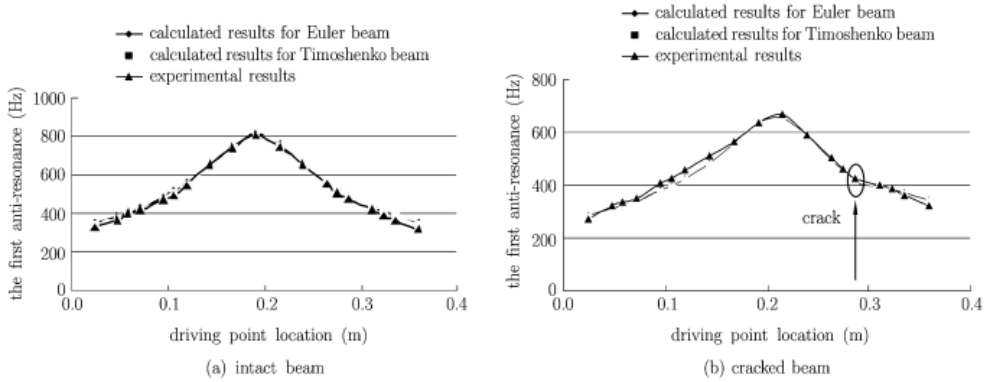

Fig. 23 – Experimental and calculated results for the first anti-resonance

1.5.2 Conclusions

The work shows that the presence of the crack will induce the changes in the mechanical impedance characteristics of the beam. At one time, the first anti-resonant frequencies and the first resonant frequencies also decrease. In addition, since the anti-resonant frequency is a local parameter, it can be used as important information for crack localization.
The numerical results show that when a crack occurs in the beam, the curve of the first anti-resonant frequency versus driving-point location will not be smooth but show discontinuity at the crack position, and the degree of the discontinuity depends on the depth of the crack. It is also concluded that the proposed technique for crack identification in a Timoshenko beam is robust to the measuring noise.

Chapter 2 A NEW APPROACH

Before introducing the new approach for crack identification, it is important to understand completely the theory behind the principle, in particular all the aspects involved in description of continuous system behaviour.

The analysis of a continuous system could be seen as the analysis of a *n gdl* discrete system with *n* that tends to ∞. The problem is to analytically realize this formal passage, indeed for continuous systems, equation of motion are in the form of PDE because depends from both space (*x,y,z)* and time (*t)*. All real systems should be studied as continuous systems but apart from the most simple cases, analytical solution could not be obtained using the continuous approach. In this cases it is indispensable the use of discrete methodology as the FEM analysis to solve the problem.

The study carried out on continuous systems is important and form the base for the method of crack identification developed in this thesis. For this purpose, we will limit the study on a single and simple case that could be treated analytically in closed-form. The case is relative to bending vibration of beams.

A beam is typically described as a structural element having one dimension (length) which is many times greater than its other dimensions (width and depth). It may be straight or curved. Beams are one of the most fundamental structural and machine components. Almost every structure or machine one can think of has one or more beam components. Buildings, steel framed structures, and bridges are examples of beam applications in civil engineering. In these applications, beams exist as structural elements or components supporting the whole structure. In addition, the whole structure can be modelled at a preliminary level as a beam. For example, a high-rise building can be modelled as a cantilever beam, or a bridge modelled as a simply supported beam. In mechanical engineering, rotating shafts carrying pulleys and gears are examples of beams. In addition, frames in machines (e.g., a truck) are beams.

Robotic arms in manufacturing are modelled as beams as well. In aerospace engineering, beams (curved and straight) are found in many areas of the aircraft or space vehicle. In addition, the whole wing of a plane is often modelled as a beam for some preliminary analysis. Innumerable other examples of beams exist.

In many of these applications, beams are subjected to dynamic loads. Imbalance in driveline shafts, combustion in crank shaft applications, wind or earthquake on a bridge or a structure, and impact load when a vehicle goes over a bump are

all examples of possible dynamic loadings that beam structures can be exposed to. All of these loads and others can excite the vibration of the beam structure. This can cause durability concerns (because of potentially excessive dynamic stresses) or discomfort because of the resulting noise and vibration.
The first part of this chapter will be dedicated to the explanation of the main principles of the new method for crack identification successively entering in the detail about an argument that formed the base of the algorithm developed during this work that is the study of transverse vibrations of beams. The equations of motion will first be derived. Solutions are then found and discussed for the natural frequencies and mode shapes of various boundary conditions using exact methods.
As studied in the first chapter of this paper, it is easy to understand that although there are several known ways to identify a crack they all have positive or negative aspects to be considered. The main goal this work is the develop a new method that must be advantageous in terms of costs and above all repeatable and efficient. Before entering in the details of the method it is useful to recall some theory principle on which it is based like *Modes of Vibration* and *Nodes.*

2.1 Modes of vibration

Any complex body (i.e. more complicated than a single mass on a simple spring) can vibrate in many different ways. I.e., there is no one "simple harmonic oscillator". These different ways of vibrating will each have their own frequency, that frequency determined by moving mass in that mode, and the restoring force which tries to return that specific distortion of the body back to its equilibrium position.
It can be somewhat difficult to determine the shape of these modes. For example one cannot simply strike the object or displace it from equilibrium, since not only the one mode liable to be excited in this way. Many modes will tend to excited, and all to vibrate together.
The shape of the vibration will thus be very complicated and will change from one instant to the next. However, one can use resonance to discover both the frequency and shape of the mode. If the frequencies of the modes are different from each other, then we know that if we jiggle the body very near the resonant frequency of one of the modes, that mode will respond a lot. The other modes, with different resonant frequencies will not respond very much. Thus the resonant motion of the body at the resonant frequency of one of the modes will be dominated by that single mode.
Doing this with strings under tension, we find that the string has a variety of modes of vibration with different frequencies. The lowest frequency is a mode where the

whole string just oscillates back and forth as one with the greatest motion in the center of the string (Fig. 24).

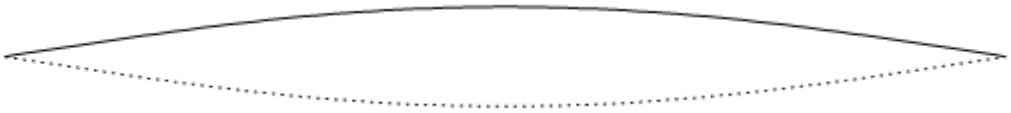

Fig. 24 – First mode of vibration

The diagram gives the shape of the mode at its point of maximum vibration in one direction and the dotted line is its maximum vibration in the other direction.
If we increase the frequency of the jiggling to twice that first modes frequency, we get the string again vibrating back and forth, but with a very different shape. This time, the two halves of the string vibrate in opposition to each other. As one-half vibrates up, the other moves down and vice versa (Fig. 25).

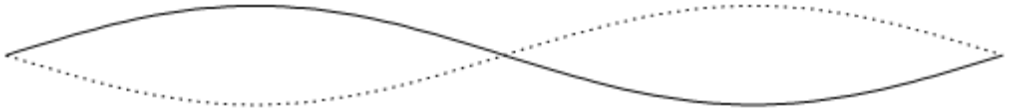

Fig. 25 – Second mode of vibration

Again the diagram gives the shape of this mode, with the solid line being the maximum displacement of the string at one instant of time, and the dotted being the displacement at a later instant (180 degrees phase shifted in the motion from the first instant).
If we go up to triple the frequency of the first mode, we again see the string vibrating a large amount– i.e. at the resonant frequency of the so-called third mode. In this case, the string is divided into three equal length section, each vibrating in opposition to the adjacent piece (Fig. 26).

Fig. 26 – Third mode of vibration

As we keep increasing the jiggling frequency, we find at each whole number multiple of the first modes frequency another mode. At each step up, the mode gets an extra

"hump" and an extra place where the string does not move at all. Those places where the string does not move are called the *nodes* of the mode. Nodes are where the quantity (in this case the displacement) of a specific mode does not change as the mode vibrates.

The modes of the string have the special feature that the frequencies of all of modes are simply integer multiples of each other. The n^{th} mode has a frequency of n times the frequency of the first mode. This is not a general feature of modes. In general, the frequencies of the modes are not related to each other. As an example, let us look at the modes of a vibrating free bar (Fig. 27). In the figure below, we plot the shape of the first three modes of a vibrating bar, together with the frequencies of the three modes. Again the solid lines are the shape of the mode on maximum displacement in one direction and the dotted the shape on maximum displacement in the other direction. Note that these are modes where the bar is simply vibrating, and not twisting. If one thinks about the bar being able to twist as well, there are extra modes. For a thin bar, the frequencies of these modes tend to be much higher than these lowest modes discussed here. However the wider the bar, the lower the frequencies of these modes with respect to the vibrational modes.

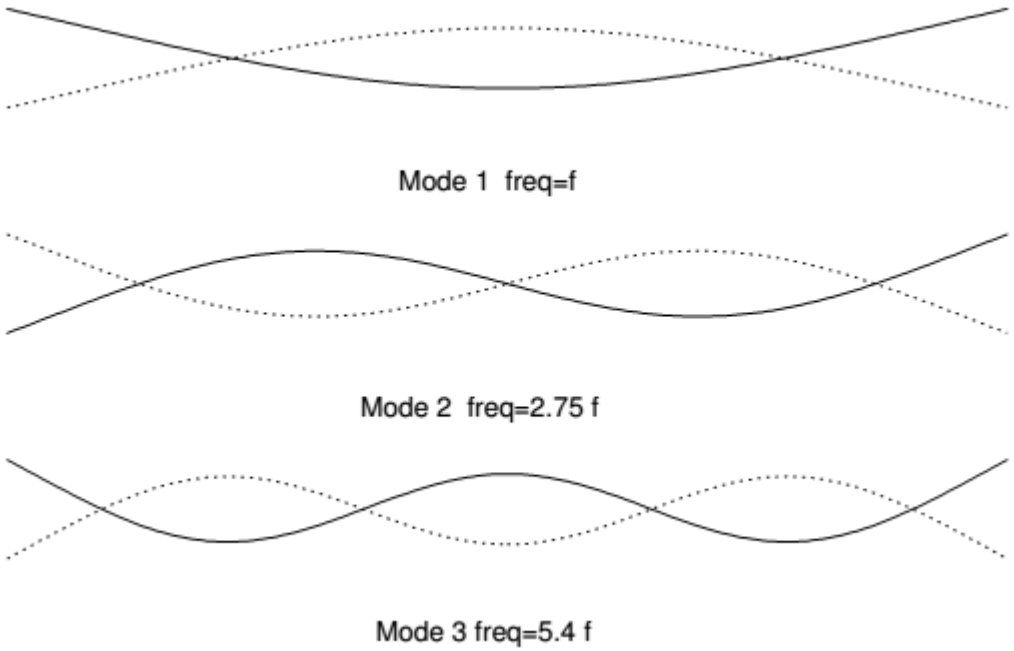

Fig. 27 – First three modes for a free bar

The concept of *Nodes* just introduced will be used as a base for locate a crack along the beam length.

2.2 Non-linear behavior

Most researchers have assumed that the crack in a structural member is open and remains open during vibration. This assumption is usually satisfied when the damage is rather large and avoids the complexity resulting from nonlinear behavior when a breathing crack is presented. On the contrary, breathing behavior is generally reported in the case the damage interests only a small portion of the cross section of the structural element but it requires a nonlinear model to take into account its effect on the system dynamics.
Nonlinear approaches require that the damage induces a nonlinear behavior in the system and are suitable for the early-detection of cracks when they behave in a breathing way. In fact, the breathing crack model considers that, during the vibration cycle of a structure, the edges of the crack come into and out of contact, leading to sudden changes in the dynamic response of the structure and these changes can be useful for the detection of cracks.
While these nonlinear effects make the response of beams more difficult to model with respect to notched beams, their appearance clearly marks the boundary between undamaged and damaged behavior.
As already demonstrated by other researchers [11], when a system with a breathing crack is excited by a single harmonic force, distinctive nonlinear features appear in the response. The excitation, in fact, forces the crack to open and close and the resulting clapping of the crack's edges produces harmonics that are integer multiple or fractional multiple of the forcing frequency. These harmonics are commonly referred as to *super-harmonics* and *sub-harmonics*, respectively. These features are easily detectable when the excitation frequency is in an integer ratio or is a multiple of a resonance frequency of the system; moreover, these would be much more sensitive to cracks characteristics than the modal properties of a linear system.
The non-linear effects that characterize a cracked beam are detectable through the Spectrogram of the beam dynamic response. A linear behavior is identified from the presence of a single line linked with the exiting frequency (Fig. 28.a). Spectrogram of a non-linear system shows instead the presence of multiple lines related to sub-harmonics and super-harmonics of forced frequency (Fig. 28.b).
Returning to the previous concept of Nodes (2.1) it is possible to ask ourselves something, "What happen if the crack is in a nodal point of the mode?"
If the crack is in the Node of the mode shape, then it is impossible to open and close cyclically, this result in a cracked beam that behave as an undamaged beam at that particular frequency. That frequency is the one that have a node of the mode coincident with the crack position. When such a thing happen, breathing behavior

of the crack is disabled and so its nonlinear features. It must be noted that observations above are valid for cracks in general but it is obvious that, in order to make possible for the crack to be perfectly in coincidence with a nodal point it is required that its size is restrained. Due to this fact, the effect on super-harmonic frequency could be also linked with the particular geometry of the crack and in particular on the influence that it has on nodal points.

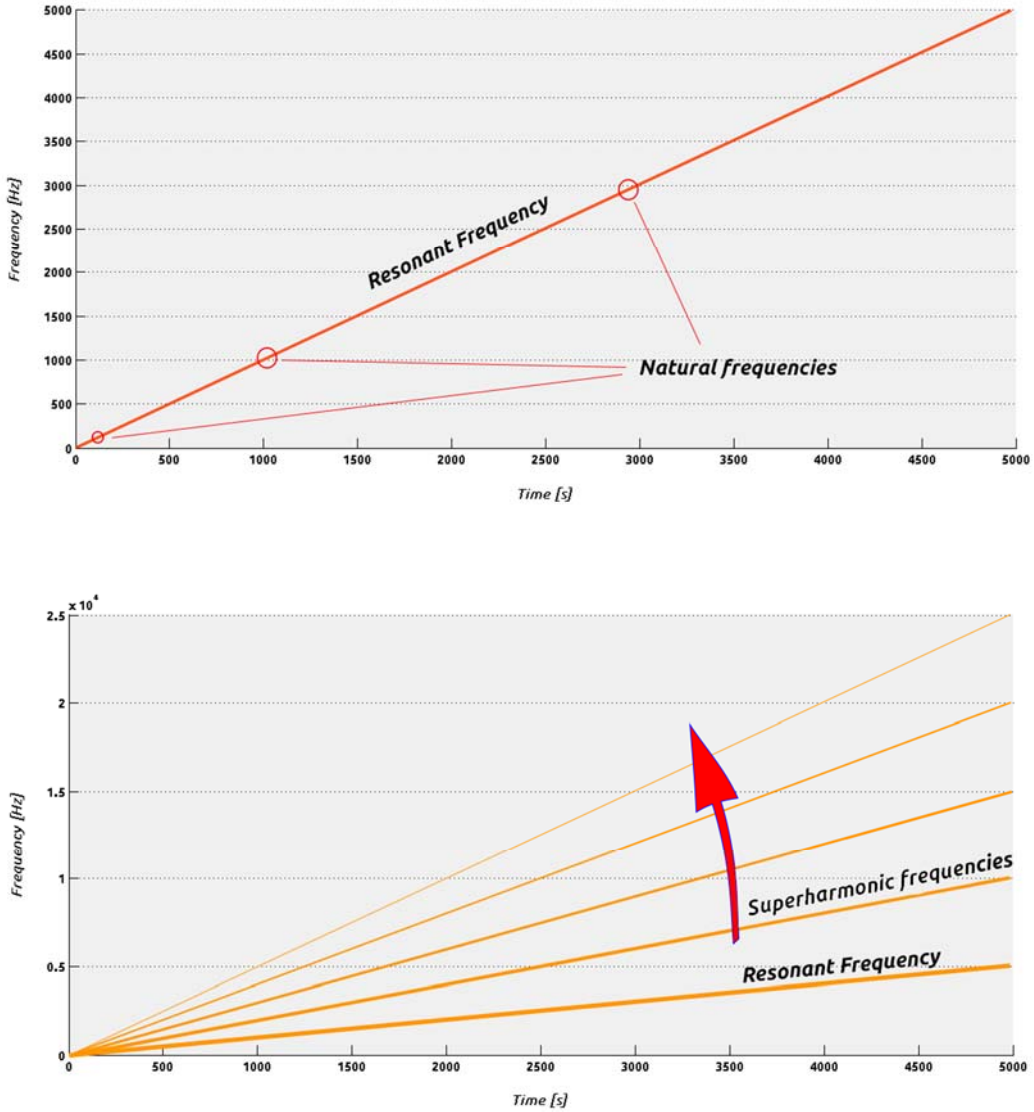

Fig. 28 – Spectrogram example for linear (a) and non-linear (b) behavior

2.3 Crack identification

The study of the Spectrogram of the beam dynamic response assume an important role in the whole procedure of crack identification that we want to present in this paper. As previously introduced, through its study it is possible to verify the presence of harmonics that are integer multiple or fractional multiple of the system forcing frequency. These frequencies, as already mentioned are named super-harmonics and sub-harmonics respectively.
In a perfect case, super-harmonics and sub-harmonics would disappear from the Spectrogram but, in realty, their expression is only damped down. This happens for different reasons especially related to the geometry of the crack.
Effects on non-linear feature are various depending on dimension and position of the crack indeed. The size and especially the spatial extension of the crack can influence different nodal point of the mode shape and for this reason, oblique crack will affect differently from longitudinal as well as transversal cracks.
In this paper, we limit the study only to the case of a transversal crack. In this way, its extension is limited to only few points of the structure and so its effects on super-harmonic frequencies will be maximized.
Information of the *Nodes* and of the system behavior can be used to develop an index useful to investigate the presence of a crack. As already written, if the crack is in a Node of the mode shape, then it will be impossible to open and close cyclically, this result in a linear behavior at that particular frequency. For this purpose, it is necessary to make the nodal points of the curvature to move along the length of the beam until they meet the crack making possible its identification. Nodal points change position gradually along the beam as frequency change so, for a correct identification, it is necessary to force the beam in a certain range of frequency studying its behavior. This fact leads to an innate connection between frequency and node displacement that must be considered during the test since a frequency step will turn into a spatial resolution for crack location.
The first step to accomplish is to obtain the position of curvature nodes of the structure at each frequency; this is possible in two different ways related to the complexity of the system itself. Simple geometries could be treated analytically while complex structures need to be analyzed with the help of a FEA software.
To first understand the analytical study of a simple case used to validate the method it is necessary to deal with the equation that describe the bending vibration of beams.

2.4 Bending vibration of beams

In this part, we introduce the study of vibrations in distributed parameter systems by dealing with the bending vibrations of a beam [8], [9].
We will treat the problem under the following assumptions:

1. Small displacements
2. Linear elastic constitutive law: we will consider a linear, isotropic relationship between stress and strain in the beam material; this assumption is normally well satisfied by metallic materials (steel, aluminum) until the plastic yield limit is achieved.
3. Constant section and homogeneous material: we will consider the section of the beam as constant in shape and dimensions along the beam axis. Furthermore, we will assume that no all-physical properties of the beam material (density, modulus of elasticity) depend upon the particular position inside the beam volume.
4. Damping effect can be neglected
5. No forces applied on the beam, except at the boundaries.
6. The beam is not subject to tension/compression.
7. Plane bending of the beam is studied, assuming that the plane where the bending motion occurs contains one of the principal axes of the beam section. It is easy to verify that, under this assumption, the plane bending motion studied is totally de-coupled from a second component of bending, occurring in an orthogonal plane which contains the other principal axis of the beam section. Therefore, the results obtained may be applied to the study of the three-dimensional bending motion of the beam, provided that the two bending motions in the two orthogonal planes are combined each other.
8. The center of gravity of the beam sections falls on the principal axis contained in the considered plane of bending: by this assumption, the bending motion studied is de-coupled from the torsional vibrations of the beam.
9. The beam is "slender", i.e. the ratio of the height h of the section over the beam length l is small :

$$\frac{h}{l} << 1$$

The last condition implies that the so-called "Euler-Bernoulli" theory can be used to describe beam bending. According to this theory, the angular distortion produced in the beam by the action of shear forces (see below) is negligible, so that if we denote

by *w(x,t)* the transversal displacements of the points along the beam axis and by *M(x,t)* the bending moment in the beam, the following relationship may be established between the two:

$$M = EJ\frac{\partial^2 w}{\partial x^2} \tag{26}$$

where *E* is the modulus of elasticity for the beam material and *J* is the geometric moment of inertia of the beam section along the principal axis orthogonal to the plane of bending. Additionally, the "Euler-Bernoulli" theory assumes that the effect of rotational inertia in the beam may be neglected (the consequence of this further assumption is discussed in detail below).
It is worth recalling that other beam models exist, allowing to consider the effect of shear deformation and/or of beam rotational inertia. The use of these theories is recommended in the study of "thick" beams, where the ratio $\frac{l}{h}$ is in the range of $\frac{1}{10}$ or more.
We consider the system represented in Fig. 29 **Errore. L'origine riferimento non è stata trovata.**and confine the study to the bending motion in the *x-z* plane, denoting by *w(x,t)* the transversal displacements of the points on the axle of the beam. The conventions introduced for shear forces *T* and bending moments *M* is also shown in the figure.

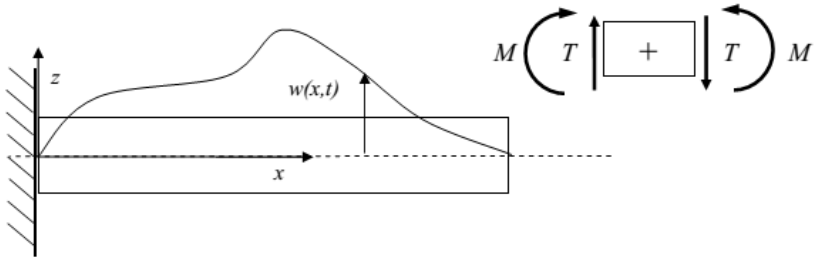

Fig. 29 – Model of the system

Now, in order to write the equation of motion for the bending vibration of the beam, we consider an element of infinitesimal length *dx* in a generical time *t*. The element is subjected to the forces shown in the figure below (Fig. 30) that, in absence of external forces are:

- The shear force *T(x,t)* and the bending moment *M(x,t)* acting on the left face of the element.

- The shear force *T(x+dx,t)* and the bending moment *M(x+dx,t)* acting on the right face of the element.
- The inertia force, expressed as the product of the infinitesimal mass of the element *dm* times the acceleration of the element $\frac{\partial^2 w}{\partial t^2}$ with the sign changed.

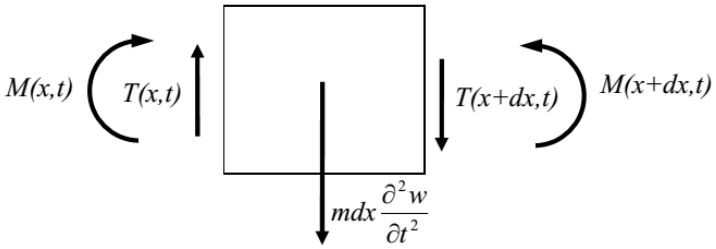

Fig. 30 – Infinitesimal element

Due to the fact that the "Eulero-Bernoulli" theory for the beam is used, we may consider as negligible the inertia torque expressed as the product of the beam element moment of inertia times the angular acceleration of the element with the sign changed (this is what was meant in the list of assumptions as "negligible rotatory inertia").
Now it is clearly possible to write, for the infinitesimal element, two dynamic equilibrium equations.

VERTICAL EQUILIBRIUM

$$T(x,t) - T(x+dx,t) - mdx\frac{\partial^2 w}{\partial t^2} = 0$$
$$T(x,t) - T(x,t) - \frac{\partial T}{\partial x}dx = mdx\frac{\partial^2 w}{\partial t^2} \qquad (27)$$
$$\Longrightarrow \quad \boldsymbol{\frac{\partial T}{\partial x} = -m\frac{\partial^2 w}{\partial t^2}}$$

ROTATION EQUILIBRIUM

$$M(x,t) - M(x+dx,t) + T(x,t)\cdot\frac{dx}{2} - T(x+dx,t)\cdot\frac{dx}{2} = 0$$
$$M(x,t) - M(x,t) - \frac{\partial M}{\partial x}dx + 2\cdot[T(x,t)\cdot\frac{dx}{2}] - \frac{\partial T}{\partial x}\cdot\frac{d^2x}{2} = 0 \qquad (28)$$
$$-\frac{\partial M}{\partial x}dx + T(x,t) = 0$$
$$\Rightarrow \quad \boldsymbol{T(x,t) = \frac{\partial M}{\partial x}dx}$$

Merging the two equilibrium equations, it is easy to obtain the following expression:

$$T(x,t) = \frac{\partial M}{\partial x} \quad ; \quad \frac{\partial T}{\partial x} = -m\frac{\partial^2 w}{\partial t^2} \qquad \Longrightarrow \qquad \boldsymbol{\frac{\partial^2 M}{\partial x^2} = -m\frac{\partial^2 w}{\partial t^2}} \tag{29}$$

Using now the relation valid for the Eulero-Bernoulli theory, it is possible to write the *indefinite equilibrium equation* that describe the bending vibration of a generic beam:

$$EJ\frac{\partial^4 w}{\partial x^4} = -m\frac{\partial^2 w}{\partial t^2} \tag{30}$$

2.4.1 Stationary solutions

To study bending motion of the beam, we seek for stationary solutions in the form

$$w(x,t) = \alpha(x)\beta(t)$$

where $\alpha(x)$ is a function of space alone describing the waveform of the stationary vibration and $\beta(t)$ is a time dependent vibration amplitude coefficient. To derive appropriate expressions for $\alpha(x)$ and $\beta(t)$ we observe that:

$$\frac{\partial^4 \alpha(x)\beta(t)}{\partial x^4} = \alpha^{IV}(x)\beta(t) \quad ; \quad \frac{\partial^2 \alpha(x)\beta(t)}{\partial t^2} = \alpha(x)\ddot{\beta}(t)$$

By introducing the above relationships in the *indefinite equilibrium equation* we get:

$$EJ\alpha^{IV}(x)\beta(t) = -m\alpha(x)\ddot{\beta(t)} \tag{31}$$

then, using the "separation of variables principle" scheme we get:

$$\frac{\ddot{\beta(t)}}{\beta(t)} = -\frac{EJ}{m}\frac{\alpha^{IV}(x)}{\alpha(x)} = -\omega^2 \tag{32}$$

Now it is possible to use the Separation of Variables method to get solution for the system. With this method is possible to separate the (32) in a second-order

differential equation in $\beta(t)$ alone and a fourth-order differential equation in $\alpha(x)$ alone:

$$\ddot{\beta}(t) + \omega^2\beta(t) = 0 \tag{33}$$

$$\alpha^{IV}(x) - \frac{m\omega^2}{EJ}\alpha(x) = 0 \tag{34}$$

the first equation provides the solution:

$$\beta(t) = Ecos(\omega t + \varphi) \tag{35}$$

to solve the second of equations we first simplify the notation by defining:

$$\gamma^4 = \frac{m\omega^2}{EJ} \tag{36}$$

so that the equation becomes:

$$\alpha^{IV}(x) + \gamma^4\alpha(x) = 0 \tag{37}$$

which is a fourth order, linear differential equation with constant parameters. The solution of this type of equation is a linear combination of four terms having the exponential form:

$$\alpha(x) = \alpha_0 e^{\lambda x} \quad \rightarrow \quad \alpha^{IV}(x) = \lambda^4\alpha_0 e^{\lambda x} \tag{38}$$

with the constant coefficient γ in the exponent being in general complex valued. By substitution of the above solution in equation (37) we get:

$$(\lambda^4 - \gamma^4)\alpha_0 e^{\lambda x} = 0 \quad \rightarrow \quad (\lambda^4 - \gamma^4)\alpha_0 = 0 \tag{39}$$

and, in order to discard the "trivial" solution $\alpha(x) = 0$

$$\lambda^4 - \gamma^4 = 0$$

that provides as solution λ :

$$\lambda_{1,2} = \pm i\gamma$$
$$\lambda_{3,4} = \pm i\gamma$$

so that the solution of eq. (37) takes the complex form:

$$\alpha(x) = \alpha_1 e^{i\gamma x} + \alpha_2 e^{-i\gamma x} + \alpha_3 e^{\gamma x} + \alpha_4 e^{-\gamma x} \tag{40}$$

now, we know from the solution of the free undamped motion of discrete systems that the first two terms in the above solution may be rewritten as:

$$\alpha_1 e^{i\gamma x} + \alpha_2 e^{-i\gamma x} = A\cos(\gamma x) + B\sin(\gamma x) \tag{41}$$

moreover, by definition of the hyperbolic cosine *Ch* and hyperbolic sine *Sh* functions we have:

$$Ch(\gamma x) = \frac{e^{\gamma x} + e^{-\gamma x}}{2} \quad ; \quad Sh(\gamma x) = \frac{e^{\gamma x} - e^{-\gamma x}}{2}$$

so that if we use the following substitutions in equation (40):

$$\alpha_3 = \frac{C + D}{2} \quad ; \quad \alpha_4 = \frac{C - D}{2}$$

in this way the global solution of $\alpha(x)$ it is given by:

$$\alpha(x) = A\cos(\gamma x) + B\sin(\gamma x) + C\cosh(\gamma x) + D\sinh(\gamma x) \tag{42}$$

and then:

$$w(x,t) = [A\cos(\gamma x) + B\sin(\gamma x) + CCh(\gamma x) + DSh(\gamma x)]\cos(wt + \varphi) \tag{43}$$

where the amplitude of the time dependent part of the solution of $\beta(x)$ has been embedded in constants A, B, C, D. The expression obtained represents the general solution for the stationary free bending vibration of a beam with constant section, regardless the boundary conditions acting on the beam at its ends. Different values of natural frequencies and modes of vibration are then associated to different boundary conditions at the ends of the beam.
In the next three sections the problem is examined evaluating different aspects related to boundary conditions. Different kinds of possible boundary conditions are first examined and translated into mathematical conditions, then the simplest case represented by the "pinned-pinned" boundary conditions is examined, and finally a

general procedure to treat the problem for arbitrary boundary conditions and for systems of beams is introduce.

2.4.2 Different boundary conditions for the bending motion

In the case of transversal vibrations of a tensioned string, one boundary condition was written for each end of the beam, thus providing a total of two boundary conditions. It could be demonstrated that the total number of boundary conditions in the problem is always equal to the maximum order of spatial derivatives in the partial derivatives differential equation to be solved. Thus we expect in the case of bending vibrations four boundary conditions, which means in turn two per each end of the beam.
In this section, we will consider three possible cases of boundary conditions that are those most frequently occurring in engineering practice. Other boundary conditions may be introduced [9] but their treatment may be deduced from the examples reported hereafter.
The first case we consider is the clamped beam end: this kind of constraints prevents the end of the beam from undergoing any vertical displacement or rotation.
If we denote by x the position of the section where the constraint is placed (this will be either $x = 0$ for the left end or $x = l$ for the right end of the beam), we must then require:

$$w(x,t)|_{x=\bar{x}} = 0 \quad \text{for any time } t$$

$$\left.\frac{\partial w}{\partial x}\right|_{x=\bar{x}} = 0 \qquad \text{for any time } t$$

where the second boundary condition is justified by the fact that if the distortions of the element produced by shear forces are negligible (in accordance with the Euler-Bernoulli beam theory). Then the rotation of the section coincides with the inclination of the beam axis, which in turn is expressed by the derivative of the transversal displacement $w(x,t)$ with respect to the spatial derivative x.
We see that in the case of a clamped end, the two boundary conditions reflect both the presence of a constraint and are then called "geometric" boundary conditions.
As a second case, we consider the "free end" boundary conditions, where the beam is not subjected to any constraint. Obviously in this case it is not possible to write geometric boundary conditions. However, if we consider an infinitesimal element of the beam that includes the free end of the beam, then there are two equilibrium

equations that we may write and will provide us with two boundary conditions that are called *"natural"* boundary conditions. In order to clarify this point we consider (without loss of generality) the case where the left end of the beam is free. The situation is depicted in Fig. 31:

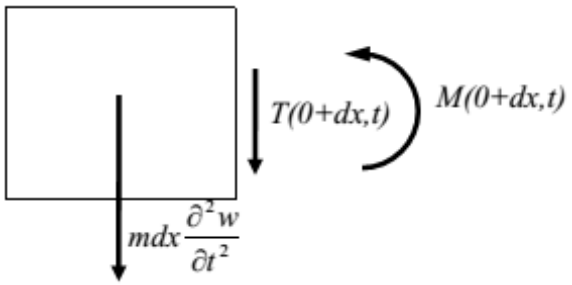

Fig. 31 – Equilibrium of an infinitesimal beam element on the left end

We may then write a dynamic equilibrium equation along the vertical direction and one dynamic equilibrium equation with respect to the rotation of the same element.

$$Vertical\ equilibrium:\ T(0,t)+\frac{\partial T}{\partial x}dx+mdx\frac{\partial^2 w}{\partial t^2}=0 \tag{44}$$

$$Rotation\ equilibrium:\ M(0,t)+\frac{\partial M}{\partial x}dx=0 \tag{45}$$

In both equations, the terms containing the infinitesimal length dx of the element are negligible with respect to the finite terms, so that we may simplify the equations in:

$$T(0,t)=0 \quad ; \quad M(0,t)=0$$

and, recalling equations (26) and (28):

$$\begin{aligned} EJ\left.\frac{\partial^3 w}{\partial x^3}\right|_{x=0}=0 \quad &\rightarrow \quad \left.\frac{\partial^3 w}{\partial x^3}\right|_{x=0}=0 \\ EJ\left.\frac{\partial^2 w}{\partial x^2}\right|_{x=0}=0 \quad &\rightarrow \quad \left.\frac{\partial^2 w}{\partial x^2}\right|_{x=0}=0 \end{aligned} \tag{46}$$

if we now remove the assumption of considering the left end of the beam, we get the general expression for the free end boundary conditions in a generic extremity of the beam x:

$$\left.\frac{\partial^3 w}{\partial x^3}\right|_{x=\bar{x}} = 0$$
$$\left.\frac{\partial^2 w}{\partial x^2}\right|_{x=\bar{x}} = 0 \tag{47}$$

we note by the way that the "natural" boundary conditions introduced in the free end involve higher order derivatives of the solution $w(x,t)$ that the "geometric" boundary conditions. Also we note that in presence of a clamp constraint, it is impossible to write any natural boundary condition, since each of the two equilibrium equations written above in the case of the free end would introduce in that case an unknown force component (either the clamping shear force or the clamping moment) associated with the presence of the constraint.

Finally, we consider a case that may be considered as intermediate between the "clamped end" and the "free end" cases. That is the case of a "pinned end", which means that the considered beam section is supported by a constraint like a hinge that prevents the section from any vertical displacement but leaves it free to rotate around a fixed point. We may introduce in this case one single geometric boundary condition that reflects the constraint acting on the vertical displacement and will thus correspond to the first of conditions found in the case of a clamped section, and additionally one single natural boundary condition that reflects the possibility for the beam section to freely rotate, and will then correspond to the second of conditions (47), found in the case of a free section. Thus, the two boundary conditions corresponding to a pinned section are:

$$w(\bar{x},t) = 0$$
$$\left.\frac{\partial^2 w}{\partial x^2}\right|_{x=\bar{x}} = 0 \tag{48}$$

2.5 The pinned-pinned beam

We consider first the case of a pinned-pinned beam to find the associated natural frequencies and modes of vibration. The advantage of considering this case is that the resulting equation is simple, allowing an analytical treatment. This is not the case for generic boundary conditions, where the use of a numerical procedure is normally needed, as will be clarified in the next section. If we consider a pinned boundary condition applied at both beam ends $\bar{x} = 0$ and $\bar{x} = l$ we get as the total set of four boundary conditions:

$$\begin{gathered} w(0,t) = 0 \quad ; \quad w(l,t) = 0 \\ \left.\frac{\partial^2 w}{\partial x^2}\right|_{x=0} = 0 \quad ; \quad \left.\frac{\partial^2 w}{\partial x^2}\right|_{x=l} = 0 \end{gathered} \tag{49}$$

we replace the general solution (43) into (49), taking into consideration that:

$$\frac{\partial^2 w}{\partial x^2} = \gamma^2[-Acos(\gamma x) - Bsin(\gamma x) + CCh(\gamma x) + DSh(\gamma x)]\cos(\omega t + \varphi) \tag{50}$$

so that we get from the first and second of (49):

$$\begin{cases} A + C = 0 \\ C - A = 0 \end{cases} \quad \rightarrow \quad \begin{cases} A = 0 \\ C = 0 \end{cases} \tag{51}$$

if we now consider the third and fourth of conditions (49), taking into account the above result, we get:

$$\begin{cases} Bsin(\gamma l) + DSh(\gamma l) = 0 \\ -Bsin(\gamma l) + DSh(\gamma l) = 0 \end{cases} \quad \rightarrow \quad \begin{cases} DSh(\gamma l) = 0 \\ Bsin(\gamma l) = 0 \end{cases} \tag{52}$$

Now, since the hyperbolic sine function is zero only for zero argument and since $\gamma l \neq 0$, the first of the two above conditions necessarily implies

$$D = 0 \tag{53}$$

On the other hand, if we consider the second of the above conditions, we may come out with two possibilities: the first one is $B = 0$, that (taken into account that we found previously $A = C = D = 0$) would imply a trivial case, where the beam remains still.

In order to avoid this trivial solution we need to set:

$$sin(\gamma l) = 0 \quad \rightarrow \quad \gamma l = k\pi \tag{54}$$

and finally, recalling the definition of γ by equation (36):

$$\frac{m\omega^2}{EJ} = \gamma^4 = \left(\frac{k\pi}{l}\right)^4 \tag{55}$$

and solving the above condition for the possible values of the pulsation ω :

$$\omega_k = \left(\frac{k\pi}{l}\right)^2 \sqrt{\frac{EJ}{m}} \quad ; \quad k = 1,2, \dots \tag{56}$$

Where ω_k take the meaning of the natural frequencies of the pinned-pinned beam in its bending vibrations. In (565656) coefficient k may assume any integer positive value, without any upper limit. In order to define the corresponding $k-th$ mode of vibration we introduce equations (51), (53) and (56) into the general expression of stationary bending vibrations, (43). From the substitutions, we easily obtain:

$$w_k(x,t) = B_k \sin\left(\frac{k\pi}{l}x\right)\cos(\omega_k t + \psi_k) \tag{57}$$

which shows that the $k-th$ mode of vibration (space function describing the shape of deformation associated with the $k-th$ natural frequency) is the same as for the transversal vibration of a tensioned string, i.e. a sinusoid having as its wavelength an integer sub-multiple of twice the beam span:

$$\alpha_k(x) = B_k \sin\left(\frac{k\pi}{l}x\right) \tag{58}$$

Fig. 32 reports the shape of the first four modes of vibration. The more general bending motion for the pinned-pinned beam in bending motion is then the combination of all motion components of the type (57):

$$w(x,t) = \sum_{k=1}^{\infty} w_k(x,t) = \sum_{k=1}^{\infty} B_k \sin\left(\frac{k\pi}{l}x\right)\cos(\omega_k t + \varphi_k) \tag{59}$$

where the amplitude parameters B_k and the phase parameters φ_k have to be determined by considering a particular set of initial conditions for the system.

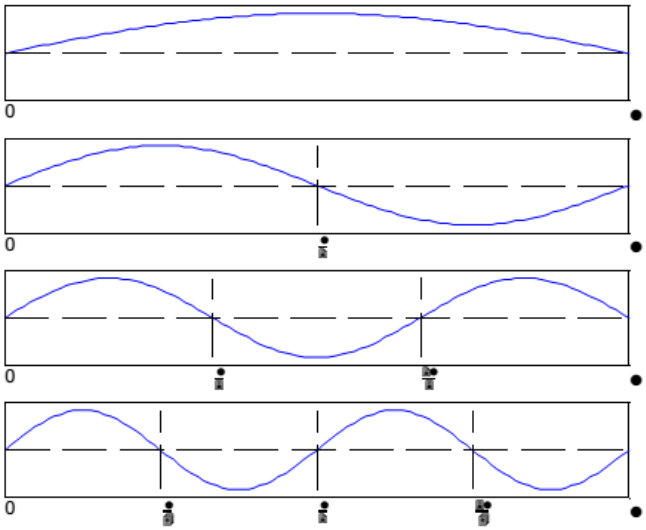

Fig. 32 – Shape of the first four modes of vibration for the pinned-pinned beam

2.5.1 Other boundary conditions

As explained above, the natural frequencies and modes of vibration of a beam in bending do not only depend upon the physical parameters of the beam (length, section, material), but also upon the particular boundary conditions considered. The same approach previously described may be used to define the natural frequencies and modes of vibration for any combination of boundary conditions, with the only difference that, in general, an analytical solution will not be possible.
We provide an example of the general procedure to consider a generic combination of boundary conditions by considering the cantilever beam, clamped at one end and free at the other, see Fig. 33.

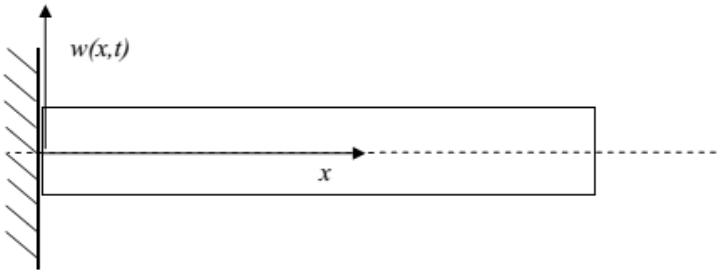

Fig. 33 – Model of the beam

In this case, the four conditions to be processed are the two of the clamped end in x=0 and the two of the free end in $\bar{x} = l$

$$\begin{aligned} w(0,t) = 0 \quad ; \quad \left.\frac{\partial w}{\partial x}\right|_{x=0} = 0 \\ \left.\frac{\partial^2 w}{\partial x^2}\right|_{x=l} = 0 \quad ; \quad \left.\frac{\partial^3 w}{\partial x^3}\right|_{x=l} = 0 \end{aligned} \tag{60}$$

It is left to the reader to verify that introducing these four conditions in the general solution (43) for the stationary bending vibration of the system, the following system of four equations in the unknowns A, B, C, D is obtained:

$$\begin{aligned} &A + C = 0 \\ &B + D = 0 \\ &-Acos(\gamma l) - Bsin(\gamma l) + CCh(\gamma l) + DSh(\gamma l) = 0 \\ &Asin(\gamma l) - Bcos(\gamma l) + CSh(\gamma l) + DCh(\gamma l) = 0 \end{aligned} \tag{61}$$

which may be rewritten in the for of the following matrix equation:

$$[H(\gamma)]\underline{x} = \underline{0} \tag{62}$$

where axis the vector formed by the four unknowns:

$$\underline{x} = \begin{Bmatrix} A \\ B \\ C \\ D \end{Bmatrix} \tag{63}$$

and $[H(\gamma)]$ has the following expression:

$$[H(\gamma)] = \begin{bmatrix} 1 & 0 & 1 & 0 \\ 0 & 1 & 0 & 1 \\ -\cos(\gamma L) & -sin(\gamma L) & Ch(\gamma L) & Sh(\gamma L) \\ sin(\gamma L) & -cos(\gamma L) & Sh(\gamma L) & Ch(\gamma L) \end{bmatrix} \tag{64}$$

By considering any other boundary conditions different from those of the cantilever beam, the same equation (62) would have been obtained, but with a different expression for matrix $[H(\gamma)]$. Now, we may observe that in equation (62):

- the term at right hand is zero (i.e., the problem is homogeneous)
- matrix $[H(\gamma)]$ depends upon parameter γ

From the first observation above, in order to get non-trivial solutions, we must require:

$$det[H(\gamma)] = 0$$

which results into a non-linear equation in parameter γ, having an infinite number of solutions γ_k, k=1,2,… Using equation (36) it is then possible to obtain the corresponding values for the natural frequencies that will be:

$$\omega_k = (\gamma_k)^2 \sqrt{\frac{EJ}{m}} \tag{65}$$

Finally, by replacing $\gamma = \gamma_k$ into equation (62), a solution x_k for that equation will be found, being formed by the four parameters A_k, B_k, C_k, D_k, where (as always in non-trivial solutions of homogeneous problems) one of the values will be chosen arbitrarily. By replacing these four values into solution (43), the $k-th$ component of the free motion for the system is defined, with the spatial part of the solution α_k representing the $k-th$ mode of vibration, associated with the $k-th$ natural frequency ω_k.
As we may see, the solution scheme to be adopted in the case of generic boundary conditions is the same as the one introduced while treating the pinned-pinned case. The difference is that in a generic case an analytical treatment of equation (62) is not possible, while in the case of the pinned-pinned beam equation (62) is easily transformed into the particular form:

$$A = 0 \ ; \ C = 0 \ ; \ D = 0 \ ; \ \sin(\gamma l) = 0 \tag{66}$$

that may be treated in a very simple way, as discussed at the beginning of section 2.5.

2.6 Systems of beams

The solutions for the free motion of beams in bending discussed in sections (2.5) and are referred to the case of a single beam with constant section, which is not subjected to any concentrated force (as could be caused by the presence of a constraint, or a concentrated spring / mass, etc.) except at its ends. However, we easily recognize that the presence of "discontinuities" along the beam axis is often encountered in the engineering practice where variations of the section, constraints and concentrated masses / springs may take place due to the particular design of the system to be studied. This could be the case e.g. of the shaft of a steam turbine + generator, normally resting on several supports that may be represented in first approximation as pins, with a mechanical scheme corresponding to that shown in Fig. 34.

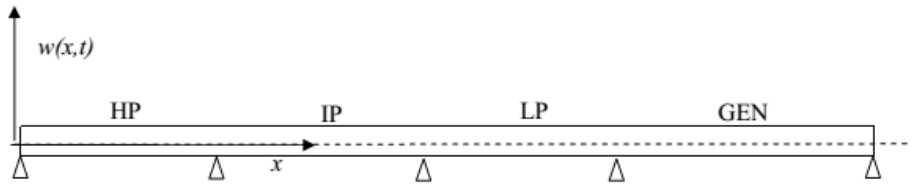

Fig. 34 – Shaft of a steam turbine + generator scheme

The scheme in Fig. 34 could also be a representative of a railway / road viaduct, which may also be considered in some cases as a continuous beam resting on multiple supports. We recognize that the situation of Fig. 34 may be described as that of a "system of beams" interconnected each other, where in the specific case each beam is represented by the single span separating two subsequent supports. Aim of this section is to describe how the solution for the free bending motion of such systems may be computed using the general solution for the free bending vibration of a single beam (43).

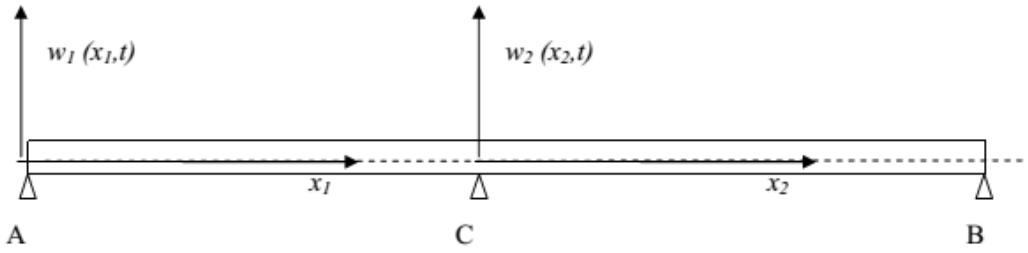

Fig. 35 – Railway / road viaduct scheme

To this end, we simplify the example in Fig. 34 to the case of a continuous beam resting on three supports, as represented in Fig. 35: this will allow us to illustrate the procedure in a simple case, but from the treatment, it should be clear that the same approach may be used for more complicate systems of beams.
In order to treat the case of Fig. 35, we observe that the assumptions under which we found solution (43) are not applicable to the whole beam (due to the presence of the central support), but instead are satisfied if we consider separately the left and right halves (spans) of the beam. Thus, we may introduce two axial coordinates x_1 and x_2, spanning respectively the left and right halves of the system, and correspondingly two solutions of the type (43) that separately apply to the left and right spans of the system:

$$\begin{aligned} w_1(x_1,t) &= [A_1\, cos(\gamma x_1) + B_1\, sin(\gamma x_1) + C_1 Ch(\gamma x_1) + D_1 Sh(\gamma x_1)]cos(\omega t + \varphi) \\ w_2(x_2,t) &= [A_2\, cos(\gamma x_2) + B_1\, sin(\gamma x_2) + C_1 Ch(\gamma x_2) + D_1 Sh(\gamma x_2)]cos(\omega t + \varphi) \end{aligned} \tag{67}$$

We observe by the way the time-dependent part of the two solutions must obviously be the same, since the motion of the two halves of the system must be synchronized. From eq. (36), it then follows that since parameter ω is equal for the two solutions in (67), then also the same γ coefficient has to be used for the two subsystems, as far as the EJ and m coefficients are the same along the whole beam.
To find the natural frequencies and modes of vibration for the system in Fig. 35, we must define a set of appropriate boundary conditions for equation (67), which will be referred to both the "external boundaries" (the ends of the system, sections A and B) and the "internal boundary" (the central pin, section C, where the two halves are connected). For sections A and C, the already encountered boundary conditions of the pinned end take place:

$$\begin{aligned} w_1(0,t) = 0 \quad ; \quad \left.\frac{\partial^2 w_1}{\partial x_1^2}\right|_{x_1=0} = 0 \\ w_2(l,t) = 0 \quad ; \quad \left.\frac{\partial^2 w_2}{\partial x_2^2}\right|_{x_2=l} = 0 \end{aligned} \tag{68}$$

Moreover, in point C four additional boundary conditions hold, the first three being geometrical (equality of displacements and rotations at the connection between the two halves of the beam, plus zero displacement due to the presence of the pin) and

the fourth one being a natural boundary condition representing the rotational dynamic equilibrium of the infinitesimal beam element cut just before and just after the central pin:

$$\begin{aligned} w_1(l,t) = w_2(0,t) \quad ; \quad \left.\frac{\partial w_1}{\partial x_1}\right|_{x_1=l} = \left.\frac{\partial w_2}{\partial x_2}\right|_{x_2=0} \\ w_1(l,t) = 0 \qquad ; \quad \left.\frac{\partial^2 w_1}{\partial x_1^2}\right|_{x_1=l} = \left.\frac{\partial^2 w_2}{\partial x_2^2}\right|_{x_2=0} \end{aligned} \tag{69}$$

we note by the way that the total number of boundary conditions (eight) equals the number of unknowns in eq. (67): $A_1, B_1 \ldots D_1$, plus $A_2, B_2 \ldots D_2$. The above listed eight boundary conditions may be written as a single matrix equation with the form (62), the only difference with the case of the cantilever beam previously treated being that in this case matrix $[H()]$ will have dimension 8 instead than 4. The same procedure to find the natural frequency and modes of vibrations described in the end of section 2.5.1 (based on computing the values of parameter that correspond to zero values of the determinant of matrix $[H]$) may be used also for the system of beams in Fig. 35 and, more generally, for any system of beams where all elementary beams have a common axis.

2.7 Clamped beam with boundary displacement

In order to validate the crack identification method based on the study of super-harmonic frequencies a different configuration must be studied for the purpose.
The idea of moving the nodal points along the length of the beam necessitate the system to be forced in a generic range of frequency. For this purpose, it is chosen the configuration presented in Fig. 36.
The configuration it's physically the same presented in section 2.5.1 with a different boundary condition due to the presence of a vertical pulsing displacement in the constrain.

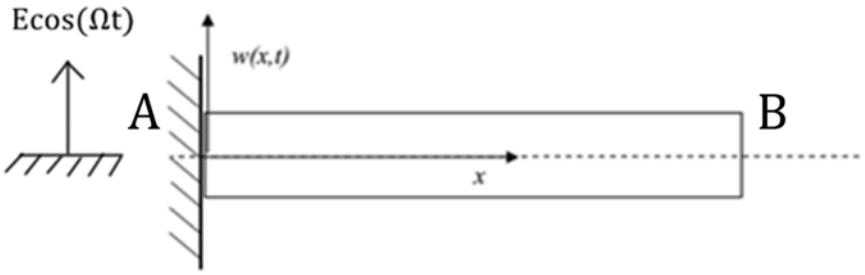

Fig. 36 – Clamped beam with boundary pulsing displacement

Now, to obtain the dynamic equation, it is possible to start from the (43) and substitute the boundary condition that are:

$$w(0,t) = Ecos(\Omega t)$$

$$\left.\frac{\partial w}{\partial x}\right|_{x=o} = 0$$

$$\left.\frac{\partial^2 w}{\partial x^2}\right|_{x=l} = 0$$

$$\left.\frac{\partial^3 w}{\partial x^3}\right|_{x=l} = 0$$

Now it is possible to use this conditions with the generic dynamic equation of motion obtained for bending vibration of beams that is equal to (43):

$$w(x,t) = [Asin(\gamma x) + Bcos(\gamma x) + Csinh(\gamma x) + Dcosh(\gamma x)] \cdot cos(\Omega t)$$

As already calculated for different boundary conditions, it is possible to create the system and obtain the unknown coefficient A, B, C, D:

$$\begin{cases} \text{Condition 1}: (B+D)cos(\Omega t) = Ecos(\Omega t) \quad \rightarrow \quad \boldsymbol{B + D = E} \\ \text{Condition 2}: \gamma(A+C) = 0 \quad \rightarrow \quad \boldsymbol{A = -C} \\ \text{Condition 3}: \boldsymbol{-Asin(\gamma L) - Bcos(\gamma L) + Csinh(\gamma L) + Dcosh(\gamma L) = 0} \\ \text{Condition 4}: \boldsymbol{-Acos(\gamma L) + Bsin(\gamma L) + Ccosh(\gamma L) + Dsinh(\gamma L) = 0} \end{cases}$$

This leads to the following matrix system in the form $[H(\gamma)]x = [Q]$ were *x* is the vector containing the unknown parameters.

$$\underline{x} = \begin{Bmatrix} A \\ B \\ C \\ D \end{Bmatrix}$$

Now the system may be rewritten as:

$$\begin{bmatrix} 0 & 1 & 0 & 1 \\ 1 & 0 & 1 & 0 \\ -\sin(\gamma L) & -cos(\gamma L) & sinh(\gamma L) & cosh(\gamma L) \\ -cos(\gamma L) & sin(\gamma L) & cosh(\gamma L) & sinh(\gamma L) \end{bmatrix} x = [Q] \tag{70}$$

In this case, vector $[Q]$ contain only coefficient *E* in the first row and then all zeros. Coefficient *E* represent the amplitude of boundary displacement so, for simplicity it could be expressed by $E = 1$ to have

$$\begin{bmatrix} 0 & 1 & 0 & 1 \\ 1 & 0 & 1 & 0 \\ -\sin(\gamma L) & -cos(\gamma L) & sinh(\gamma L) & cosh(\gamma L) \\ -cos(\gamma L) & sin(\gamma L) & cosh(\gamma L) & sinh(\gamma L) \end{bmatrix} \begin{bmatrix} A \\ B \\ C \\ D \end{bmatrix} = \begin{bmatrix} 1 \\ 0 \\ 0 \\ 0 \end{bmatrix} \tag{71}$$

Since we are seeking the analytical expression of parameter A, B, C, D, we may write:

$$\begin{bmatrix} A \\ B \\ C \\ D \end{bmatrix} = \begin{bmatrix} 0 & 1 & 0 & 1 \\ 1 & 0 & 1 & 0 \\ -\sin(\gamma L) & -cos(\gamma L) & sinh(\gamma L) & cosh(\gamma L) \\ -cos(\gamma L) & sin(\gamma L) & cosh(\gamma L) & sinh(\gamma L) \end{bmatrix}^{-1} \begin{bmatrix} 1 \\ 0 \\ 0 \\ 0 \end{bmatrix} \tag{72}$$

The expression obtained (72) contain the inverse matrix of the system that must be solved to obtain the unknown coefficient.
Using the Adjoint method to calculate the inverse matrix we get:

$$\begin{bmatrix} A \\ B \\ C \\ D \end{bmatrix} = \frac{1}{\det[H(\gamma)]} \begin{bmatrix} Cof(H_{11}) & Cof(H_{12}) & Cof(H_{13}) & Cof(H_{14}) \\ Cof(H_{21}) & Cof(H_{22}) & Cof(H_{23}) & Cof(H_{24}) \\ Cof(H_{31}) & Cof(H_{32}) & Cof(H_{33}) & Cof(H_{34}) \\ Cof(H_{41}) & Cof(H_{42}) & Cof(H_{43}) & Cof(H_{44}) \end{bmatrix}^{T} \begin{bmatrix} 1 \\ 0 \\ 0 \\ 0 \end{bmatrix} \tag{73}$$

We proceed with the calculus of the $\det[H(\gamma)]$

$$det\begin{bmatrix} 0 & 1 & 0 & 1 \\ 1 & 0 & 1 & 0 \\ -\sin(\gamma L) & -\cos(\gamma L) & \mathrm{Sh}(\gamma L) & \mathrm{Ch}(\gamma L) \\ -\cos(\gamma L) & \sin(\gamma L) & \mathrm{Ch}(\gamma L) & \mathrm{Sh}(\gamma L) \end{bmatrix} =$$

$$= -1 \cdot det\begin{bmatrix} 1 & 1 & 0 \\ -\sin(\gamma L) & \mathrm{Sh}(\gamma L) & \mathrm{Ch}(\gamma L) \\ -\cos(\gamma L) & \mathrm{Ch}(\gamma L) & \mathrm{Sh}(\gamma L) \end{bmatrix} - 1 \cdot det\begin{bmatrix} 1 & 0 & 1 \\ -\sin(\gamma L) & \cos(\gamma L) & \mathrm{Sh}(\gamma L) \\ -\cos(\gamma L) & \sin(\gamma L) & \mathrm{Ch}(\gamma L) \end{bmatrix}$$

$$= [-Sh^2(\gamma L) + cos(\gamma L)Ch(\gamma L) + Ch^2(\gamma L) - sin(\gamma L)Sh(\gamma L)]$$

$$+ [cos(\gamma L)Ch(\gamma L) + sin^2(\gamma L) + cos^2(\gamma L) + sin(\gamma L)Sh(\gamma L)]$$

This leads to

$$det\begin{bmatrix} 0 & 1 & 0 & 1 \\ 1 & 0 & 1 & 0 \\ -\sin(\gamma L) & -\cos(\gamma L) & \mathrm{Sh}(\gamma L) & \mathrm{Ch}(\gamma L) \\ -\cos(\gamma L) & \sin(\gamma L) & \mathrm{Ch}(\gamma L) & \mathrm{Sh}(\gamma L) \end{bmatrix} = \mathbf{2 + 2cos(\gamma L)Ch(\gamma L)} \quad (74)$$

Substituting (74) in (73), the system become:

$$\begin{bmatrix} A \\ B \\ C \\ D \end{bmatrix} = \frac{1}{2 + 2cos(\gamma L)Ch(\gamma L)} \begin{bmatrix} Cof(H_{11}) & Cof(H_{12}) & Cof(H_{13}) & Cof(H_{14}) \\ Cof(H_{21}) & Cof(H_{22}) & Cof(H_{23}) & Cof(H_{24}) \\ Cof(H_{31}) & Cof(H_{32}) & Cof(H_{33}) & Cof(H_{34}) \\ Cof(H_{41}) & Cof(H_{42}) & Cof(H_{43}) & Cof(H_{44}) \end{bmatrix}^T \begin{bmatrix} 1 \\ 0 \\ 0 \\ 0 \end{bmatrix}$$

And transcribing the transposed matrix we get:

$$\begin{bmatrix} A \\ B \\ C \\ D \end{bmatrix} = \frac{1}{2 + 2cos(\gamma L)Ch(\gamma L)} \begin{bmatrix} Cof(H_{11}) & Cof(H_{21}) & Cof(H_{31}) & Cof(H_{41}) \\ Cof(H_{12}) & Cof(H_{22}) & Cof(H_{32}) & Cof(H_{42}) \\ Cof(H_{13}) & Cof(H_{23}) & Cof(H_{33}) & Cof(H_{43}) \\ Cof(H_{14}) & Cof(H_{24}) & Cof(H_{34}) & Cof(H_{44}) \end{bmatrix} \begin{bmatrix} 1 \\ 0 \\ 0 \\ 0 \end{bmatrix}$$

Solving the right part of the system, we may rewrite:

$$\begin{bmatrix} A \\ B \\ C \\ D \end{bmatrix} = \frac{1}{2 + 2cos(\gamma L)Ch(\gamma L)} \begin{bmatrix} Cof(H_{11}) \\ Cof(H_{12}) \\ Cof(H_{13}) \\ Cof(H_{14}) \end{bmatrix} \quad (75)$$

Expression (75) can be rewritten using analytical expressions of cofactors that are:

$$Cof(H_{11}) = det\begin{bmatrix} 0 & -cos(\gamma L) & sin(\gamma L) \\ 1 & Sh(\gamma L) & Ch(\gamma L) \\ 0 & Ch(\gamma L) & Sh(\gamma L) \end{bmatrix} = sin(\gamma L)Ch(\gamma L) + cos(\gamma L)Sh(\gamma L)$$

$$Cof(H_{12}) = -det\begin{bmatrix} 1 & -sin(\gamma L) & -cos(\gamma L) \\ 1 & Sh(\gamma L) & Ch(\gamma L) \\ 0 & Ch(\gamma L) & Sh(\gamma L) \end{bmatrix} = 1 + cos(\gamma L)Ch(\gamma L) - sin(\gamma L)Sh(\gamma L)$$

$$Cof(H_{13}) = det\begin{bmatrix} 1 & -sin(\gamma L) & -cos(\gamma L) \\ 0 & -cos(\gamma L) & sin(\gamma L) \\ 0 & Ch(\gamma L) & Sh(\gamma L) \end{bmatrix} = -cos(\gamma L)Sh(\gamma L) - sin(\gamma L)Ch(\gamma L)$$

$$Cof(H_{14}) = -det\begin{bmatrix} 1 & -sin(\gamma L) & -cos(\gamma L) \\ 0 & -cos(\gamma L) & sin(\gamma L) \\ 1 & Sh(\gamma L) & Ch(\gamma L) \end{bmatrix} = 1 + cos(\gamma L)Ch(\gamma L) + sin(\gamma L)Sh(\gamma L)$$

In this way, system (75) can be organized as follows

$$\begin{cases} A = \dfrac{1}{\det[H(\gamma)]} \cdot Cof(H_{11}) \\ B = \dfrac{1}{\det[H(\gamma)]} \cdot Cof(H_{12}) \\ C = \dfrac{1}{\det[H(\gamma)]} \cdot Cof(H_{13}) \\ D = \dfrac{1}{\det[H(\gamma)]} \cdot Cof(H_{14}) \end{cases}$$

Using analytical expression obtained from (74) and from cofactors calculation, it is now possible to solve the system (73) and obtain the values of unknown coefficient.

$$\begin{cases} A = \dfrac{1}{2 + 2cos(\gamma L)Ch(\gamma L)} \cdot sin(\gamma L)Ch(\gamma L) + cos(\gamma L)Sh(\gamma L) \\ B = \dfrac{1}{2 + 2cos(\gamma L)Ch(\gamma L)} \cdot 1 + cos(\gamma L)Ch(\gamma L) - sin(\gamma L)Sh(\gamma L) \\ C = \dfrac{1}{2 + 2cos(\gamma L)Ch(\gamma L)} \cdot -cos(\gamma L)Sh(\gamma L) - sin(\gamma L)Ch(\gamma L) \\ D = \dfrac{1}{2 + 2cos(\gamma L)Ch(\gamma L)} \cdot 1 + cos(\gamma L)Ch(\gamma L) + sin(\gamma L)Sh(\gamma L) \end{cases} \quad (76)$$

Analytical expressions from (76) can be substituted inside the general solution (43) to obtain displacement values of every portion of the beam.

$$w(x,t) = [Asin(\gamma x) + Bcos(\gamma x) + Csinh(\gamma x) + Dcosh(\gamma x)]\cos(wt + \varphi)$$

This is one of the most important part for the crack identification method proposed since with expression just written is possible to calculate the curvature nodes position of the structures and use these information to locate the crack as already explained in section 2.3.

2.8 Curvature node position

Simple geometries could be analytically treated and it is possible to find the position of curvature nodes at each frequency studying the expression of $w(x,t)$ already obtained. Curvature parameter is expressed by κ and it is defined as the second derivative of the deflection:

$$\kappa = \frac{\partial^2 w}{\partial x^2} \tag{77}$$

Using the dynamic equation (43) we get:

$$\begin{aligned} &\frac{\partial w}{\partial x} = \gamma \cdot [Acos(\gamma x) - Bsin(\gamma x) + Ccosh(\gamma x) + Dsinh(\gamma x)] \\ &\frac{\partial^2 w}{\partial x^2} = \gamma^2 \cdot [-Asin(\gamma x) - Bcos(\gamma x) + Csinh(\gamma x) + Dcosh(\gamma x)] \end{aligned} \tag{78}$$

Moreover, to obtain the nodal points related with the curvature of the mode of vibration we must search for

$$-Asin(\gamma x) - Bcos(\gamma x) + Csinh(\gamma x) + Dcosh(\gamma x) = 0$$

Where A, B, C, D are the parameters found before, x is the coordinate along the length of the beam and finally

$$\gamma = \sqrt{\omega\sqrt{\frac{m}{EJ}}} \quad \rightarrow \quad \gamma = \sqrt[4]{\frac{m\omega^2}{EJ}} \tag{79}$$

Results obtained from analytical calculations are used to create a graph that links frequency and position of the nodes along the length of the beam.
To easily get the position of nodal points for the simple geometry just examined a Matlab function called *clamped_beam_flexure.m* is created. Function developed uses parameters A, B, C, D to give results for the beam configuration considered and give in output the chart to be used to locate the crack (Fig. 37). Blue points in fact represent the transition to zero for the curvature values of the different vibration modes of the beam. Axe x contain the frequency used to force the system and axe y the position of the node expressed as a percent of the length x/l.

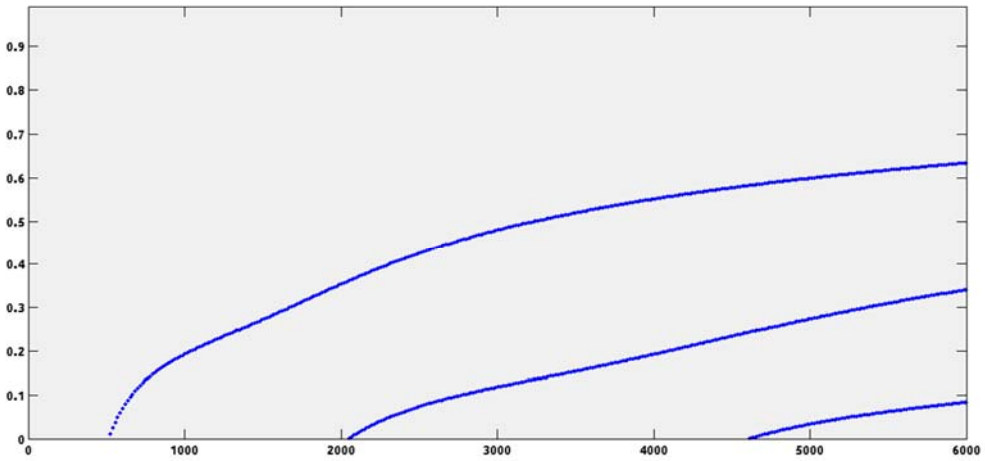

Fig. 37 – Curvature nodes position at different frequency for a generic beam

As is possible to see, different lines are present since node numbers increase as modes changes during the frequency increasing. This graph will be used to investigate the presence of a crack in a generic point as well as to deny its presence.
Before testing it on a specific case it is now time to introduce the parameter used to get the right value to enter on it that is the *Non-Linearity Index*.

2.9 Non-Linearity Index

Crack identification method introduced in this paper has the aim of weigh the non-linear behavior of a structure with the purpose to locate the position of a crack. This is possible using, as a point of start, the Matlab Spectrogram function of the response. As explicatory example, Fig. 38 shows two spectrogram of the response recorded from a damaged and an undamaged beam. Observing the figures, it is possible to see difference in their behavior. Non-linear behavior is clearly noticeable for damaged

beam since different lines representing the super-harmonic frequencies appear in the graph (Fig. 38 (b)).
In particular, the target is to find out where these lines disappear gathering frequencies that show a linear behavior despite the presence of the crack. This fact implies that the crack cannot open in its position at that particular frequency suggesting that its location is actually in a curvature node.
Using the analytical model created in section (2.7) it is possible to track the location of the crack since it is known where the nodes at positioned for every frequency.

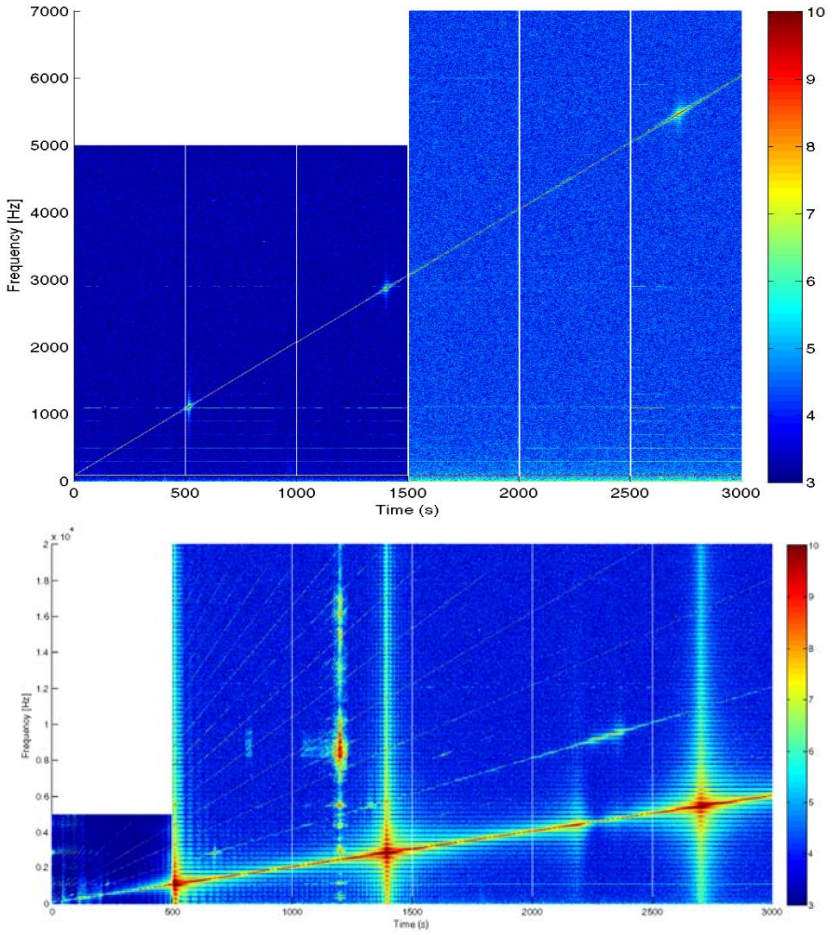

Fig. 38 – Spectrogram of linear (a) and non-linear (b) system

For this purpose, a *Non-Linearity Index* is created to weigh the non-linear behavior of the beam at each frequency. To do that is necessary to examine result obtained from Spectrogram and in particular, the matrix S that it creates. To make it easy

applicable, a script is created in Matlab. This script scans the entire matrix *S* column-by-column collecting the peak values at each resonant frequency and weighting the super-harmonic frequencies contributes as shown in Fig. 39.
Non-Linearity Index is so defined as:

$$NL_{Index}(i) = 1 - \frac{Peak_0 + Peak_1 + Peak_2}{Peak_0} \tag{80}$$

Where i is the considered frequency, $Peak_0$ is the resonant frequency value, $Peak_1$ and $Peak_2$ are the first and the second super-harmonic frequencies respectively.

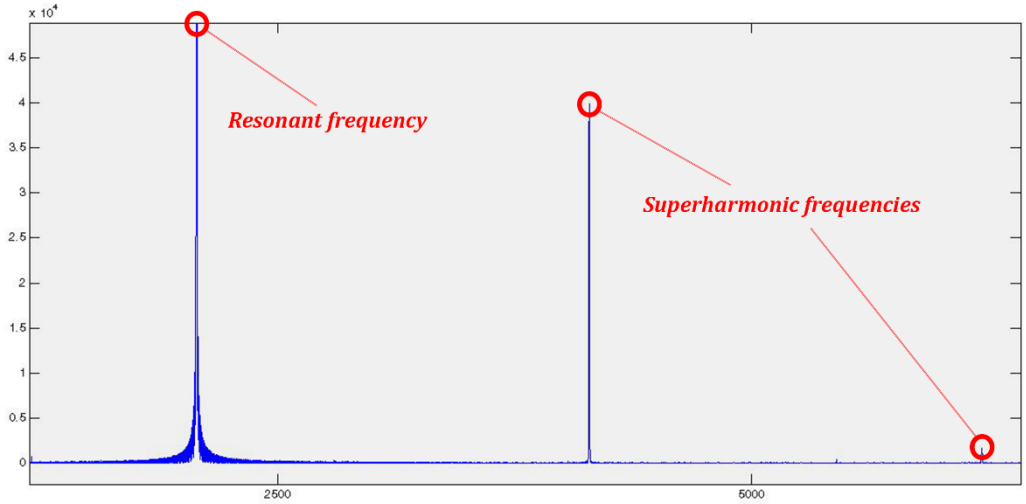

Fig. 39 – Contributes of resonant and super-harmonic frequencies

Linear behavior of the structure will be identified by the minimum values of this index. These minimum points correspond to particular frequencies in which the crack seems to have no breathing behavior. When the frequency that correspond to a minimum of the *Non-Linearity Index* is obtained it is possible to locate the position of the crack entering with it in the *Curvature Node Graph* (Fig. 37).
Procedure is schematically reported in Fig. 40 and consist of:

1. Frequency corresponding to *Non-Linearity Index* is used to enter in axe *x* of the graph.
2. Interception with node position line is obtained.
3. Node position line is used to intercept axe y that report position in percent of beam length. This is the possible crack position.

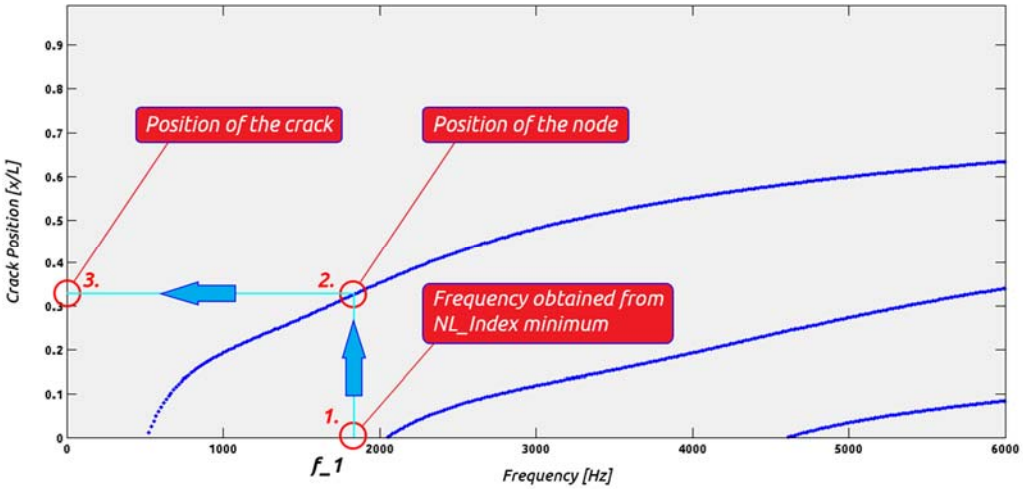

Fig. 40 – Example #1 on the use of NL_Index to locate the crack

Now to find further confirmation about the presence of the crack it is possible to use the node position just obtained to verify it on other modes (Fig. 41).

4. Horizontal line is traced from node position obtained and is intercepted with following lines that correspond to other modes.
5. Another frequency is obtained on axe *x*. This value is used to check if it correspond to another minimum of the *Non-Linearity Index.*

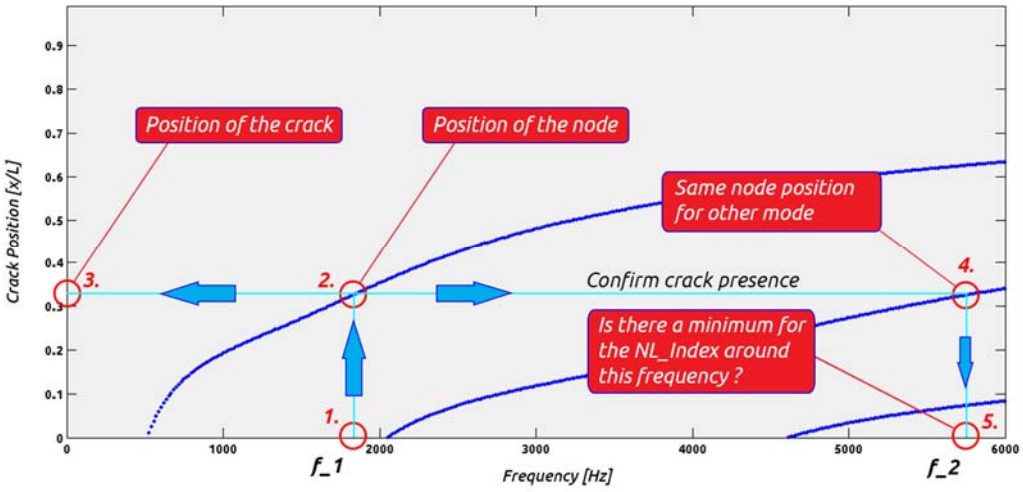

Fig. 41 – Example #1 investigation on higher mode

It is important to highlight that results may not be univocal due to the presence of more than one node at high frequency. In this case, the procedure is the same:

1. Frequency corresponding to *Non-Linearity Index* is used to enter in axe *x* of the graph. This leads to two nodes because it correspond to second mode.
2. Two possible position of the crack are located on *y* axe (Fig. 42 (a)).
3. Now it is possible to check the nodes position on higher or lower frequency modes to verify if they correspond to other minimum points of the *Non-Linearity Index* and so indicating the presence of the crack (Fig. 42 (b)).

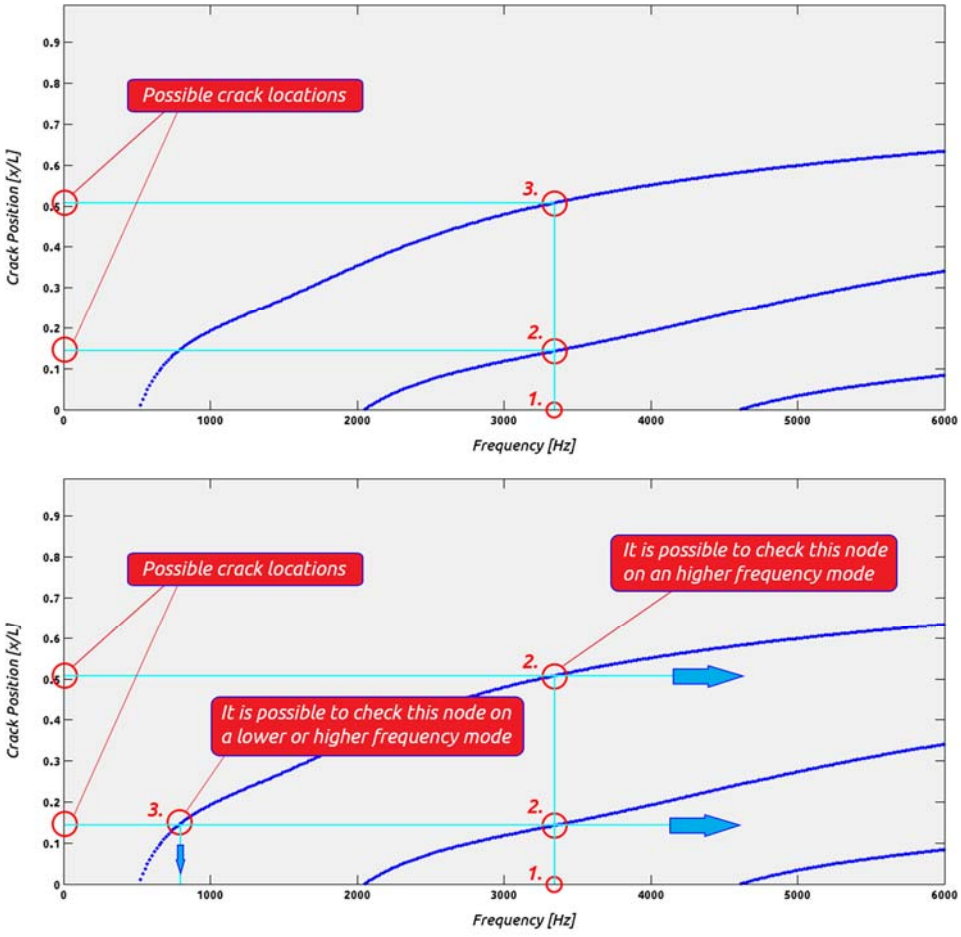

Fig. 42 – Example #2 on the use of NL_Index

The method presented could so be used to validate as well as deny the presence of a crack in a certain point due to the possibility to verify the *Non-Linearity Index* of the same node at different frequencies.

Chapter 3 NUMERICAL SOLUTION

Crack identification method presented in Section 2.3 is strictly based on the study of curvature nodes position of the structure that must be analyzed. This is not a priori knowledge and so must be examined for each structure. This problem can be faced off using the equations that describe continuous systems when a simple geometry is considered, but in the most cases, we need to deal with complex structures that are not easily solvable analytically. In this case curvature nodes position is still achievable using the *Finite Element Analysis.*
The case of clamped beam examined in the previous chapter is simple and the relation obtained between frequency and node position could be naturally obtained in the same way with numerical simulation.

3.1 A brief history

Finite Element Analysis (FEA) was first developed in 1943 by R. Courant, who utilized the Ritz method of numerical analysis and minimization of variational calculus to obtain approximate solutions to vibration systems. Shortly thereafter, a paper published in 1956 by M. J. Turner, R. W. Clough, H. C. Martin, and L. J. Topp established a broader definition of numerical analysis. The paper centered on the "stiffness and deflection of complex structures".
By the early 70's, FEA was limited to expensive mainframe computers generally owned by the aeronautics, automotive, defense, and nuclear industries. Since the rapid decline in the cost of computers and the phenomenal increase in computing power, FEA has been developed to an incredible precision. Present day supercomputers are now able to produce accurate results for all kinds of parameters.
Finite Element Analysis is one of several numerical methods that can be used to solve complex problems and is the dominant method used today. As the name implies, it takes a complex problem and breaks it down into a finite number of simple problems. A continuous structure theoretically has an infinite number of simple problems, but finite element analysis approximates the behaviour of a continuous structure by analysing a finite number of simple problems. Each element in a finite element analysis is one of these simple problems. Each element in a finite element model will have a fixed number of nodes that define the element boundaries to which loads and boundary conditions can be applied. The finer the mesh, the closer we can approximate the geometry of the structure, the load application, as well as the stress and strain gradients. However, there is a tradeoff: the finer the mesh, the more

computational power is needed to solve the complex problem. The strategy of optimizing the mesh size can greatly reduce an analyst's time without compromising on the quality of analysis results.
In spite of the great power of FEA, the disadvantages of computer solutions must be kept in mind when using this and similar methods: they do not necessarily reveal how the stresses are influenced by important problem variables such as materials properties and geometrical features, and errors in input data can produce wildly incorrect results that may be overlooked by the analyst.

A finite element analysis usually consists of three principal steps:

1. *Pre-processing:* The user constructs a model of the part to be analyzed in which the geometry is divided into a number of discrete sub-regions, or "elements," connected at discrete points called "nodes." Certain of these nodes will have fixed displacements, and others will have prescribed loads. These models can be extremely time consuming to prepare, and commercial codes vie with one another to have the most user-friendly graphical "preprocessor" to assist in this rather tedious chore. Some of these preprocessors can overlay a mesh on a preexisting CAD file, so that finite element analysis can be done conveniently as part of the computerized drafting-and-design process.

2. *Analysis:* The dataset prepared by the preprocessor is used as input to the finite element code itself, which constructs and solves a system of linear or nonlinear algebraic equations

$$K_{ij}u_j = f_i$$

where u and f are the displacements and externally applied forces at the nodal points. The formation of the K matrix is dependent on the type of problem being attacked, and this module will outline the approach for truss and linear elastic stress analyses. Commercial codes may have very large element libraries, with elements appropriate to a wide range of problem types. One of FEA's principal advantages is that many problem types can be addressed with the same code, merely by specifying the appropriate element types from the library.

3. *Post-processing:* In the earlier days of finite element analysis, the user would pore through reams of numbers generated by the code, listing displacements

and stresses at discrete positions within the model. It is easy to miss important trends and hot spots this way, and modern codes use graphical displays to assist in visualizing the results. A typical postprocessor display overlays colored contours representing stress levels on the model, showing a full-field picture similar to that of photo elastic or more experimental results.

3.2 Creation of the model

The first step for planning a numerical analysis is the creation of the model, for this purpose it is chosen to use *Abaqus* from *Dessault Systemes*. In this part is important to take into consideration some aspects related to the experimental test that will be carried out in the following steps and in particular about the physical model that is available to validate the crack identification method. To avoid future modification of the model and the repetition of the complete numerical simulation all physical element such as dimensions, material and boundary condition are chosen in this part. Considering the analytical model seen in the previous chapter (Fig. 43) both a model for the undamaged and damaged beam were created.

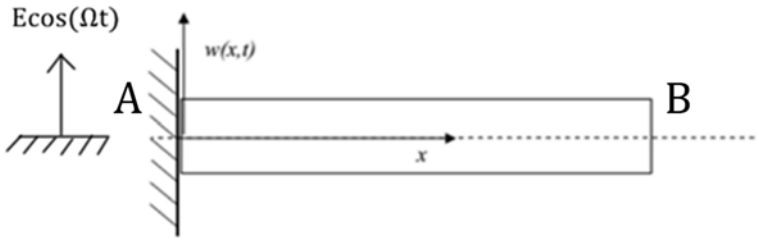

Fig. 43 – Model used for analytical analysis

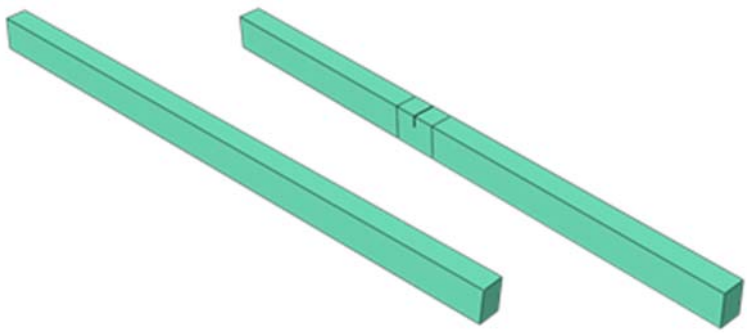

Fig. 44 – Abaqus model for undamaged (a) and damaged (b) beam

Material chosen for the beam is aluminum; section is rectangular with dimension of $15\ mm\ x\ 10\ mm$ and a total length of $260\ mm$. Crack is modelled as a simple cut

of depth 5 mm and width 0.25 mm that cover all the width of the beam (Fig. 45). All physical details like mass and density are resumed in Tab. 2.

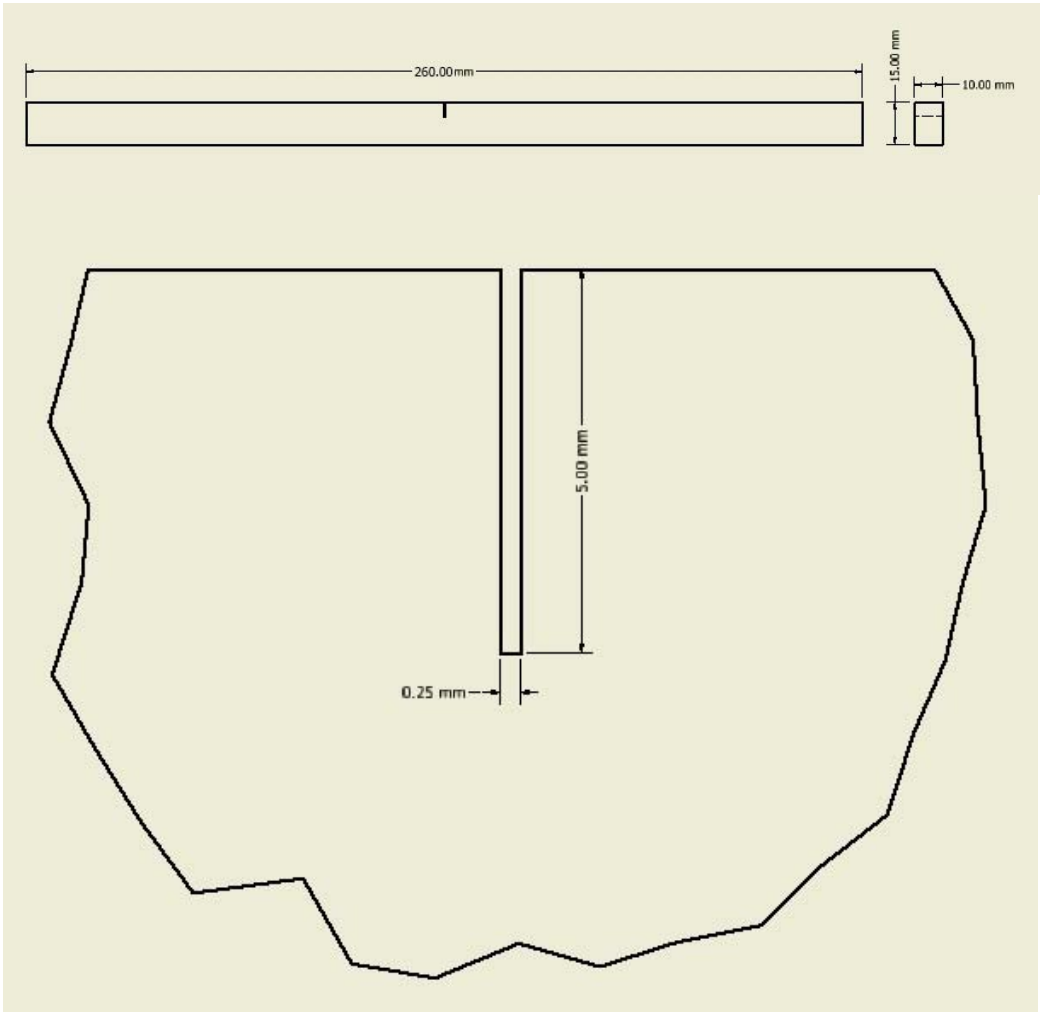

Fig. 45 – Damaged beam geometry (a); Crack details (b)

Tab. 2 – Physical detail for the beam

Material	*Aluminum*
Density	*2800 [kg/m3]*
Young's Modulus	*70000 [Mpa]*
Poisson ratio	*0.33*

For a more complete analysis, and to investigate about the change in natural frequencies due to the presence of the crack two different models are created for the damaged beam. Fig. 46 show the different crack configuration used for this purpose.

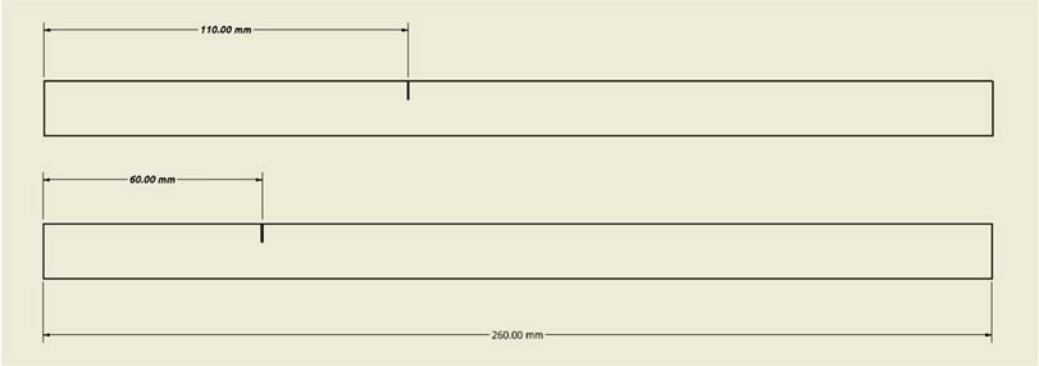

Fig. 46 – Crack configurations geometry

When all physical characteristics are defined, it is possible to complete the model inside Abaqus (Appendix A).

3.3 Natural frequencies

The first operation accomplished is about to verify the quality of the analytical model used to find the position of the curvature nodes. To evaluate that, is possible to check the difference in natural frequencies between analytical model and numerical ones. This can give an idea of the correspondence between the two models used and of the error that could be committed using one model instead the other.
In order to accomplish a good simulation, the 3D model previously created is used. The main reason for this choice relay on the fact that it will be possible to see all the mode of vibration of the beam and not only the ones that we will force with the boundary displacement. This will be useful especially during the experimental test on the real physical model (Appendix B).
Tab. 3 shows the results obtained from the simulation.

Tab. 3 – Natural frequencies of system for analytical and numerical analysis

	ANALYTICAL [Hz]	NUMERIC [Hz]	ERROR
Mode 1	177.5	177.78	0.15 %
Mode 2	1115	1097.1	1.6 %
Mode 3	3122	3001	3.8 %
Mode 4	6119	5696.4	6.9 %

Since the computational effort for this kind of simulation is not elevate and the mode shapes involves all axes *x,y,z*, the first ten *Natural Frequencies* ω_{oi} of the clamped beam are estimated for both damaged and undamaged model in order to observe changes due to the presence of the crack. Results are presented in Tab. 4.

Tab. 4 – Results obtained from Abaqus analysis on both model

		ABAQUS SYMULATION MODEL		
		UNCRACKED BEAM	CONFIGURATION 1	CONFIGURATION 2
Mode	Axis	Nat Freq [Hz]	Nat Freq [Hz]	Nat Freq [Hz]
1	X-Z	117,3	116,54	115,41
2	X-Y	177,78	173,31	167,21
3	X-Z	730,12	720,55	729,89
4	X-Y	1097,1	1044,2	1096,6
5	X-Z	2022,8	2013	2005
6	Y-Z	2430,4	2407,2	2396,6
7	X-Y	3001	2953,9	2902,8
8	X-Z	3905,4	3875,4	3854,8
9	X-Y	4815,7	4695	4643,4
10	X-Y	5696,4	5571,7	5510,5

Since the vertical displacement considered in analytical study (Paragraph 2.10) involves only plane *x-y* we expect to see only natural frequency highlighted in yellow during the simulation that we will carry out. From the table it is easy to see that crack changes natural frequencies of the beam as studied in the theory (Chapter 1). For the completeness of the results, in Fig. 47 the shapes of the vibration modes obtained from the simulation are presented.

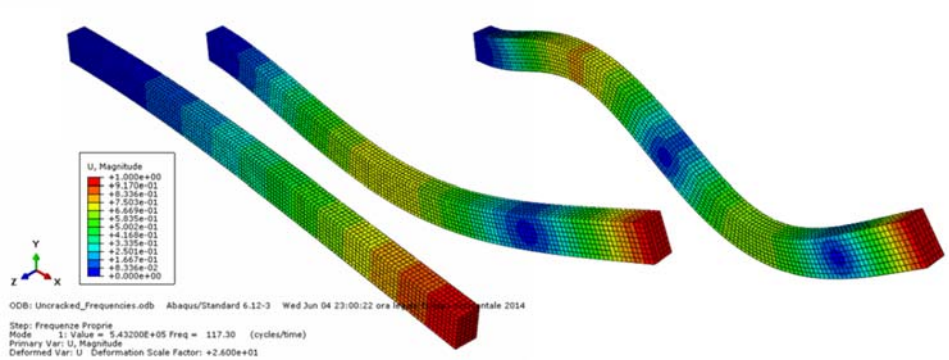

Fig. 47 – Shapes of vibration modes

3.4 Frequency response and curvature

In order to validate the performance of the crack identification method, the most important information obtainable from the FEA analysis is the system *Frequency Response.* This information is important because through it, it is possible to evaluate the position of the curvature nodes at each frequency. Since we need information in a certain range of frequency, it is used a Sweep to force the whole system in the boundary constrain (Appendix B).
Undamaged Beam Model is used for this purpose; this because we need to investigate where the cracked beam behave linearly and so, computational effort to solve a non-linear system would become useless.
Database created contain displacement values at each step-frequency of the sweep implemented. Information obtained will be used to calculate the curvature of the beam through the second derivative of the vertical displacement $w(x, f)$

$$\kappa = \frac{\partial^2 w}{\partial x^2}$$

As already done in Section 2.11 it is necessary to study the trend of such parameter and find where $\kappa = 0$ to find position of nodes at each frequency. For this purpose, a node-set is created (Appendix B.2) for the model and information are extracted for displacement, frequency and position respectively (Fig. 48).
It is obvious that precision of parameter κ is directly linked with the number of nodes used to divide the length of the structure. In order to obtain good results it is necessary to choose dimension of the mesh cleverly so that the distance between points is not too high.

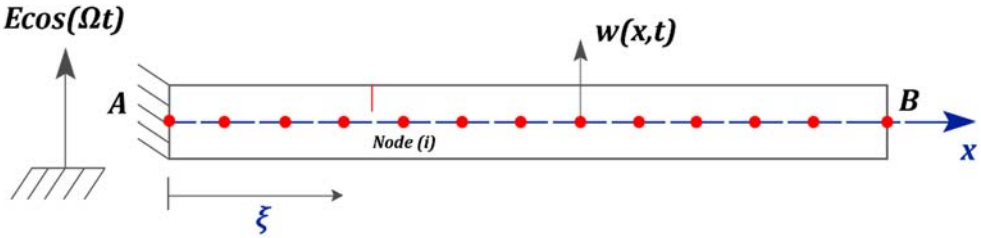

Fig. 48 – Set of points used to extract displacement values

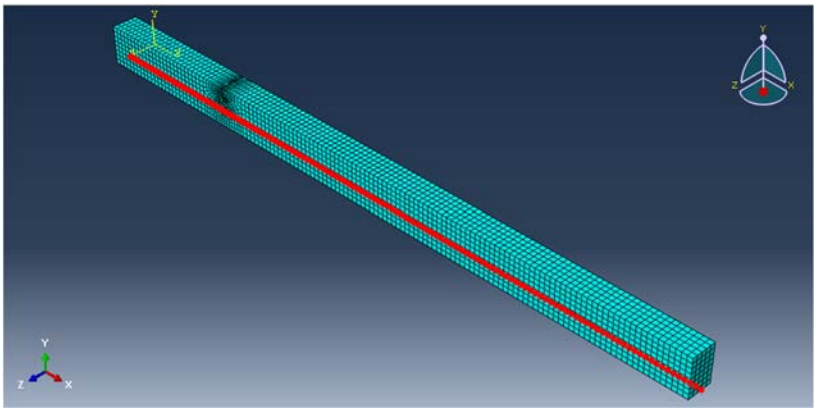

Fig. 49 – Set of points used in Abaqus 3D Model

From the simulation's field output a matrix and two vectors are created, *Pos(i)_NodeDisp, Pos(i)_NodeCoord* and *Pos(i)_Freq* and imported in the workspace of Matlab. Vector *Pos(i)_NodeCoord* contain coordinate values ξ_i of each node, *Pos(i)_Freq* contain frequency values in which the displacement is evaluated and finally matrix *Pos(i)_NodeDisp* contain displacement values for each node (rows) calculated for the single frequencies considered in the analysis (columns).
Data collected permitted the creation of the curvature κ function and so to obtain the same graph already obtained from analytical study of Section 2.11 (Fig. 50).

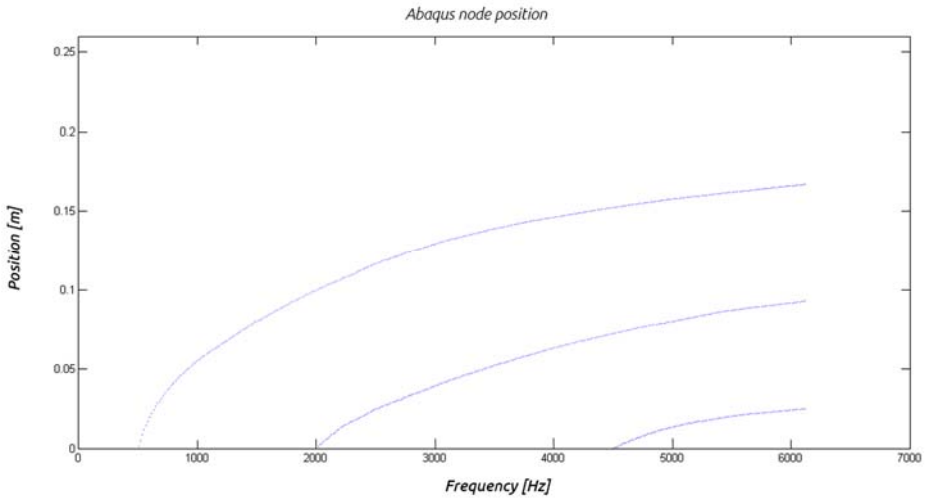

Fig. 50 – Curvature node position at each frequency

Now that Curvature node chart is obtained it is possible to test the crack identification method on a real system that will reproduce the one studied up to this time.

Chapter 4 EXPERIMENTAL TEST

Experimental test is the most critical part because will give us an idea on how much the method developed is precise and above all efficient. The main purpose of this section is to examine the possibility of estimating location of a crack by measuring the response of the free end of the beam when exited with a pulsing displacement in the constraint. This is achieved checking minimum of the Non-Linearity Index and using frequencies obtained as input for the *Curvature Node Graph*.

Frequency response of the system can be obtained using a Vibrant Table but, since the need is to reach high frequencies, it is important to choose it accurately.

For the purpose of the experiment an LDS Shaker Vibrator is used (Fig. 51). Datasheet report a *Useful Frequency Range* of 5 Hz – 9 kHz that make it ideal for our experimental test.

Performance Parameters and Characteristics*		
Shaker	**V406**	**V408**
Standard LDS Amplifier	PA500L	
Sine Force (peak) – forced air cooled	196 N	196 N
Armature Resonance (f_n)	9 kHz	9 kHz
Useful Frequency Range	5 Hz – 9 kHz	5 Hz – 9 kHz
Effective Mass of Moving Element	0.200 kg	0.200 kg
Velocity (sine peak)	1.78 m/s	1.78 m/s
Maximum Acceleration (sine peak) – naturally cooled	50 g	50 g
Maximum Acceleration (sine peak) – forced air cooled	100 g	100 g
Max. Random Force (rms)	89 N	89 N
Displacement (pk–pk) – continuous	17.6 mm	17.6 mm
Suspension Axial Stiffness	12.3 N/mm	12.3 N/mm
Aux. Suspension Axial Stiffness	35.1 N/mm	35.1 N/mm
Shaker Body Mass – base mounted	14.1 kg	14.1 kg
Shaker Body Mass – trunnion mounted	22.7 kg	22.7 kg
Impedance at 500 Hz	2.5 Ω	2.5 Ω
Cooling Air Flow	0.014 m^3/s	0.014 m^3/s
Armature Diameter	38 mm	38 mm
Armature Insert Pattern:		
Centre Insert	1	1
2.54 mm PCD†	6	6
Insert Threads	M4	10/32 UNF

Fig. 51 – LDS Vibrator V406 and V408 datasheet

Data will be recorded from two accelerometer positioned in the constraint and at the free end of the beam, in this way it is possible to obtain the transfer function of the system that will be used for a comparison with the analytical and numerical model. The choice of the accelerometer to use for data acquisition is linked to two aspects, the first, more important, directly connected with the maximum energy that the

Vibrator can introduce in the system and the other to the necessity to not affect the behavior of the system.
This second aspects is valid only for the accelerometer that will be applied on the free end of the beam that could move the natural frequency of the system due to its mass. Looking at the LDS Vibrator datasheet (Fig. 51), we note that it is reported a maximum acceleration equal to:

$$max_{acc} = 100 \cdot 9.8 \left[\frac{m}{s^2}\right] = 980 \left[\frac{m}{s^2}\right]$$

For the constrain it is worth to use a *200 G* accelerometer in this case and at least a *500 G* accelerometer for the free end since we expect to observe greater acceleration in this point. Final choice was for PCB Model 353B02 and 352A25 for the constrain and the free end respectively (Fig. 52).

Fig. 52 – Accelerometer used for constrain (a) and free end (b)

The complete equipment used for experimental test consist of (Fig. 53):

- LDS V406/8 Series Vibrator
- LDS PA100E Power Amplifier
- Agilent – Function Waveform generator Model 33220A
- PCB – ICP Accelerometer Model 352A25
- PCB – ICP Accelerometer Model 353B02
- PCB – Amplifier Model 482A16
- National Instruments – cDAQ-9178 Chassis
- National Instruments – NI 9239 Input Module

Fig. 53 – Complete equipment used for acquisitions

The system used in our experimental test must be identical to the one used in analytical study (Fig. 43), so it is necessary to physically reproduce the constraint for boundary condition in point A. With the help of *Autodesk Inventor* a clamp it is created and it is used to fix the beam to the *LDS Vibrator*. Dimension of the constraint must be considered for this purpose to permit the attachment of the beam to the instrument (Fig. 54).

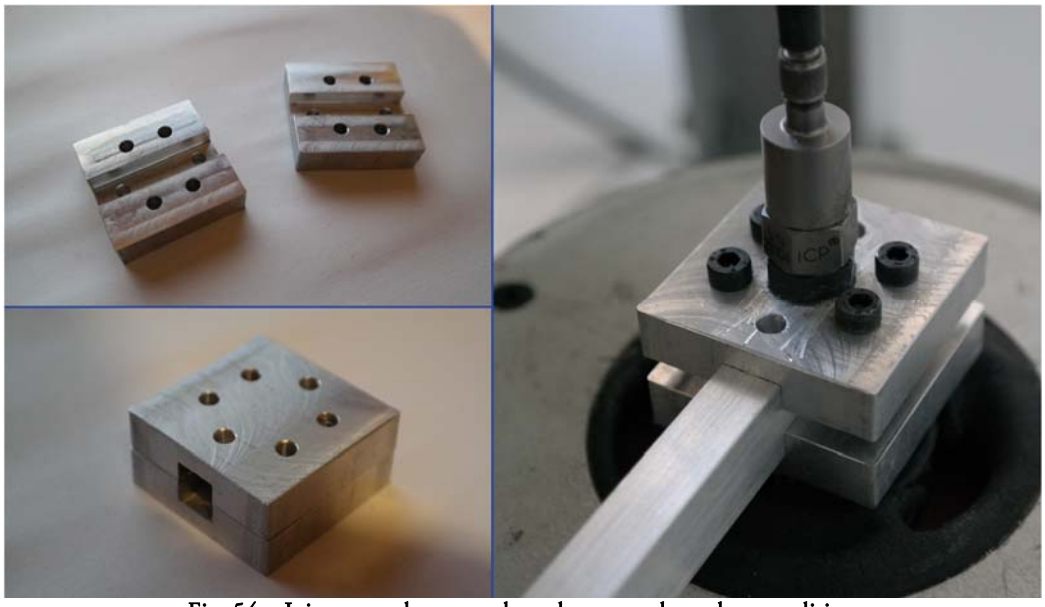

Fig. 54 – Joint created to reproduce the system boundary condition

To maintain coherence with the Abaqus model used in previous chapter, a set of aluminum bar of the same section is created. Crack is obtained using a 0.25 mm blade from a *Mechanical Precision Processing*.
The clamp created guarantee attachment to the LDS Vibrator through its M4 holes and make it possible to reproduce the boundary condition used for the analytical model (Fig. 36).
Now the last important aspect to study before pratical experimental acquisition is relative to the influence of the free end accelerometer on the system behavior. This operation could easily dealt with Abaqus using the model already created.

4.1 Accelerometer physical influence on system behavior

Results obtained from numerical simulations do not take into account the influence that the accelerometer could have on the system behavior. To check if its inertia may distort the results it is possible to edit Abaqus model verify how the accelerometer change natural frequencies positions.
Since dimensions and weight are reported in the datasheet (Tab. 5), it was possible to calculate the inertial contribute given to the system.

Tab. 5 – Accelerometer physical properties

PHYSICAL PROPERTIES	
Weight	0.6 grams
Height	3.6 mm
Length	11.4 mm
Width	6.4 mm

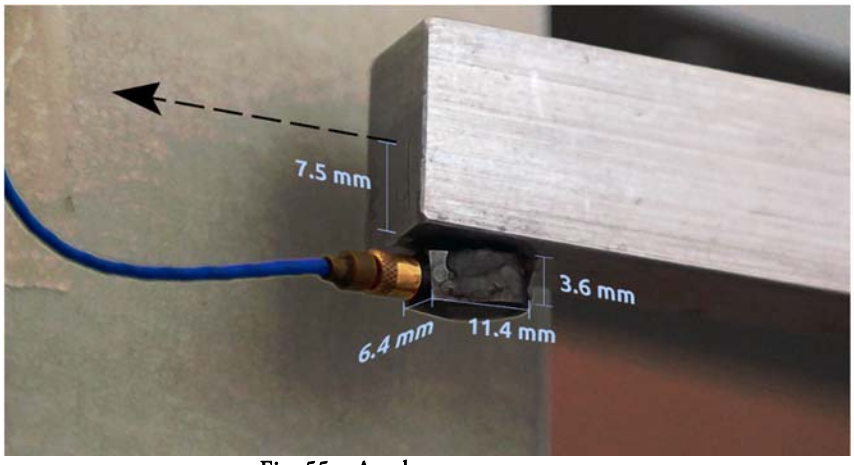

Fig. 55 – Accelerometer geometry

Considering the setup shown in Fig. 55 it is possible to calculate the values to be used for mass and inertia inside the numerical simulation.
Mass parameter must be inserted as *ton* instead of *kg* as already saw in Appendix A so:

$$m = 0.6 \cdot 10^{-3}[kg] = 6 \cdot 10^{-7}[tonn]$$

Now it is possible to calculate the whole inertia given to the system. The generic formula for a continuous body is:

$$J = \int_V \rho r^2 dV$$

that become

$$J = b \cdot \rho \int_A (x^2 + y^2) dA$$

$$J_z = \left(\frac{6.4 \cdot 11.4^3}{12} + \frac{6.4 \cdot 3.6^3}{12} \right) [mm^4] \cdot \frac{6 \cdot 10^{-7}[tonn]}{6.4 \cdot 3.6 \cdot 11.4\ [mm^3]} \cdot 6.4[mm]$$

And so

$$J_z = 1.2 \cdot 10^{-5}[tonn \cdot mm^2]$$

Now we proceed calculating

$$J_{ZT} = m \left(7.5 + \frac{3.6}{2} \right)^2 [mm^2] = 5.2 \cdot 10^{-5}\ [tonn \cdot mm^2]$$

The calculus for inertial value finally is:

$$J_{tot} = 6.4 \cdot 10^{-5}[ton\ mm^2]$$

This value obtained is used in Abaqus to evaluate the influence of the accelerometer on the natural frequency.
Results obtained from simulation are resumed in the following table.

Tab. 6 – Influence of accelerometer on natural frequencies

	Mode 1	Mode 2	Mode 3
Natural frequency	175.82	1085.05	2968.23
Difference	1.1%	1%	1%

It is noticeable that an accelerometer, as the one chosen, can cause a 1% natural frequency variation. This is totally acceptable and suggest that results won't be distorted by the weight of the instrument used.

4.2 Transfer function

The first test is about to verify if the physical model is compatible with the one used for numerical and analytical study. This part is achievable simply comparing the natural frequency obtained from the evaluation of the transfer function.
System is excited in the proper frequency range to contain the first three natural frequency and the transfer function is obtained with the help of Matlab.
Since the *Vibrator* has a sweep limitation of *500 seconds*, different windows were used in order to have a step of $1\ Hz/sec$.

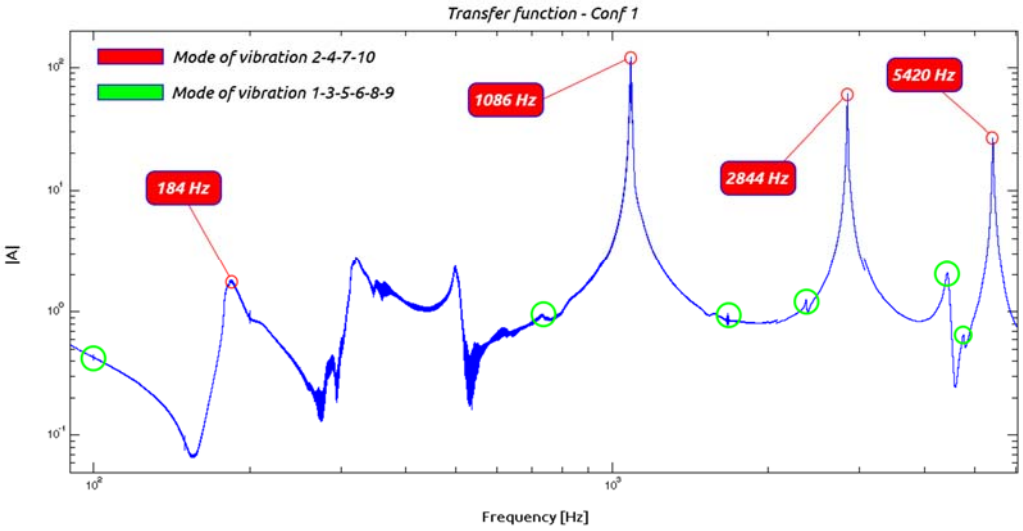

Fig. 56 – Transfer function for crack configuration #1

Transfer function obtained is compared with Tab. 3 in order to verify results compatibility. Fig. 56 and Fig. 57 show that all the natural frequencies obtained from analytical and numerical simulation are present. Values are different since the crack has the property of changing natural frequencies in different ways depending on the mode considered and its position along the beam.
Minimum peaks are observable for modes that do not involve *y* axe. Other peaks and antiresonances are present and this could be related with Vibrator Table features that has a bad performance at particular frequencies and with the joint that could only in part emulate the behavior of a perfect clamp.

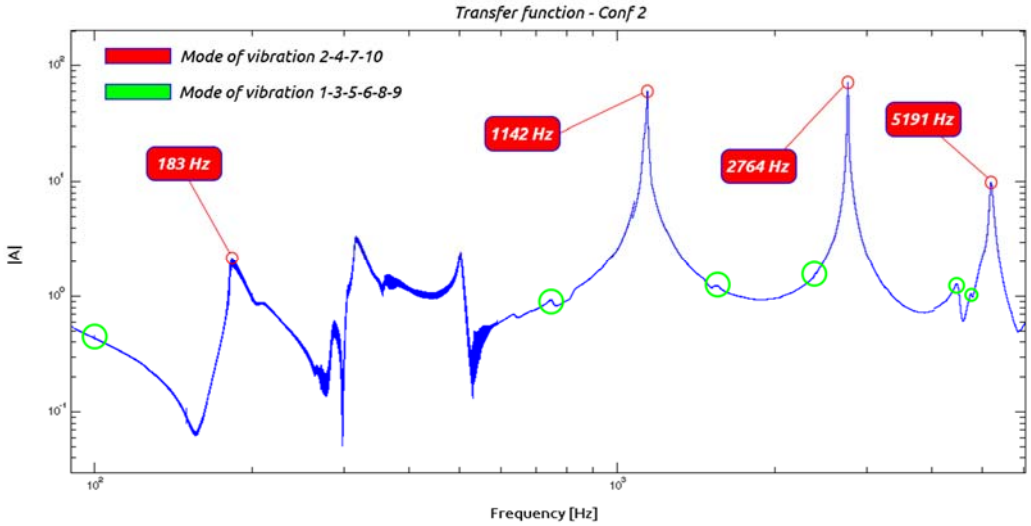

Fig. 57 – Transfer function for crack configuration #2

To investigate the reason of such behavior in the range 200 Hz – 600 Hz an acquisition on the Vibrator Head is performed using only the PCB Model 353B02 Accelerometer. Fig. 58 shows results obtained using the Fourier Transform algorithm.

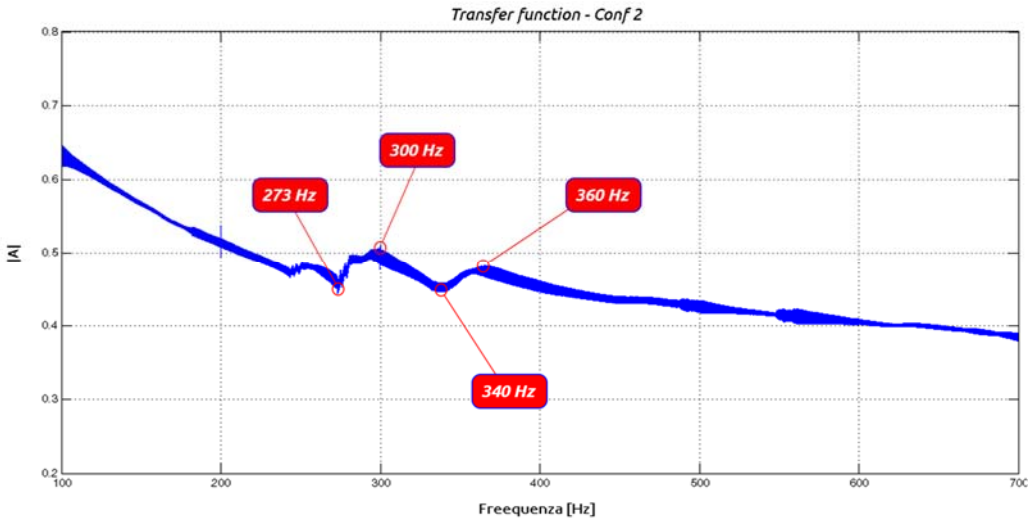

Fig. 58 – Frequency response for Vibrator's head

From Fig. 58 it is observable that only the first two peaks are attributable to the ones reported in the transfer function studied in Fig. 56-57. It is concluded that Frequency

range from 200 Hz to 600 Hz is disturbed from the presence of the joint used to clamp the beam that is not perfect as the one obtainable with numerical analysis.

4.3 Application of the algorithm of crack identification

Equipment used in this experimental test permits to excite the system up to *9 kHz* but for the purpose it is used *5 kHz* as limit. For this reason, it is necessary to acquire at least at 50 kHz in order to analyze the super-harmonic frequencies due to the non-linear behavior of the system.
Frequency resolution is evaluated as:

$$\Delta f = \frac{1}{T} = 0.002\ Hz$$

Since the Nyquist frequency is:

$$f_{Nyquist} = \frac{f_{samp}}{2} = \frac{50\ kHz}{2} = \mathbf{25\ kHz}$$

With this sampling frequency, it will be possible to observe up to four super-harmonic frequencies of the resonant.
For the generation of the boundary displacement it is used a *Sine Wave Generator.* Starting frequency it is chosen at *500 Hz* for two reasons, firstly Vibrator has the difficulty to transfer enough energy to the system at low frequency and finally the *Curvature Node Graph* has the first curve from about *500 Hz*.
As already mentioned it is important to consider the intrinsic connection between frequency-step and spatial resolution because of the node repositioning at every frequency. Since it is important to excite the system in all frequency range, it is important to choose intelligently Sweep-Step parameter to avoid bad results.
To gain better results it is a good procedure to first perform a fast sweep of $1\ Hz\ /\ sec$ maximum and then perform slowest sweeps in important frequency windows.
Acceleration of the free end is acquired for both damaged beams and *NL_Index* is generated with the script created in Matlab. Fig. 59 shows results obtained for the first beam relative to *Crack Configuration #1* in which the damage is located *100 mm* from the constrain.

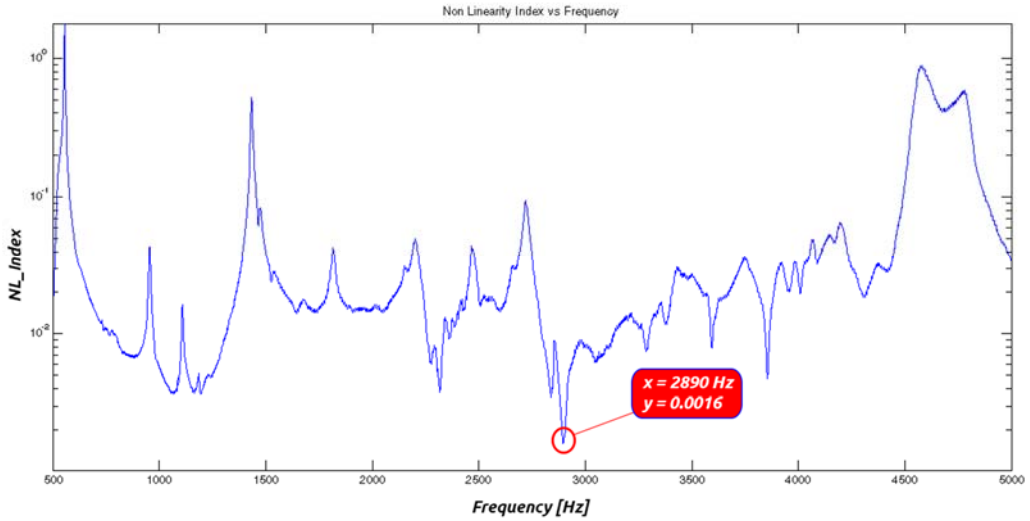

Fig. 59 – *NL_Index* for Configuration #1 (Crack located at 42.3% of length)

Frequency obtained gives a crack located at *46.7%* of the beam length that correspond to *121 mm.* The error is about *4.5%* that is totally acceptable (Fig. 60).

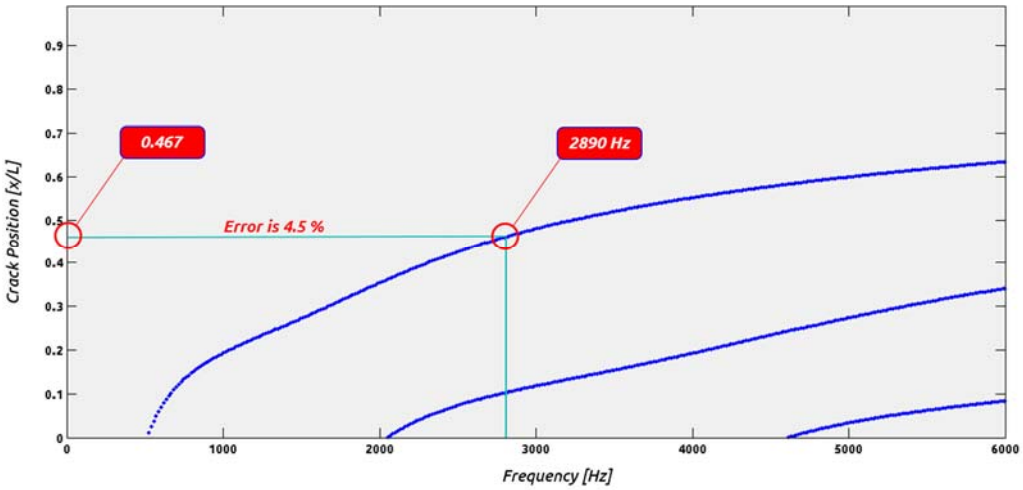

Fig. 60 – Estimation of damage location for Crack Configuration #1

Now an important observation on the use of the graph in Fig. 60. As is possible to see, the frequency related to the *NL_Index* minimum leads to two blue lines of the curvature nodes. The solution could not be univocal indeed; in this case, it is necessary to investigate about the other possible crack location detected. First blue line intercepted would indicate a position at 11% of beam length and this should necessary leads to *NL_Index* minimum at 684 Hz (Fig. 61).

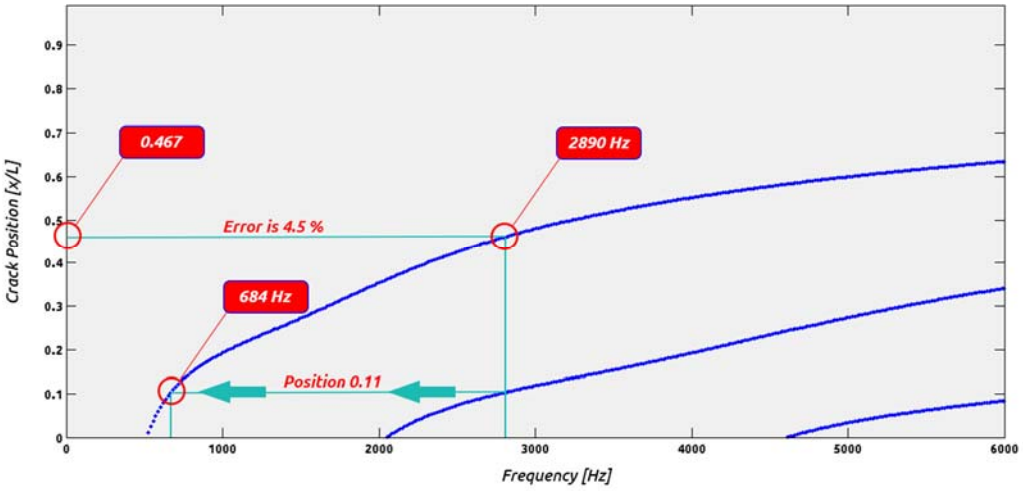

Fig. 61 – Investigation about the first node for Configuration #1

Returning with this frequency in the *NL_Index* plot it is easy to see that there is no minimum point at that particular frequency so this indicate that the crack is on the second node of the curvature as previously shown (Fig. 62).

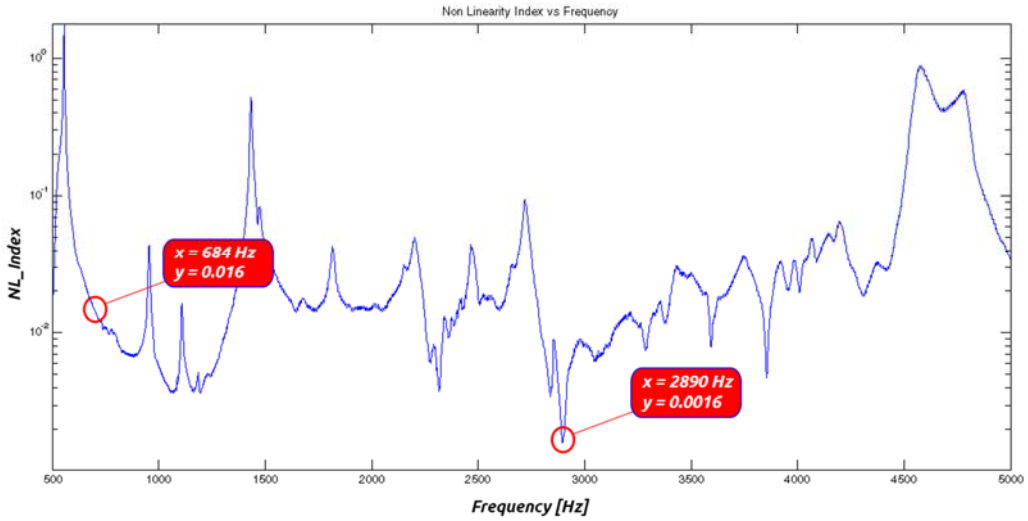

Fig. 62 – Investigation about the first node for Configuration #1

Same tests were performed on *Crack Configuration #2 Beam.* Results obtained from *NL_Index* (Fig. 63) show a mimimum at 1240 Hz that should indicate a crack located at 23.5% of beam length (Fig. 64). In this case error is only 0.4%.

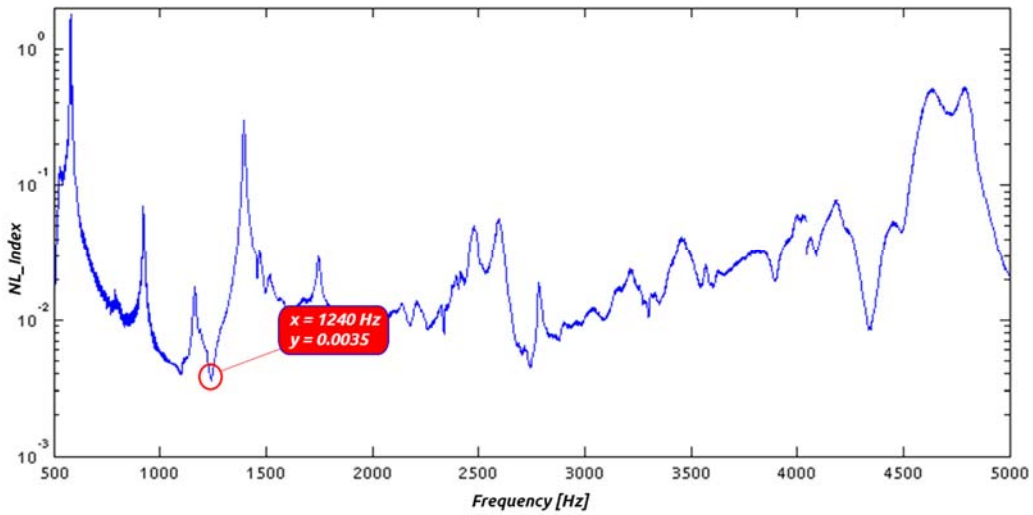

Fig. 63 – *NL_Index* for Configuration #2 (Crack located at 60 mm)

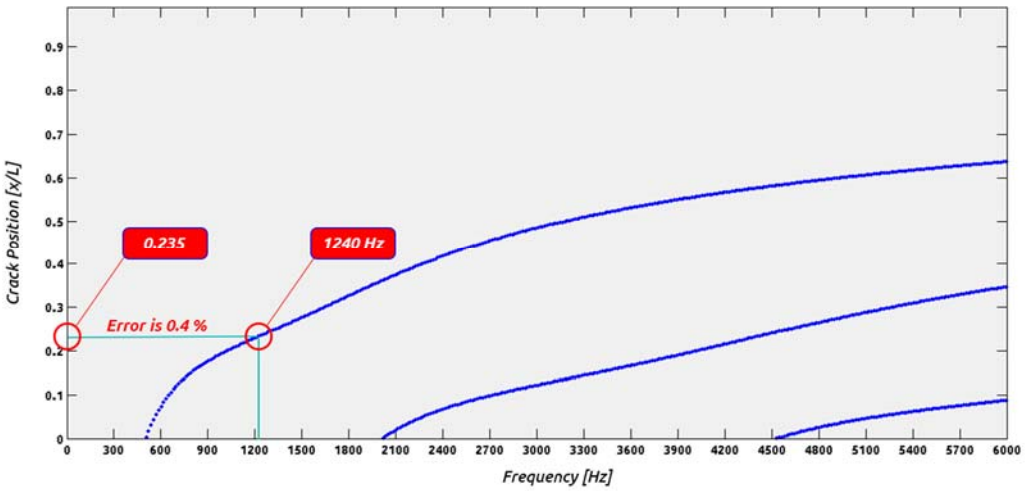

Fig. 64 – Crack location for Configuration #2

The second blue curve could be used to find a validation on the position just obtained. Position 23.5% would be linked with another minimum of the *NL_Index* related to frequency 4421 Hz (Fig. 65).
Frequency just recorded it is used inside *NL_Index* plot to find out if it correspond to a minimum of its trend (Fig. 66).

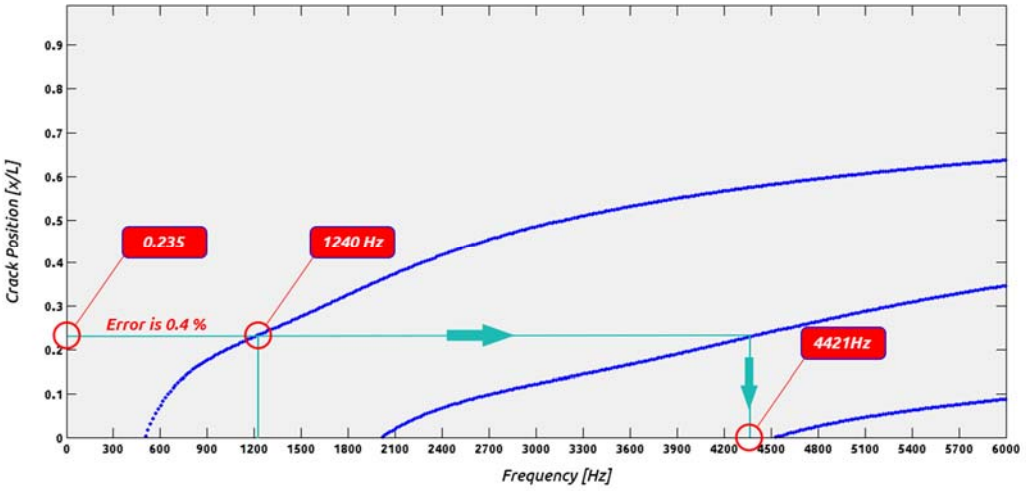

Fig. 65 – Investigation on higher modes

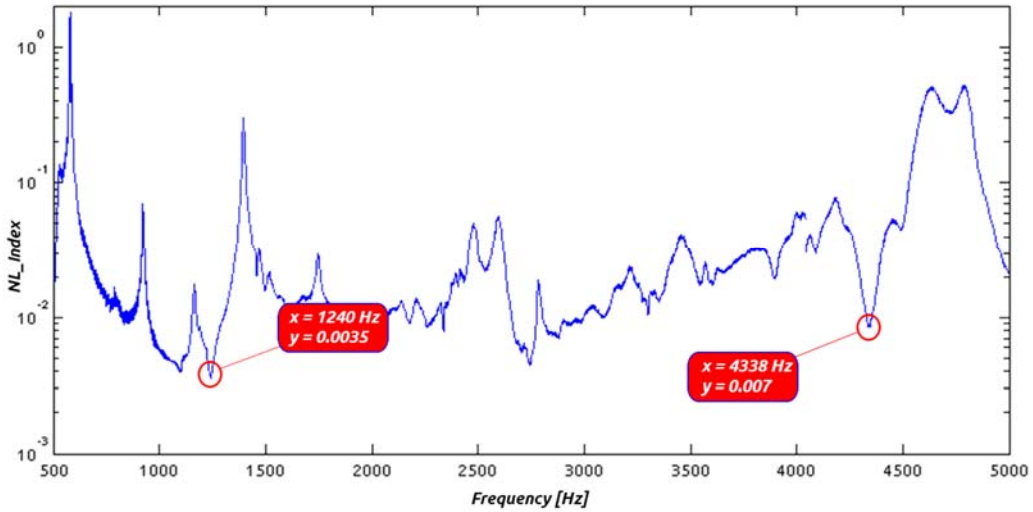

Fig. 66 – NL_Index Investigation on higher modes

It is notable that there is a minimum point at frequency 4338 Hz that is compatible with what we were searching. In this case, an error of 1.8% leads to the conclusion that the crack is certainly located at 23.5% of beam length.
This procedure could be used also to check validation on other minimum highlighted from *NL_Index,* for example frequency 2740 Hz (Fig. 67).

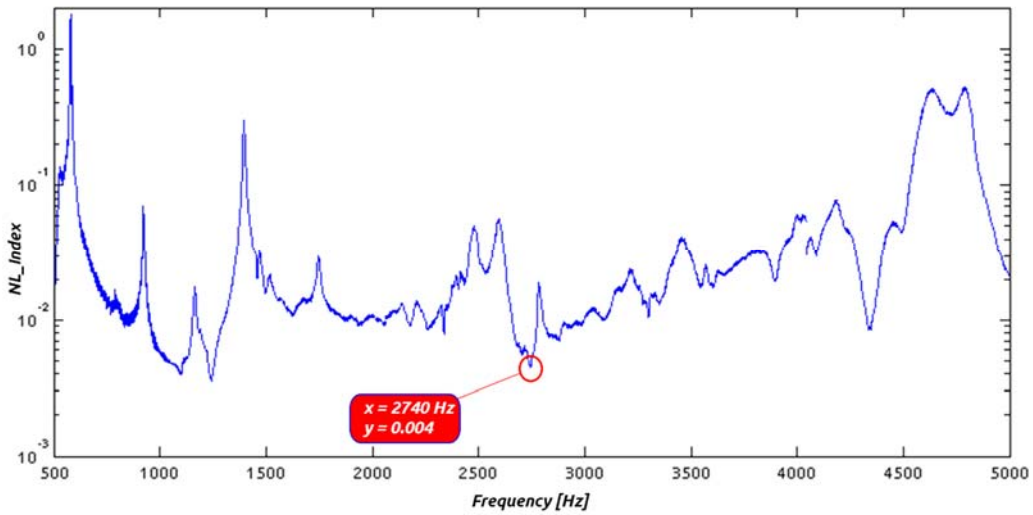

Fig. 67 – Investigation on other minimum points

Entering with this value in the *Curvature Node plot* it is found a relation with a possible crack located at 10.6 % of beam length (Fig. 68). This is the first curvature node of the second vibration mode but is also the only node for mode 1 at frequency 664 Hz.

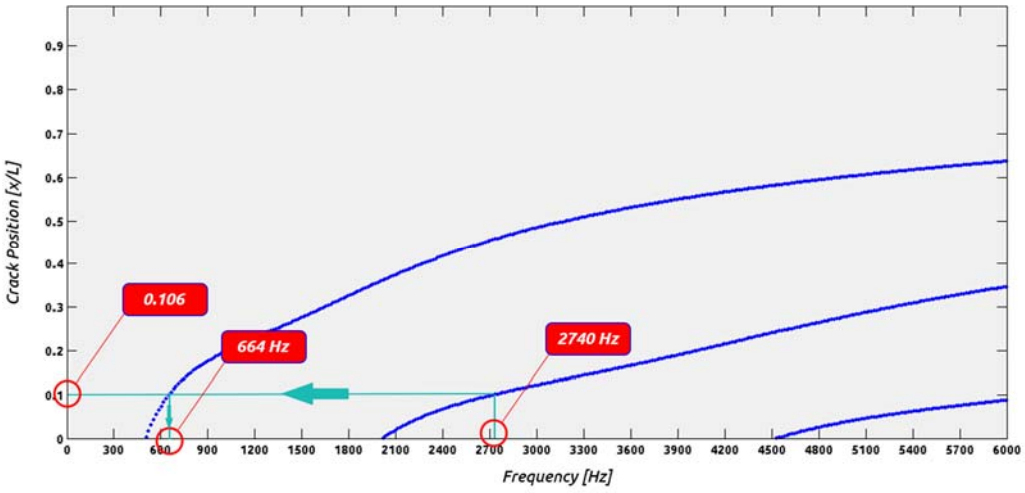

Fig. 68 – Possible crack location for other minimum point

NL_Index trend shows no minimum at this frequency and so, there is no crack located at 10.6 % of beam length (Fig. 69).

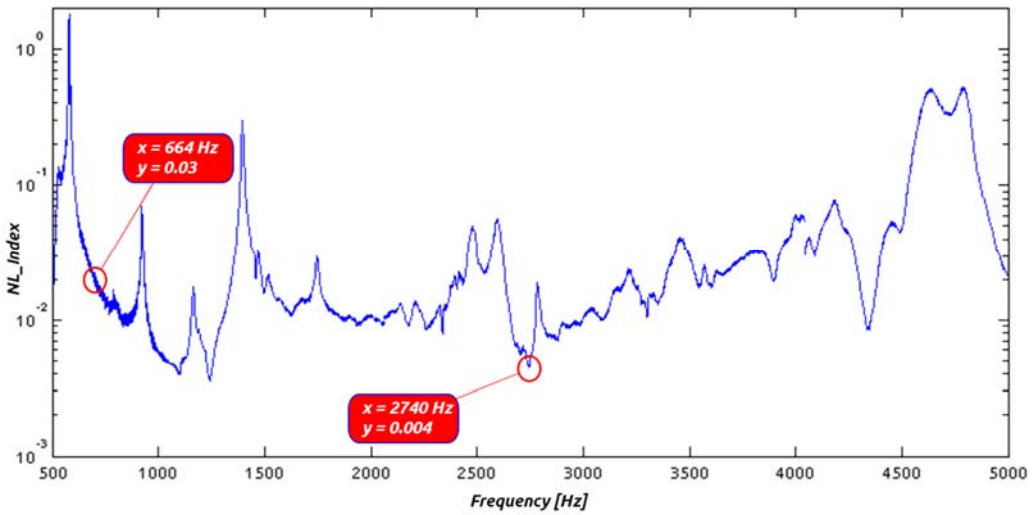

Fig. 69 – NL_Index value at frequency 664 Hz

From the previous experiment, it is easy to understand that this procedure is useful to confirm as well as to deny the presence and the location of a crack.

CONCLUSIONS

With the objective of developing a Non-Destructive method to locate the presence of a crack in a structure it was studied the frequency behavior of the system when exited with a pulsing displacement.
The method presented was tested on a real model that include two cracked beams and a system to force them in a certain range of frequency.
The main advantage of this method despite the others studied in the first part of this paper, is the possibility to obtain useful information to locate the crack with only a single sensor measuring in a single point of the structure.
Data are obtained from an accelerometer and processed in Matlab were the Scripts created permitted the creation of the *Non-Linearity Index* in automatic way.
For the success of the method is necessary to have the position of the curvature node at each frequency, this can be achieved in two way, by analytical study and by numerical study. The case used for the experiment was a simple clamped beam and so has given the opportunity of using both method due to geometry simplicity.
Model created were compared using results obtained from their natural frequencies extraction and shows that difference is minimal. This justify the use of a costly method like the analytical one for simple geometries as beams.
On the other hand, FEA software analysis is expensive but more flexible and permits to treat complex geometries easily extending the usability of the method to all mechanical structures.
Real physical tests highlighted problems involved in the methodology that need to be faced to improve the performance. First of all the implicit difference that will ever exist between a numerical or more generally ideal boundary condition and a real one.
Anyway, results obtained are encouraging and demonstrate that the crack location is identifiable with the method presented. Crack identification was successful in both cases locating the crack with a maximum error of 4.5%. This could be in part related to the 1% influence of the accelerometer inertia and in part to the joint behavior.
Results suggest that the method is applicable and future studies could be conducted on the subject. Versatility of the method and innovation on the use of super-harmonics lead to a possible publication to describe completely this new crack identification method and its possible enhancement to improve overall performance and to be adapted for the localization of different type of cracks.

Appendix A

Creation of the model is a delicate part since it is important to reproduce accurately the physical model that must be analysed. There are different ways to obtain a good model and they are all related with the type of analysis to be carried out.

Inside the *Part Module* of Abaqus is possible to choose the kind of model to use for the analysis (Fig. 70). For the creation of complex systems as the ones represented from cracked beams it is better to use a 3D Deformable Solid Shape while for undamaged beam and other kind of simple geometry it is possible to use Wire Shapes. It is important to specify that Wire Shapes Models are more simple to treat with since Mesh operations are easier.

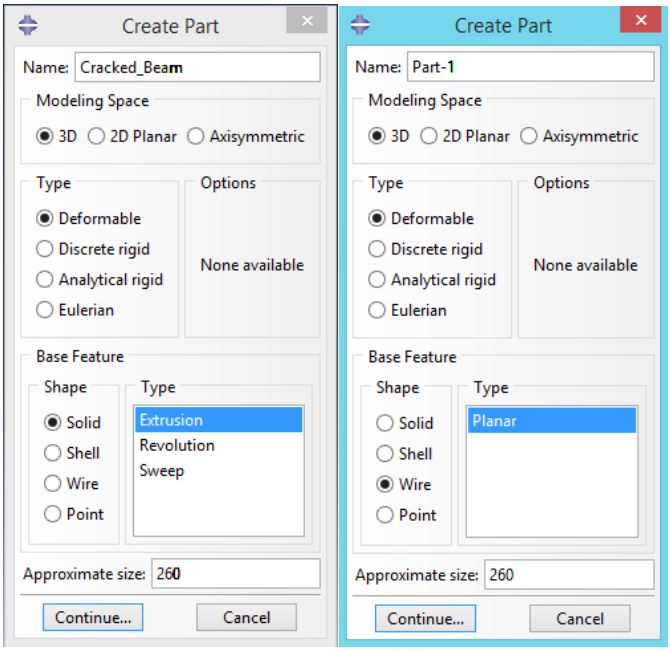

Fig. 70 – Creation of the Part

After that geometry is assigned in *Part Module* it is possible to assign all physical properties to the shape with the *Property Module* (Fig. 71).

Since we need to deal with a real physical model in the following steps, it is important to choose these parameters correctly to prevent further modification of the model.

Tab. 2 resume all physical properties used to create the model. Since geometry created is measured in $[mm]$ and the Young's Modulus is defined in $[N/mm^2]$ it is

important to use $[ton/mm^3]$ instead of $[kg/m^3]$ for material density value to avoid wrong results.

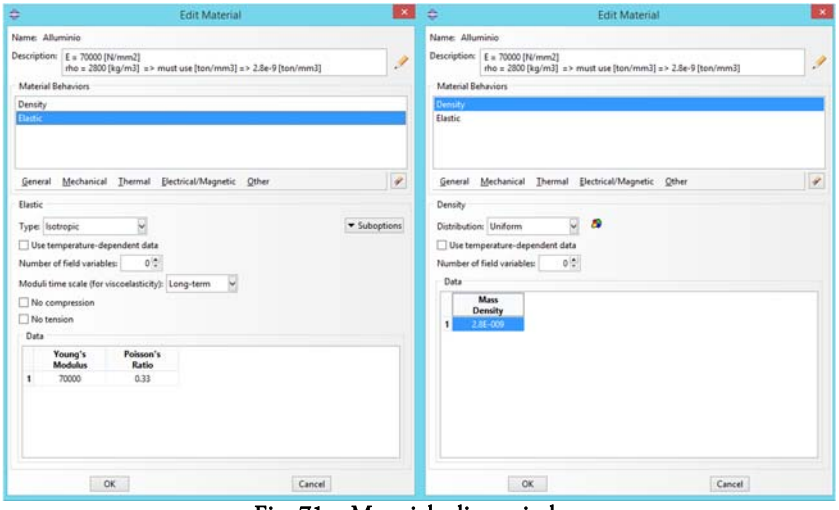

Fig. 71 – Material editor window

Now that geometry and physical properties are assigned it is necessary to reproduce the boundary conditions used in the analytical configuration used in Section 2.7. Analytical model consist of a clamped beam with a pulsing boundary displacement. Moving forward to the *Load Module* the boundary conditions are chosen.
Since point A represent the clamped constrain (Fig. 43) it is necessary to insert a Displacement and Rotation boundary condition at the left side of the beam as initial condition (Fig. 72).

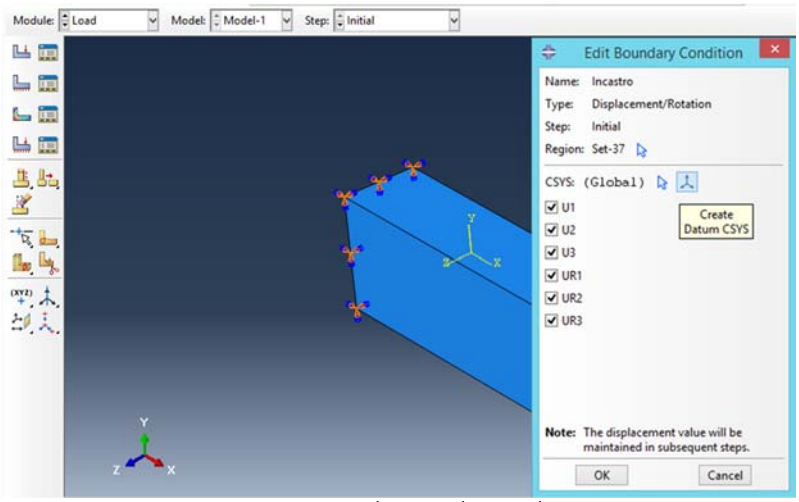

Fig. 72 – Boundary condition editor

In this section, the boundary pulsing displacement it is not considered and will be inserted for the simulation that require it to run properly.
Once boundary condition are reproduced as in the analytical model studied, it is time to enter in *Mesh Module* to define number and type of element to use.
Even though for following analysis it is used a Wire Shape model, it is show how to deal with complex geometries and so how to mesh a 3D Solid Shape model.
Mesh operation is the critical part in this kind of simulation, the goal is to have an accurate discretization of the model but at the same time maintain low computational effort. In order to achieve this result a good compromise is mandatory so it is chosen to divide the model in 3 different sections as in Fig. 73. In this way it is possible to choose two different element size dimension for the mesh, the first smaller to describe the behavior in the neighborhood of the crack and the second largest for the parts far from it (Fig. 74).

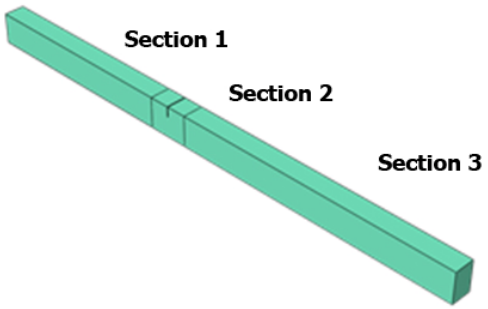

Fig. 73 – Partition of the model for numerical analysis

It is important to note that there is no a right or wrong element dimension for the creation of the Mesh. In order to achieve good results it is first important that the size of the element fits well in the geometry of the shape; sometimes it takes several attempts before achieving a satisfactory result.

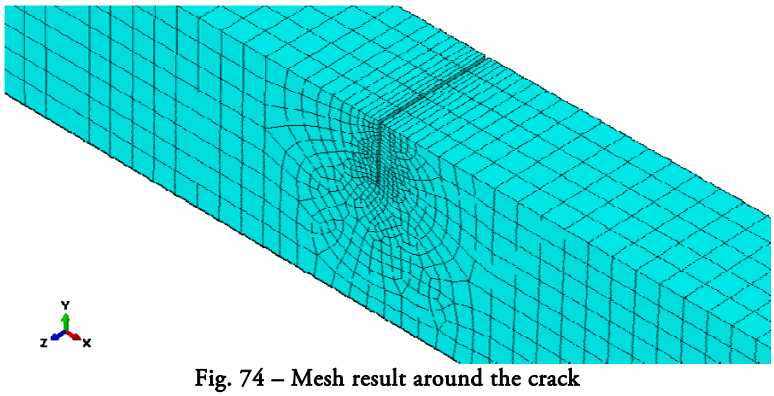

Fig. 74 – Mesh result around the crack

When element dimension is defined, it is possible to choose the type of element to assign at each session. For the kind of simulation to carry out on the model it is sufficient to assign *3D Stress Linear Elements* (Fig. 75).

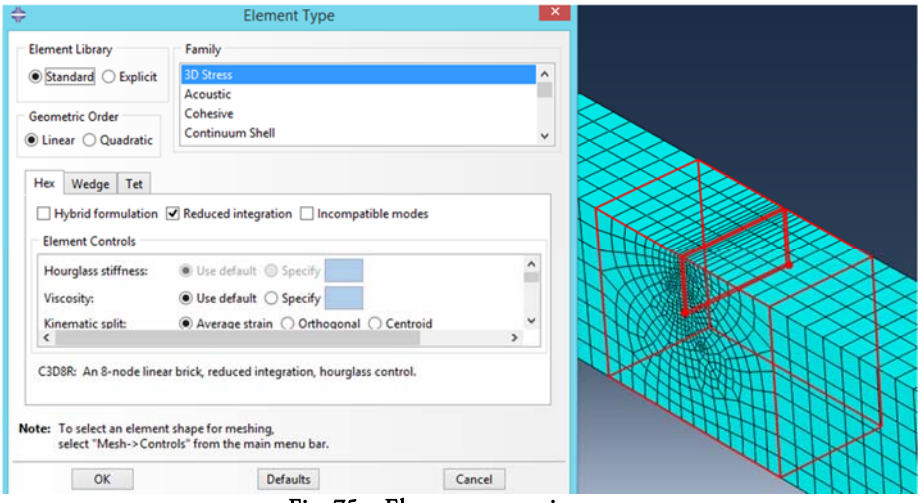

Fig. 75 – Element type assignment

After the completion of the mesh it is possible to implement the numerical analysis useful to get information for the application of the crack identification method. This is practicable editing the *Step Module* of Abaqus that provide numerous tools to accomplish every kind of simulation that is needed.

Appendix B

Natural frequency estimation

To obtain natural frequencies and mode of vibration it is necessary to go inside the *Step Module* of Abaqus and create a new step. Inside the editor, it is necessary to choose *Linear Perturbation Procedure* → *Frequency* (Fig. 76).

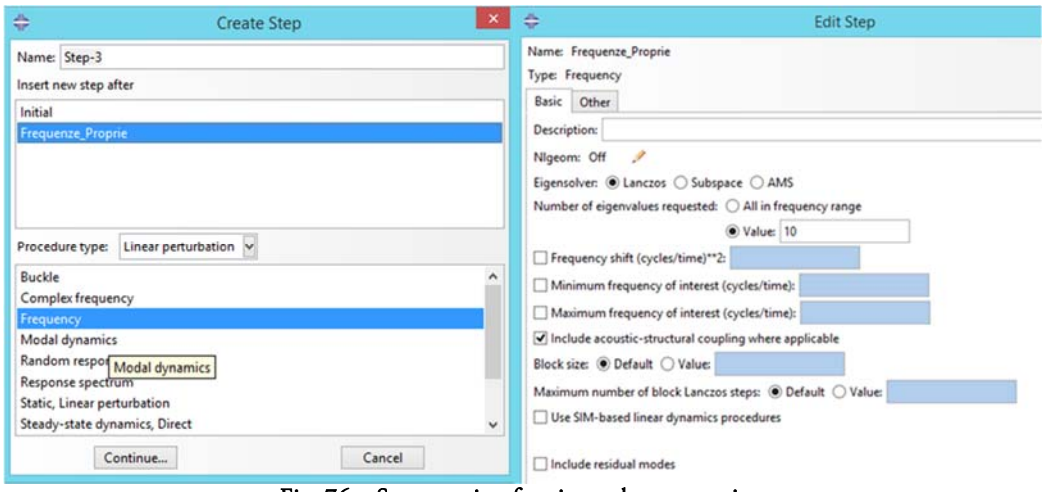

Fig. 76 – Step creation for eigenvalues extraction

In the following window it is possible to setup the Eigen-solver to use as well as the number of natural frequencies to acquire. Since computational effort is not elevate for this kind of numerical analysis it is best to extract the first 10 natural frequencies especially because the model used is free to vibrate in the whole space and so modes of vibration will include all $x - y - z$ axes.

Frequency response

Frequency response of the system is important to achieve displacement information of the beam at each frequency.
The operation consist of setting up a frequency sweep for the pulsing displacement at the constrain. To do that it is necessary to create another step inside the *Step Module* of Abaqus, this will be called "Sweep" to prevent confusion. The new step is created choosing a *Linear Perturbation* procedure and then *Steady-State Dynamic, Direct* (Fig. 77 (a)).

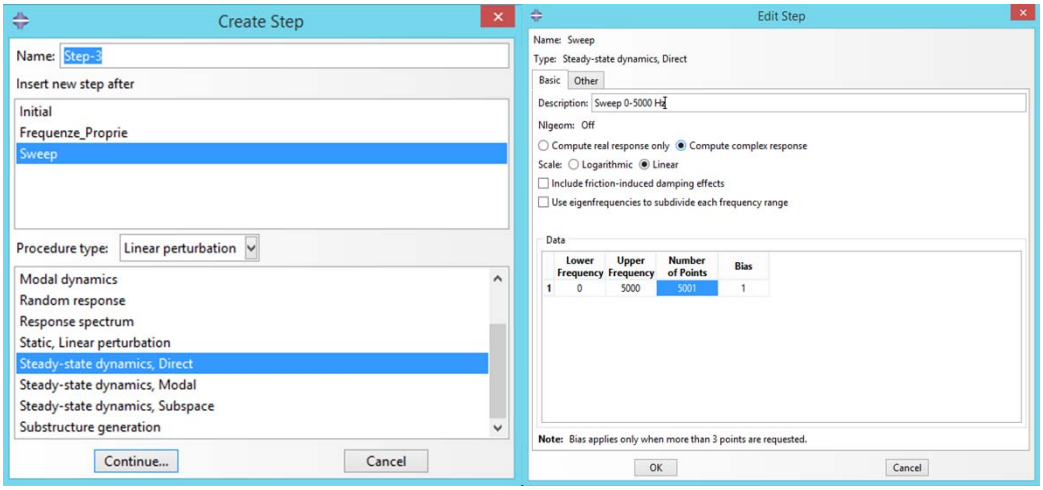

Fig. 77 – Step creation for sweep frequency response

The new window in (Fig. 77 (b)) shows useful parameter to be edited. It is possible to choose the Lower and the Upper frequency of the sweep as well as the number of points that substantially correspond to the frequency resolution that we need in the results. For the purpose of the numerical analysis that will be executed on the model it is set up a frequency sweep from 0 Hz to 5000 Hz with a step of 1 Hz and so choosing 5001 points.

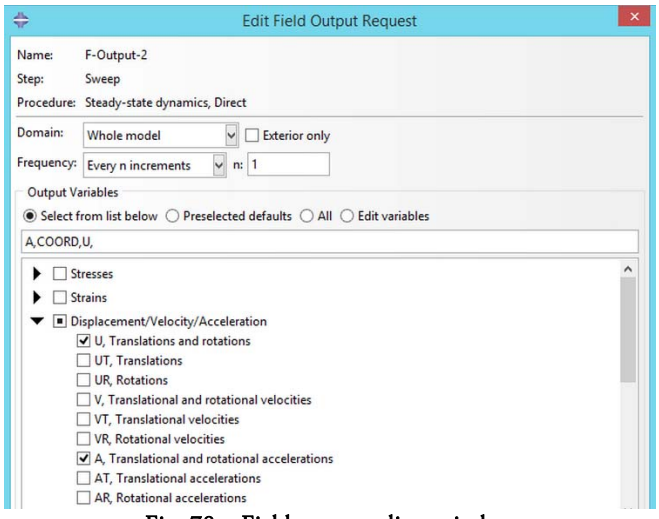

Fig. 78 – Field output editor window

Sweep Simulation is computationally hard and so it is a good procedure to edit the *Field Output* of Abaqus (Fig. 78) and leave only the calculus that effectively are needed. In this case, the necessity is to extract coordinates, displacements and

accelerations. For this purpose a set of nodal points is created to easily extract tabular data from them. This is done in *Tools* → *Set* → *Create* and selecting on the viewport the points to include in the set (Fig. 79)

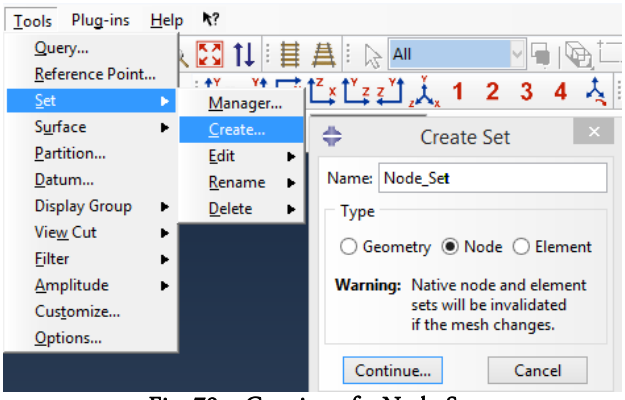

Fig. 79 – Creation of a Node-Set

Once the sweep step is created, it is necessary to edit boundary condition for it. This is done inside the *Load Module.* To obtain the same results of the analytical model studied it is necessary to setup the vertical displacement of the constrain. In the *Boundary condition Editor* it is possible to chose the interested step and so on to change values for each degree of freedom. In this case d.o.f. U2 is edited as shown in Fig. 80.

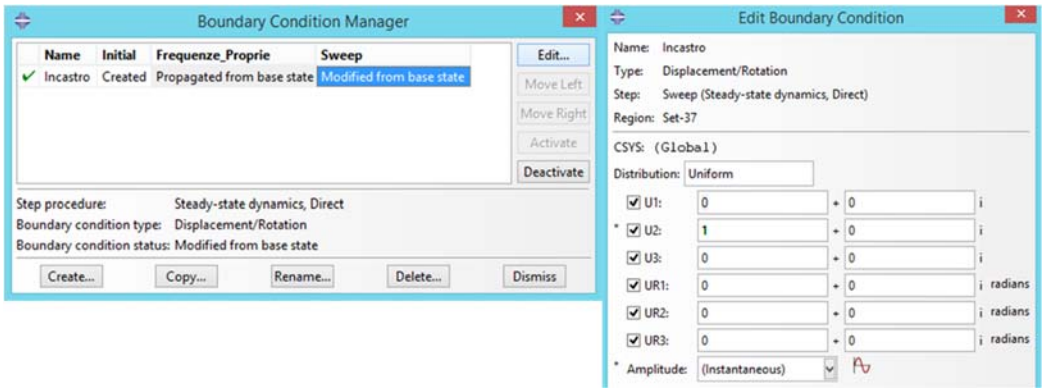

Fig. 80 – Boundary condition editor for the Sweep step

REFERENCES

[1] Lele SP, Maiti SK - Modeling of transverse vibration of short beams for crack detection and measurement of crack extension - Journal of Sound and Vibration 2002; 257:559–83.

[2] L.J. Hadjileontiadis et al. Crack detection in beams using kurtosis - Computers and Structures 83 (2005) 909–919.

[3] B. Li, X.F. Chen, J.X. Ma, Z.J. He - Detection of crack location and size in structures using wavelet finite element methods - Journal of Sound and Vibration 285 (2005) 767–782.

[4] Leonard F. et al - Free vibration behaviour of a cracked cantilever beam and crack detection - Mechanical Systems and Signal Processing (2001) 15(3), 529-548.

[5] Wang Dansheng et al - Impedance analysis for crack detection in the Timoshenko beam based on the anti-resonance technique - Acta Mechanica Solida Sinica, Vol. 20, No. 3, September, 2007.

[6] P.F. Rizos, N. Aspragathos, A.D. Dimarogonas - Identification of crack location and magnitude in a cantilever beam from the vibration modes - Journal of Sound and Vibration 138 (3) (1990) 381-388.

[7] M.H.H. Shen, Y.C. Chu - Vibrationsof beams with a fatigue crack - Computers and Structures 45 (1) (1992) 79-93.

[8] S. Bruni - Dynamics of continuous systems – bending vibrations of beams – Politecnico di Milano

[9] G. Diana, F. Cheli – Dinamica dei sistemi meccanici – Politecnico di Milano, Polipress 2010.

[10] Finite Element Analysis - David Roylance Department of Materials Science and Engineering Massachusetts Institute of Technology Cambridge, MA 02139.

[11] F. Semperlotti, K.W. Wang, E.C. Smith, Localization of a breathing crack using super-harmonic signals due to system nonlinearity, AIAA Journal, 47 (9), (2009) 2076-2086